

# Studies on some non-conjugated and conjugated polymer systems for holographic recording

Thesis submitted to  
Cochin University of Science and Technology  
in partial fulfillment of the requirements  
for the award of the degree of  
Doctor of Philosophy

By

**Anshad A**  
(Reg. No: 4106)



Department of Physics  
Cochin University of Science and Technology  
Cochin-682 022, Kerala, India

December 2018

# **Studies on some non-conjugated and conjugated polymer systems for holographic recording**

Ph.D. thesis in the field of Applied Optics

*Author*

**Anshad A**

Applied Optics Division  
Department of Physics  
Cochin University of Science and Technology  
Cochin-682 022, Kerala, India  
E-mail: anshadlathara@gmail.com

*Supervising Guide*

**Dr. C. Sudha Kartha**

Professor (Retired)  
Emeritus Scientist  
Applied Optics division  
Department of Physics  
Cochin University of Science and Technology  
Cochin-682 022, Kerala, India  
E-mail: karthasudha@gmail.com

December 2018

**DEPARTMENT OF PHYSICS**  
**COCHIN UNIVERSITY OF SCIENCE AND TECHNOLOGY**  
**KOCHI - 682022, INDIA**



---

**Dr. C. Sudha Kartha**  
Emeritus Scientist

Mob: 9847322578  
email: karthasudha@gmail.com

---

## Certificate

Certified that the thesis entitled **“Studies on some non-conjugated and conjugated polymer systems for holographic recording”** submitted by **Mr. Anshad A** in partial fulfilment of the requirements for the award of degree of Doctor of Philosophy in Physics to Cochin University of Science and Technology, is an authentic and bonafide record of the original research work carried out by him under my supervision at the Department of Physics. Further, the results embodied in this thesis, in full or part, have not been submitted previously for the award of any other degree. All the relevant corrections and modifications suggested by the audience during the pre-synopsis seminar and recommended by the Doctoral committee have been incorporated in the thesis.

Cochin - 22  
31-12-2018

**Dr. C. Sudha Kartha**  
(Supervising Guide)



## *Declaration*

I hereby declare that the work presented in the thesis entitled **“Studies on some non-conjugated and conjugated polymer systems for holographic recording”** is based on the original research work done by me under the guidance of Dr. C. Sudha Kartha, Emeritus Scientist, Department of Physics, Cochin University of Science and Technology, Cochin-22, India and no part has been included in any other thesis submitted previously for the award of any degree.

Cochin - 22  
31-12-2018

**Anshad A**



*Dedicated to*  
*My Parents & Beloved Teachers*



---

## *Words of gratitude...*

At this moment I express my heartfelt gratitude to my supervising guide Dr. C. Sudha Kartha, Emeritus Scientist, Department of Physics, CUSAT for her sustained interest, creative suggestions, motivation, guidance and support throughout my research period. I also express my sincere gratitude to Dr. K Sreekumar, Professor, Department of Applied Chemistry. Without his expert advice and help, my work would not have been completed. I also indebted to Dr. Rani Joseph, Emeritus Scientist, Department of Polymer Science and Rubber Technology and Dr. K P Vijayakumar, Emeritus Scientist, Department of Physics for their valuable suggestions.

I am grateful to Prof. M Junaid Bushiri, Head of the department of Physics, CUSAT and all former Heads of the department of Physics for granting me to access all facilities in the department to carry out my research work and for their support and co-operation.

I remember with gratitude the affection and commitment that Prof. MK Jayaraj has shown in clearing my doubts regarding my thesis work. I am thankful to my M. Sc. co-ordinator, Prof. Titus K Mathew for his friendly approach, affection and consideration. He has been a continuous source of inspiration since my post graduate classes. I have no suitable word that can fully describe Prof. Ramesh Babu's everlasting inspiration to love Physics and in improving my teaching skill.

I am grateful to all the faculty members and office staff of Department of Physics and university officials for their helping hands whenever needed.

The financial assistance from Cochin University of Science and Technology and UGC (RFSMS), India is greatly acknowledged.

A big thanks to my friends and family, I couldn't have done it without you.

*Anshad A*



## Preface

The thesis reports the studies made on synthesized low cost photoconducting polymers (both non-conjugated and conjugated polymers) which could be used as photorefractive material for holographic recording. Photorefractive effect in polymer was first reported in 1991. Photorefractive effect is the inhomogeneous variation in the refractive index of a material when it is exposed to nonuniform illumination. This effect was first reported in  $\text{LiNbO}_3$  crystal in 1966 and reported as an unwanted phenomenon. Soon after, researchers demonstrated holographic recording in  $\text{LiNbO}_3$  crystal through photorefractive effect. Photorefractive materials are now being studied for erasable holographic recording. The basic requirements for observing photorefractivity in a medium are photoconductivity and electro-optic effect. Photoconductivity results in the formation of space charge in the medium and electro-optic effect results in modulation of refractive index of material in the presence of the space charge electric field. This effect was reported earlier only in inorganic crystals. Organic photorefractive materials have several advantages over inorganic materials for producing photorefractivity such as wide flexibility to vary the chemical functions in a material, low dielectric constants, easy processing, and orientation effects. Nowadays the performance of these photorefractive polymers overcomes the performance of the inorganic crystals.

The polymers discussed in this thesis belong to two classes; non-conjugated polymers and donor-acceptor (D-A) conjugated polymers. All these polymers were synthesized by our group, taking into account the requirements of photorefractive effect. Experiments were conducted for analyzing the photoconducting properties and nonlinear properties of these polymers. Demonstration of photorefractive effect was also done by doing two beam coupling experiment.

The thesis is comprised of six chapters.

**Chapter 1** gives the basics of photorefractive effect in polymers. An introduction to the basics of photoconductivity in polymers and various types of photoconducting polymer systems are also presented.

**Chapter 2** presents the photophysical and photoconductive properties of three non-conjugated, benzoxazine polymers, which are found to have enough photoconducting properties to exhibit photorefractive effect. The molecules studied are poly(6-tert-butyl-3-Phenyl-3,4-dihydro-2H-1,3-benzoxazine) labelled as PBZ, poly([4-(6-tert-butyl-4H-benzo[e][1,3]oxazin-3-yl)phenyl]-phenyldiazene) labelled as AZO-PBZ and poly(4-tert-butyl-2-{{ethyl(4-nitrophenyl)amino}methyl}6{{methyl(4-phenylazophenyl)amino}methyl}phenol) labelled as AZO-PNA. All these polymers were synthesized using solvent free, thermally activated cationic ring opening polymerization. These polymers exhibited good thermal stability. Experiments were carried out to explore its photophysical, electrochemical, and photoconducting properties. These polymers showed optical absorption at higher frequencies of visible spectrum and exhibited good fluorescence emission. Influence of typical photosensitizer [6, 6]-phenyl-C<sub>61</sub>-butyric acid methyl ester labelled as PCBM on photoconductivity was investigated by preparing PBZ/AZO-PBZ/AZO-PNA:PCBM blend films, with polymer to PCBM weight ratios of 1:0.5 and 1:1. The photocurrent through the PCBM blend films was measured as a function of electric field to recognize the field dependence on carrier generation and photoconductive sensitivity. Internal photocurrent efficiency of the order of  $10^{-6}$ ,  $10^{-5}$  and  $10^{-4}$  were achieved in the PBZ:PCBM, AZO-PBZ:PCBM and AZO-PNA:PCBM blend films, respectively. Also, photoconductive sensitivities of the order of  $10^{-12}$ ,  $10^{-11}$  and  $10^{-10}$  S W<sup>-1</sup>cm, were achieved in the PBZ:PCBM, AZO-PBZ:PCBM and AZO-PNA:PCBM blend films respectively.

**Chapter 3** discusses the details of the preparation of photorefractive composite based on polybenzoxazine. The photorefractive composite is prepared through guest-host approach. The composite consists of PBZ:PCBM, which act as the host matrix, Disperse red 1 (DR 1), which acts as NLO chromophore (guest) and N-ethyl carbazole which reduces the glass transition temperature of the resulting composite. For photorefractive experiment, the devices were fabricated by sandwiching a thin layer of composite between two ITO coated glass plates. The photoconductivity measurements of the composite were done using He-Ne laser. Two beam coupling experiment was conducted to check whether it exhibits photorefractivity. The composite showed asymmetric coupling of two interfering beams. The photorefractive gain obtained was  $87 \text{ cm}^{-1}$ .

**Chapter 4** mainly focuses on the studies of the photoinduced charge transfer properties of low band gap donor-acceptor  $\pi$ -conjugated copolymer poly(2,5-(3,4-ethylenedioxythiophene)-alt-2,7-(9,9-dioctylfluorene)) labelled as P(EDOT-FL). Donor-acceptor coupling between EDOT and fluorene resulted in an absorption band in the visible region representing intramolecular charge transfer. The photoinduced charge transfer nature of the pristine polymer has been investigated through solvatochromic and photoconductivity studies. The positive solvatochromism exhibited by the P(EDOT-FL) reveals its photoinduced charge transfer nature of absorption and emission bands. Influence of PCBM on the photogeneration of free carriers is studied by comparing the fluorescence spectra and photoconductive properties of the P(EDOT-FL):PCBM blend films with the pristine polymer films. The blend films exhibited quenching of fluorescence and showed increased photoconductivity. Internal photocurrent efficiency and photoconductive sensitivity of pristine P(EDOT-FL) films and P(EDOT-FL):PCBM blend films were calculated as a function of electric field, by measuring the photocurrent generated in the sample. Blend films exhibit higher internal photocurrent efficiency of 86% and photoconductive sensitivity of  $5.44 \times 10^{-7} \text{ SW}^{-1} \text{ cm}$  at  $70 \text{ V}/\mu\text{m}$ .

**Chapter 5** describes the photophysical and photoconductive properties of a newly synthesized low band gap donor-acceptor conjugated polymer based on benzothiadiazole (BTZ), which is widely used as an acceptor moiety in combination with numerous donor moieties. The donor moieties selected are triphenylamine (TPA), 3-hexylthiophene (HT) and dihexyloxythiophene (HXT). The copolymers studied are poly(benzothiadiazole-triphenylamine) labelled as P(BTZ-TPA), poly(benzothiadiazole-hexylthiophene) labelled as P(BTZ-HT) and poly(benzothiadiazole-dihexyloxythiophene) labelled as P(BTZ-HXT). Initially the photophysical and photoconductive aspects of P(BTZ-TPA) were studied in detail. Here solvatochromic experiments of P(BTZ-TPA) were carried out using a binary mixture consisting of toluene and acetonitrile to understand the solvent dependence on the ground state and excited states of this polymer. It is concluded that there is high degree of intramolecular charge transfer through the polymer backbone. P(BTZ-TPA) thin films exhibited good photoresponse over the entire visible region, with promising internal photocurrent efficiency. Drastic quenching of fluorescence emission was observed when this polymer was blended with PCBM and is assigned to the charge transfer reaction between copolymer and PCBM, and is confirmed by the substantial increment in photoconductivity of the blend films. An internal photocurrent efficiency of 17.4% was obtained in the blend films for a biasing field of 10 V/ $\mu\text{m}$ . The photoconductive performance of the P(BTZ-TPA):PCBM blend films was then compared with the performance of P(BTZ-HT):PCBM and P(BTZ-HXT):PCBM blend films. It was observed that PCBM act as a good acceptor for P(BTZ-TPA). But P(BTZ-HT):PCBM and P(BTZ-HXT):PCBM gave only lesser values. Even then, the performance of all these polymers were comparable with the reported values of the well-known PVK based photorefractive polymer systems developed for holographic recording.

**Chapter 6** includes the conclusions made out of the studies and a comparison of the performance of all the non-conjugated and conjugated photoconducting polymers synthesized and studied are also given. Thesis is concluded by giving the future scope for this study and suggesting other applications of the materials studied.



# Contents

## Chapter 1

### **Photorefractive Polymers – An Introduction .....01 - 37**

1.1	Photorefractive effect and mechanism .....	02
1.2	Why photorefractive polymers? .....	08
1.3	Photorefractive polymer classes .....	09
1.4	Conducting polymers .....	11
1.5	Photoconductive polymers .....	12
1.5.1	Photogeneration of charge carriers .....	14
1.5.2	Charge transport .....	15
1.5.3	Trapping .....	16
1.5.4	Sensitizers .....	17
1.5.5	Mechanism of exciton dissociation at the donor- acceptor interface .....	18
1.5.6	Photoconductivity .....	21
1.6	NLO chromophores .....	24
1.7	Plasticizers .....	26
1.8	Outline of the thesis .....	27
	References.....	29

## Chapter 2

### **Photoconductivity studies on Polybenzoxazine**

### **based polymers .....39 - 86**

2.1	Introduction .....	40
2.2	Sample preparation .....	42
2.3	Poly(6-tert-butyl-3-phenyl-3-4-dihydro-2H-1,3-benzoxazine) .....	43
2.3.1	Electrochemical properties .....	44
2.3.2	Optical properties of PBZ .....	45
2.3.3	Temperature dependence of electrical conductivity.....	47
2.3.4	Steady state photocurrent measurement in PBZ film .....	48
2.3.5	PCBM as an acceptor.....	48
2.3.6	Optical properties of PBZ:PCBM blend .....	50
2.3.7	Steady state photocurrent measurement .....	52
2.3.7.1	Photocurrent action spectra.....	52
2.3.7.2	Intensity dependence of photocurrents.....	55
2.3.7.3	Internal photocurrent efficiency and photoconductive sensitivity .....	56

2.4	Poly([4-(6-tert-butyl-4H-benzo[e][1,3]oxazin-3-yl)phenyl]-phenyldiazene) .....	58
2.4.1	Electrochemical properties .....	60
2.4.2	Optical properties of AZO-PBZ .....	60
2.4.3	Temperature dependence of electrical conductivity .....	62
2.4.4	Steady state photocurrent measurement in AZO-PBZ film .....	63
2.4.5	Optical properties of AZO-PBZ:PCBM blend.....	63
2.4.6	Steady state photocurrent measurement .....	65
2.4.6.1	Photocurrent action spectrum .....	65
2.4.6.2	Intensity dependence of photocurrent .....	68
2.4.6.3	Internal photocurrent efficiency and photoconductive sensitivity .....	68
2.5	Poly(4-tert-butyl-2- {[ethyl(4-nitrophenyl)amino]methyl}6 {[methyl(4-phenylazophenyl)-amino]methyl}phenol) .....	70
2.5.1	Electrochemical properties .....	71
2.5.2	Optical properties of AZO-PBZ .....	72
2.5.3	Temperature dependence of electrical conductivity.....	73
2.5.4	Steady state photocurrent measurement in AZO-PNA film .....	74
2.5.5	Optical properties of AZO-PNA:PCBM blend .....	74
2.5.6	Steady state photocurrent measurements .....	76
2.5.6.1	Photocurrent action spectrum .....	76
2.5.6.2	Intensity dependence of photocurrent .....	78
2.5.6.3	Internal photocurrent efficiency and photoconductive sensitivity .....	79
2.7	The band diagram .....	81
2.8	Summary .....	82
	References.....	83

### Chapter 3

#### **Photorefractive effect in PBZ composite ..... 87 - 102**

3.1	Introduction.....	87
3.2	Poly(6-tert-butyl-3-phenyl-3,4-dihydro-2H-1,3-benzoxazine) based guest- host photorefractive composite .....	89
3.3	Photorefractive device fabrication .....	90
3.3.1	Patterning of ITO for standard electrodes .....	91
3.3.2	Preparation of the photorefractive polymer composite .....	92
3.3.3	Device fabrication .....	93
3.4	Optical absorption .....	94
3.5	Photoconductivity in photorefractive device .....	94

3.6	Two beam coupling experiment .....	95
3.6.1	Theory .....	95
3.6.2	Experiment and results .....	96
3.7	Summary.....	100
	References.....	100

## Chapter 4

### Photoconductive Properties of P(EDOT-FL) ..... 103 - 133

4.1	Introduction .....	104
4.2	Experimental .....	106
4.3	Poly(2,5-(3,4-ethylenedioxythiophene)-alt-2,7-(9,9-dioctylfluorene)) .....	107
4.4	Studies on pristine P(EDOT-FL) .....	109
4.4.1	Electrochemical properties .....	109
4.4.2	Optical properties .....	110
4.4.2.1	Optical absorption .....	110
4.4.2.2	Fluorescence emission .....	111
4.4.2.3	Solvatochromic Experiment .....	112
4.4.3	Electrical conductivity of P(EDOT-FL) thin films .....	114
4.4.4	Steady state photocurrent measurements in P(EDOT-FL) films ..	116
4.4.4.1	Intensity dependence of photocurrent .....	116
4.4.4.2	Internal photocurrent efficiency and photoconductive sensitivity.....	117
4.5	Studies on P(EDOT-FL):PCBM blend .....	119
4.5.1	Optical Absorption.....	119
4.5.2	Fluorescence quenching.....	120
4.5.3	Steady state photocurrent measurements in P(EDOT-FL):PCBM films .....	121
4.5.3.1	Intensity dependence of photocurrent .....	121
4.5.3.2	Internal photocurrent efficiency and photoconductive sensitivity .....	122
4.6	Band diagram and photoinduced charge separation.....	124
4.7	Summary .....	127
	References.....	128

## Chapter 5

### Photoconductive Aspects of Benzothiadiazole

### Copolymers ..... 135 - 179

5.1	Introduction.....	135
5.2	Experimental.....	139

5.3	Studies on P(BTZ-TPA) .....	140
5.3.1	Optical properties of P(BTZ-TPA) .....	141
5.3.1.1	Optical absorption.....	141
5.3.1.2	Fluorescence emission .....	142
5.3.1.3	Solvatochromic analysis.....	144
5.3.2	Steady state photocurrent measurements .....	147
5.3.2.1	Photocurrent action spectrum .....	147
5.3.2.2	Intensity dependence of photocurrent .....	149
5.3.2.3	Internal photocurrent efficiency and photoconductive sensitivity .....	150
5.4	Studies on P(BTZ-TPA):PCBM .....	152
5.4.1	Optical properties of P(BTZ-TPA):PCBM .....	152
5.4.1.1	Optical absorption .....	152
5.4.1.2	Fluorescence quenching .....	153
5.4.2	Steady state photocurrent measurements .....	154
5.4.2.1	Photocurrent action spectrum .....	154
5.4.2.2	Intensity dependence of photocurrent .....	155
5.4.2.3	Internal photocurrent efficiency and photoconductive sensitivity .....	156
5.5	Studies on P(BTZ-HT) .....	158
5.5.1	Optical properties of P(BTZ-HT):PCBM.....	159
5.5.1.1	Optical absorption.....	159
5.5.1.2	Fluorescence quenching .....	160
5.5.2	Steady state photocurrent measurements .....	161
5.5.2.1	Photocurrent action spectrum .....	161
5.5.2.2	Intensity dependence of photocurrent .....	162
5.5.2.3	Internal photocurrent efficiency and photoconductive sensitivity .....	162
5.6	Studies on P(BTZ-HXT) .....	164
5.6.1	Optical properties of P(BTZ-HXT):PCBM .....	165
5.6.1.1	Optical absorption.....	165
5.6.1.2	Fluorescence quenching .....	166
5.6.2	Steady state photocurrent measurements .....	167
5.6.2.1	Photocurrent action spectrum .....	167
5.6.2.2	Intensity dependence of Photocurrent .....	168
5.6.2.3	Internal photocurrent efficiency and photoconductive sensitivity .....	169
5.7	The band diagram and photoconductivity .....	170
5.8	Summary .....	173
	References.....	174

**Chapter 6**

**Summary and Future Scope .....181 - 189**

6.1 Summary of the present work..... 181

6.2 Future scope ..... 187

References ..... 188



## List of Publications

### Journal Publications

- [1] “Photophysical and photoconductive aspects of donor-acceptor low band gap conjugated copolymer” **Anshad Abbas**, Jisha J. Pillai, K. Sreekumar, Rani Joseph, C. Sudha Kartha *Optical Materials* 84 (2018) 813–820.
- [2] “Study on the photoconductive properties of charge carriers in donor-acceptor copolymer P(EDOT-FL) and P(EDOT-FL):PCBM blend” **Anshad Abbas**, Jisha J. Pillai, Sona Narayanan, K. Sreekumar, Rani Joseph, C. Sudha Kartha. *Synthetic Metals* 233 (2017) 52–57.
- [3] “Synthesis and experimental investigations on the photoconductivity of p-aminoazobenzene based non-conjugated polybenzoxazine system” Jisha J. Pillai, **Anshad Abbas**, Sona Narayanan, K. Sreekumar, C. Sudha Kartha, Rani Joseph. *Polymer* 137 (2018) 330-337.
- [4] “Low band gap donor-acceptor phenothiazine copolymer with triazine segment: Design, synthesis and application for optical limiting devices” Sona Narayanan, **Anshad Abbas**, C.P. Anjali, Sowmya Xavier, C. Sudha Kartha, K.S. Devaky, Krishnapillai Sreekumar, Rani Joseph. *Journal of Luminescence* 198 (2018) 449–456.
- [5] “Theoretical and experimental investigations on the photoconductivity and nonlinear optical properties of donor–acceptor p conjugated copolymer, poly(2,5-(3,4-ethylenedioxythiophene)-alt-2,7-(9,9-dioctylfluorene))” Sona Narayanan, **Anshad Abbas**, Sreejesh Poikavila Raghunathan, Krishnapillai Sreekumar, Cheranellore Sudha Kartha and Rani Joseph. *RSC Adv.*, 2015, 5, 8657.
- [6] “Synthesis and third-order nonlinear optical properties of low band gap 3,4-ethylenedioxythiophene–quinoxaline copolymers” Sona Narayanan, Sreejesh Poikavila Raghunathan, Sebastian Mathew, M.V. Mahesh Kumar, **Anshad Abbas**, Krishnapillai Sreekumar, Cheranellore Sudha Kartha, Rani Joseph. *European Polymer Journal* 64 (2015) 157–169.

## Conference Proceedings

- [1] “Influence of LUMO level on the charge transfer at the polymer:PCBM interface in D-A conjugated polymers” **Anshad Abbas**, Sona Narayanan, Jisha J. Pillai, K. Sreekumar, PHOTONICS-2018: International Conference on Fiber Optics and Photonics, 12<sup>th</sup> – 15<sup>th</sup> December 2018, Organized by IIT, Delhi, India.
- [2] “Photogeneration studies at the P(EDOT-FL): PCBM interface for using as a photorefractive polymer” **Anshad A**, Jisha J Pillai, Sudha Kartha C, in the 29th Kerala Science Congress held at Marthoma college, Thiruvalla during 28-30 January 2017. (BEST PAPER AWARD)
- [3] “Photoconductivity studies on poly(2,5-(3,4-ethylenedioxythiophene)-alt-2,7-(9,9-dioctylfluorene)) sensitized with Phenyl-C61-butyric acid methyl ester” **Anshad A**, Sona Narayanan, Jisha J Pillai, Sudha Kartha C, Sreekumar K and Rani Joseph. 22nd DAE-BRNS National Laser Symposium (NLS-22), Jan 08-14, 2014, Organized by Department of Atomic and Molecular Physics, MIT, Manipal University, Manipal, Karnataka, India-576 104
- [4] “Photoconductivity studies on Poly(6-tertiary-butyl-3-phenyl-3,4-dihydro 2H-1,3-benzoxazine) sensitized with Phenyl-C61-butyric acid methyl ester” Jisha J Pillai, **Anshad A**, Sudha Kartha C, Sreekumar K and Rani Joseph. 24th DAE-BRNS National Laser Symposium (NLS-24), Dec 02-05, 2015, Organized by Raja Ramanna Centre for Advanced Technology, Indore-452 013.
- [5] “Synthesis, Characterization and Photoconductivity Studies of p-Aminoazobenzene Based Polybenzoxazine System”, Jisha J P, **Anshad A**, Sudha C K, Sreekumar K, Rani J. MatCon 2016, held at Cochin University on 2016, Organized by Department of Chemistry, CUSAT.

## Photorefractive Polymers – An Introduction

### Abstract

Holographic 3D displays provide highly realistic images without the need for special eyewear, making them valuable tools. Current commercially available holographic 3D displays employ photopolymers that lack image updating capability, resulting in their limited use and high cost per 3D image. Photorefractive polymers are dynamic holographic materials that permit recording of highly efficient reversible holograms. The present chapter gives a brief introduction to photorefractive polymers. Mechanism of photorefractive polymers, requirement of photorefractive medium and different materials used for the fabrication of photorefractive devices are discussed in detail. Theoretical and experimental techniques used for design, fabrication and characterization of photorefractive polymers are also outlined. Discussions are also focused on conducting polymers, especially on conjugated photoconducting polymers. Moreover, the role of photosensitizers for achieving higher carrier generation efficiencies are presented.

## 1.1 Photorefractive effect and mechanism

Photorefractive (PR) effect is the non-local and non-uniform refractive index change of a material when it is subjected to a non-uniform intensity distribution of light. This phenomenon was first reported in 1966 in electro-optic crystal,  $\text{LiNbO}_3$  (Lithium Niobate) by Ashkin *et al.* and described as an undesirable “optical damage” [1]. Photorefractivity is a multi-step process comprising of two distinct phenomena such as photoconductivity and electro-optic effect [2]. A variety of valuable applications were reported using the photorefractive effect. In order to visualize the PR effect in a better way, the PR material is exposed to an interference pattern, resulting from the intersection of two coherent laser beams. In 1968, phase recording of optical information (holographic data storage) was done in lithium niobate crystals using PR effect [3]. Usual holographic materials such as photopolymers, photochromics, thermoplastics, etc. belong to WORM type material; write once read many. Unlike these permanent recording materials, holograms can be written and erased in PR materials many times without any chemical processing [4]. Photorefractive materials are now considered to be promising candidates for holographic storage and information processing applications. In 1991, Moerner and co-workers established the photorefractive effect in organic polymers [5]. Research on photorefractive polymers have shown remarkable progress in terms of efficiency, speed, and operating wavelengths. Today, performance of photorefractive polymers excels the performance of the best inorganic photorefractive crystals.

As mentioned, photorefractive effect is the combined effect of photoconductivity and first order electro-optic effect, also known as

Pockel's effect. Photoconductivity refers to an increase in electrical conductivity of a material due to the absorption of electromagnetic radiation of appropriate energy. On the other hand, Pockel's effect is the nonlinear change in the refractive index of a noncentrosymmetric material due to the application of the electric field.

A three dimensional refractive index inhomogeneity is produced in a photorefractive material when it is exposed to non-uniform intensity distribution. Assume two coherent laser beams intersecting in a photorefractive material. The spatially modulated intensity distribution pattern formed can be represented by the relation [6,7],

$$I(x) = I_0[1 + m \cos(2\pi/\Lambda)] \quad (1)$$

Where  $I_0 = I_1 + I_2$  is the sum of the intensities of the two beams, i.e., the total incident intensity,  $m = 2(I_1 I_2)^{\frac{1}{2}}/(I_1 + I_2)$  is the fringe visibility and  $\Lambda$  is the periodicity or the spatial wavelength. For the tilted transmission geometry,

$$\Lambda = \frac{\lambda}{2n \sin[(\alpha_2 - \alpha_1)/2]} \quad (2)$$

where  $n$  index of refraction of the material,  $\lambda$  is the wavelength of incident light beam in vacuum and  $\alpha_1$  and  $\alpha_2$  are the angles made by the incident beams with respect to sample normal. If optical frequencies are selected as the writing beams, periodicity of light intensity distribution  $\Lambda$  varies from  $0.3 \mu m$  to  $20 \mu m$ . Grating vector  $K$  is defined in a direction perpendicular to the bright and dark planes with a magnitude of  $K = 2\pi/\Lambda$ .

The intersecting writing beams produce an interference pattern within the photorefractive material, which leads to the generation of the electron-hole pairs in the brighter regions of the pattern, especially in the high intensity region. Typically, the charge carriers with high mobility (usually holes in polymers) get migrated from the brighter region to darker region leaving behind the counter charge at the brighter region.

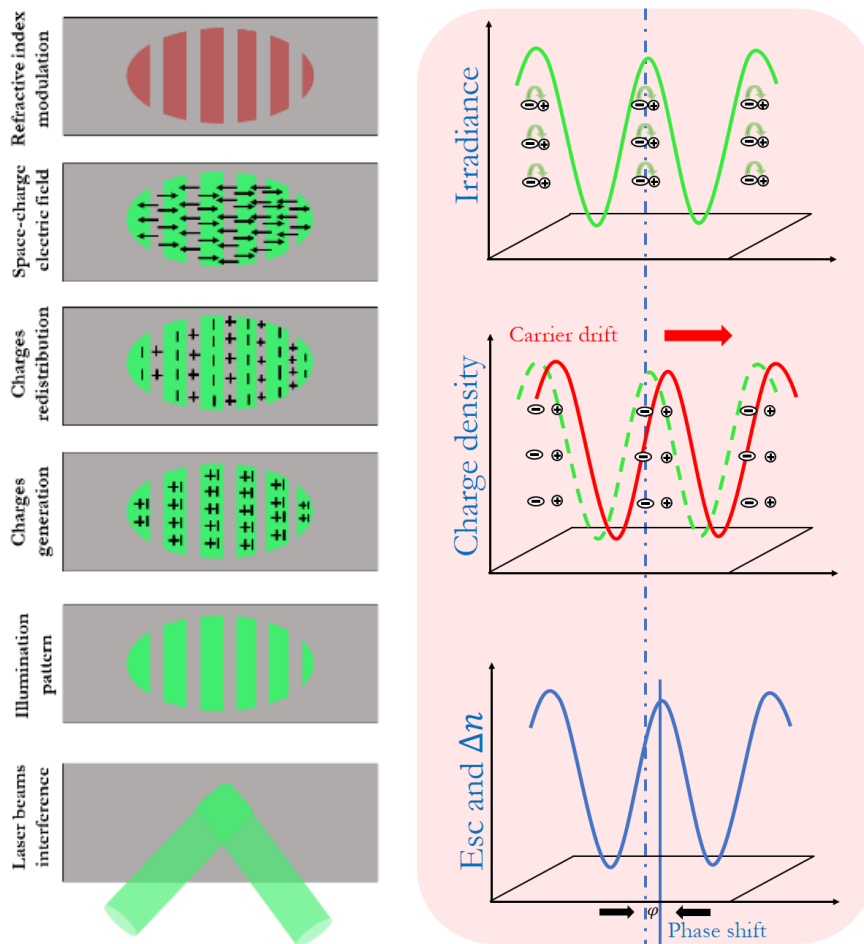


**Fig. 1.1:** Schematic representation of the mechanism of photorefractive effect

Diffusion due to concentration gradient or externally applied electric field may act as the driving force to drive the charge carriers to the dark regions. The traps present in the material limit the migration of the charge carriers towards the low intensity regions of the pattern. The charge carriers left behind in the high intensity region and the counter charge carriers trapped at low intensity regions result in the formation of inhomogeneous space charge distribution. Fig. 1.1 explains the different steps involved such as charge generation, charge transport and charge trapping corresponding to one dimensional light distribution.

If the space charge distribution is considered as one dimensional, then the induced electric field resulting from the space charge can be obtained from the Poisson's equation  $dE_{sc}/dx = 4\pi\rho(x)/\epsilon$ , where  $E_{sc}$  is the space charge electric field,  $\rho(x)$  is the charge density and  $\epsilon$  is the dielectric constant of the photorefractive material. This space charge electric field shows a phase shift ( $\varphi$ ) with respect to the intensity distribution of the incident light. If the driving force for the charge transport is diffusion alone, then the phase shift is  $\pi/2$ , otherwise this phase shift depends on the strength of the diffusion and external field. The amplitude of the periodic space charge electric field is,

$$E_{sc} = m \left[ \frac{(E_0^2 + E_d^2)}{\left(1 + \frac{E_D}{E_q}\right)^2 + \left(\frac{E_0}{E_q}\right)^2} \right]^{1/2} \quad (3)$$

Where,  $E_0$  is the component of the external electric field in the direction of the grating vector,  $E_D = Kk_bT/e$ , called diffusion field and  $E_q = eN_T/K\epsilon\epsilon_0$ , called trap limited current. Here K is the grating vector,

$k_b$  is the Boltzmann constant,  $T$  is the temperature,  $\epsilon$  is the permittivity of the medium,  $\epsilon_0$  is the permittivity of free space,  $N_T$  is the trap density and  $e$  is the electronic charge [8,9].

Again, the phase shift  $\varphi$  can also be expressed in terms these electric fields as,

$$\varphi = \arctan \left[ \frac{E_D}{E_0} \left( 1 + \frac{E_D}{E_q} + \frac{E_0^2}{E_D E_q} \right) \right] \quad (4)$$

The final process in the photorefractive grating development is the modulation of the refractive index of the material in the presence of this space charge electric field through linear electro-optic effect (Pockel's effect). Assuming pure linear electro-optic effect, the refractive index modulation is given by,

$$\Delta n(x) = -\frac{1}{2} n^3 r_e E_{sc}(x) \quad (5)$$

More details of the electro-optic effect will be discussed in the forthcoming section.

There are several local mechanisms for holographic grating recording in different materials such as thermochromism, photochromism, thermorefraction, photopolymerization, generation of excited states etc., which bring the refractive index modulation in accordance with the incident intensity distribution [10,11]. But in photorefractive systems, nonlocal properties arises owing to the physical motion of charges with in the material (up to a distance of the order of  $\mu m$ ) [12]. This charge transport results in a phase shift between the incident light intensity pattern and the refractive index modulation (Pockel's effect follows the space charge electric field).

This phase shift is unique for photorefractive materials [13]. This phase shift leads to asymmetric energy transfer (asymmetric two beam coupling) between two interfering beams in the photorefractive medium, i.e., after passing through the photorefractive medium, one of the writing beams get amplified and the other get weakened (Fig. 1.2).

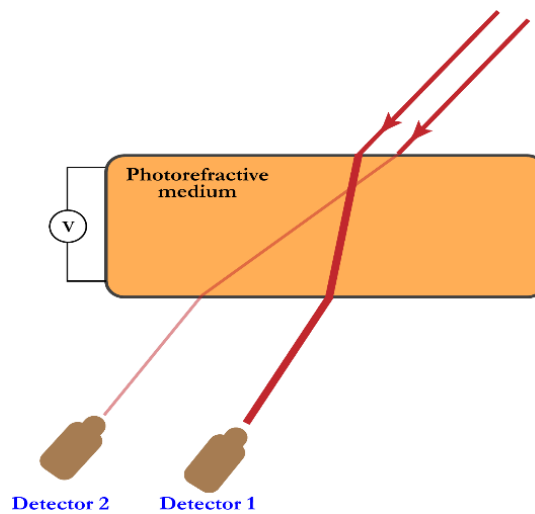


**Fig. 1.2:** Asymmetric energy transfer between two interfering beams in a photorefractive medium (Schematic representation)

The asymmetric energy transfer will not occur in a thick hologram fabricated using any local material. So the asymmetric two beam coupling (TBC) is treated as the finger print of photorefractive effect. Several novel applications have been proposed, and demonstrated based on the TBC gain which include simulations of neural networks and associative memories, coherent image amplification, self-pumped phase conjugation, novelty filtering and beam fanning optical limiters [14–19].

## 1.2 Why photorefractive polymers?

After the discovery of photorefractive effect in  $\text{LiNbO}_3$  in 1966, many research groups were working in this field and articulated various inorganic crystals in this class such as  $\text{KNbO}_3$ ,  $\text{BaTiO}_3$ ,  $\text{Bi}_{12}\text{SiO}_{20}$  (BSO),  $\text{Sr}_x\text{Ba}_{1-x}\text{NbO}_3$ ,  $\text{InP:Fe}$ ,  $\text{GaAs}$ , multiple-quantum-well semiconductors[19–21]. Also, several novel applications were proposed as mentioned in section 1.1, which rely on TBC effect. However, difficulties in crystal growth and sample preparation limited the use of these inorganic crystals in the proposed applications. On the other hand, organic materials mostly polymeric or glassy materials offer ease of fabrication and flexibility in sample preparation. This is one of the major reasons for pursuing organic photorefractive materials, especially photorefractive polymers. Another motivation comes from the concept of figure of merit, defined as  $Q = n^3 r_e / \epsilon_r$ , where  $n$  is the refractive index of the material,  $r_e$  is the electro-optic coefficient and  $\epsilon_r$  is the dielectric constant. Figure of merit can be roughly defined as the ratio of optical nonlinearity to the screening of the internal space charge electric field. In inorganic crystals, the large ionic polarizability predominantly contributes to optical nonlinearity.  $Q$  therefore does not vary significantly from material to material. However, the optical nonlinearity in organic materials is a molecular property, which is determined by the charge asymmetry of the electronic distribution in the ground state and excited state [22]. So, in organic materials, large electro-optic coefficient is not accompanied by large dielectric constant. Thus, figure of merit in organic photorefractive material can be improved up to a factor of ten or more.

Research on photoconducting polymers began in 1960s and poly(N-vinylcarbazole) is one pioneering polymer in this class. Since 1980, research was conducted to achieve electro-optic properties in organic nonlinear optical (NLO) materials. In 1990, photorefractivity was reported in organic semiconducting materials [23]. In the succeeding year, holographic recording was successfully proven in a polymeric material [5]. After this, numerous polymer systems were reported in literature; many of them were better than the best inorganic crystals and many have commercial applications. These photorefractive polymers are also known as photorefractive polymer composites.

### 1.3 Photorefractive polymer classes

Photoconductivity and electro-optic effect are the basic requirements of any photorefractive system. Photoinduced charge generation, transport of the generated carriers, trapping of charge carriers and electro-optic response are key features influencing the photorefractivity in all systems. Typically, there are two types of photorefractive polymer systems: guest-host polymer systems and fully functionalized polymers. Among the various polymer systems, guest-host approach is widely preferred owing to its extreme flexibility. Here, the necessary functional species are physically mixed to a host polymer. One can control the proportion of the active dopant molecules and hence can tune the molecular properties affecting the photorefractivity. The first reported photorefractive polymer system belongs to this class where an electro-optic polymer was used as polymer host and a charge transport agent, sensitizer and chromophore molecules were doped into the nonlinear optical polymer [5]. At the same time, the

interest of scientists also concentrated in the development of organic light emitting diodes, organic thin film transistors and photovoltaic cells [24–26]. The photoinduced charge generation and transport of charge carriers through photoconductive material plays central role in such applications, which is a common phenomenon found in photorefractive materials also. Research in these fields has enabled the development of many novel organic polymers exhibiting substantial photoconductive performance. So, in many of the recently reported guest-host photorefractive polymer systems, photoconducting polymers are used as polymer host. In photoconducting polymers, charge transport occurs through polymer backbone and thus the inert material used for charge transport can be reduced. The phase separation of the doped components is the main drawback of guest-host approach, which will affect the stability of the PR composite. However, a 100% diffraction efficiency was reported in a guest-host polymer system in which poly(N-vinylcarbazole) was used as the photoconducting host [27].

To overcome the phase stability issue, another class of polymers were introduced, commonly referred to as fully functionalized polymers. In this case, the required components are directly attached to polymer backbone through chemical reaction. Either the NLO chromophore is covalently linked to a photoconducting polymer backbone or NLO molecule is functionalized with photoconducting moieties [28–30]. Most of the fully functionalized polymers exhibit higher glass transition temperature (above room temperature) which limit the orientational enhancement of electro-optic response. So poling is necessary to obtain electro-optic activity in these polymers. Also, these orientational enhancement is low and very slow,

compared to the same process in the guest-host systems. Further, the space charge formation is a slow process in fully functionalized polymers which significantly affect the holographic response time. The refractive index modulation and two beam coupling gain is also reported to be very low in these fully functionalized polymers. Though the fully functionalized polymers exhibit stability against phase separation of the multicomponent in the guest-host approach, it cannot fulfill the other demands of photorefractive effect [31].

## 1.4 Conducting polymers

In general, polymers are treated as insulators due to their poor electrical conductivity. In 1977, it was shown that, an intrinsically insulating polymer, polyacetylene (PA) become highly conducting one, on treatment with oxidizing or reducing agents [32]. This process is referred as doping. Following this achievement, a variety of polymers were reported as conducting polymers such as poly(p-phenylene sulphide), polypyrrole, polythiophene, polyfuran etc. Planar structure and presence of conjugated system along the polymer backbone are the two structural features providing the increased electrical conductivity on doping. Presence of alternate single and double bond is called conjugation. One of the bonds in double bond ( $\pi$  bond) is highly delocalized so that electrons in this bond can be easily removed when it is doped with electron accepting molecule. On doping with an oxidizing agent, the electrons in the  $\pi$  bond get partially transferred to the dopant by leaving a hole in polymer backbone. This brings higher electrical conductivity in the conducting polymers[33–35].

In 1988, it was reported that, conjugated backbone was not a necessity for electrical conductivity in polymers [36]. Electrical conductivity was obtained in specific non-conjugated polymers with one double bond and three single bonds in the repeat unit when doped with iodine. Cis-polyisoprene, trans—polyisoprene and poly(dimethylbutadiene) are examples for non-conjugated polymers. The conductivity in non-conjugated polymers depend on the fraction of double bonds per repeat unit. Higher the fraction of double bond per repeat unit, larger will be the electrical conductivity. In addition, a polymer having no double bond in the repeat unit cannot be conducting due to the lack of  $\pi$  electron for charge transfer reaction during doping. The maximum value of the fraction is  $\frac{1}{2}$  which indicate the conjugated polymers.

## **1.5 Photoconductive polymers**

Photoconductivity is the essential part of photorefractive polymer systems. Photoconductors are generally insulators and become more conducting when it is illuminated with photon flux of suitable energy. The absorption of electromagnetic radiation results in the generation of free electron-hole pairs. Transport of the newly generated carriers in the presence of biasing electric field increase conductivity of the material. The difference in electrical conductivity of the photoconductor before and after illumination is a quantitative measure of this phenomenon and is termed as photoconductivity ( $\sigma_{ph}$ ). Physics of photoconductivity in polymers is entirely different from that in inorganic crystals. In polymers, photoconductivity is influenced by several factors such as photogeneration of charge carriers, charge transport and trapping which in turn depends on the wavelength of illumination, incident intensity, biasing electric field, HOMO-LUMO

energy levels of polymers and dopants, structural morphology of the polymer and its distribution in solid state form etc.

Poly(N-vinylcarbazole), commonly called as PVK is a renowned photoconducting polymer widely used in copy machines (xerography). This innovative polymer was studied for past two decades in photorefractive systems as a photoconducting host matrix and reported many fruitful outcomes. There is a review article “carbazole photorefractive materials” published which shows its wide acceptance as a photoconductor [37]. Nearly 100% diffraction efficiency with a coupling gain of more than  $200 \text{ cm}^{-1}$  and a response time in the range of millisecond for two beam coupling measurement were reported for PVK based photorefractive polymer systems [27,38–40]. Recently, in a carbazole based photorefractive polymer composite, photorefractivity was established through the surface plasmon effects of gold nanoparticles [41].

PVK is a hole transporting photoconducting polymer. Hole mobility of pristine PVK polymers is much low, of the order of  $10^{-7} - 10^{-6} \text{ cm}^2 \text{ V}^{-1} \text{ S}^{-1}$  which limits the photorefractive response time in ten or hundreds of millisecond regime. Triphenylamine or tetraphenyldiaminophenyl based polymers were introduced to achieve faster response time since they possessed high hole mobility [42,43]. Hole mobility of the order of  $10^{-5} - 10^{-4} \text{ cm}^2 \text{ V}^{-1} \text{ S}^{-1}$  has been reported for tetraphenyldiaminophenyl based polymer [44]. Also, a triphenylamine based photorefractive polymer system with high hole mobility ( $10^{-3} - 10^{-2} \text{ cm}^2 \text{ V}^{-1} \text{ S}^{-1}$ ) was reported [45]. This polymer is less efficient because the high hole mobility in this

polymer resulted in large dark current, which easily lead to dielectric break down under low electric field [45–47].

### **1.5.1 Photogeneration of charge carriers**

Initial process in the photoconductivity of a material is the absorption of light and subsequent generation of electron-hole pairs, followed by its transport. The primary excitations in crystalline materials directly generate electron-hole pairs, without the formation of any intermediate excited state. These free electrons and holes are distributed in the conduction band and valence band immediately after the photon absorption. Radiative recombination of the electrons and holes are responsible for the luminescence effect in such materials. Photogeneration of charge carriers in inorganic crystals is independent of temperature, applied electric field, trap densities etc. while the radiative recombination is affected by temperature [48].

When an organic molecule is optically excited, the excited state can either relax to the ground state by radiative or non-radiative decay process, or it can form a bound-electron hole pair called excitons. The electron and hole can localize on the same molecule or different molecules. These excitons can either dissociate into free carriers (charge separation) or undergo recombination (geminate recombination) due to Coulombic attraction between the electron-hole pair. In organic materials geminate recombination dominates the charge separation due to its low dielectric constant. This results in a low photogeneration efficiency (number of charge carriers generated per absorbed photon) of the organic materials.

The charge separation of the bound electron-hole pairs is enabled through the thermal motion or by applying electric field. The external electric field decreases the Coulomb potential and thereby increases the chances of charge separation. In contrast to inorganic crystals, in the case of photoconductive polymers, photogeneration efficiency is highly field dependent [8].

### 1.5.2 Charge transport

The ability of a material for the charge transport is usually described by the physical quantity, mobility. In inorganic materials, once free carriers are generated, they are drifted/diffused to the dark region and get accumulated there. Mobility of the charge carriers are generally field independent [21]. Band transport theory can successfully explain the charge transport in inorganic crystals [49]. On the other hand, organic materials especially polymers, are disordered materials (amorphous materials). Recent research articles regarding the charge transport in organic materials discuss the wide scope of the organic electronics. In this case, mobility of the charge carriers is highly field dependent and temperature dependent, and in many cases,  $\ln \mu \propto E^{1/2}$  [50]. Also, charge transport in these polymers is facilitated through hopping mechanism, which is evident from the strong mobility dependence of carriers on inter-particle distance between the transport molecules [51]. The charge carriers experience different energetic environment in each hopping site due to the disordered nature. This type of charge transport in polymers is generally termed as dispersive charge transport [52]. The temperature and field dependence of carrier mobility is successfully explained by Gaussian disorder or hopping model [53]. For

photorefractive polymer systems, the proposed model is valid for temperatures below the glass transition temperature.

### 1.5.3 Trapping

Traps play a major role in the photorefractive performance of a polymer composite since they hold the mobile charges to build the space charge. Traps are defined as the local regions within the material where the mobile charges are localized for some period of time. Impurities and structural defects can also be treated as traps. The mobility of the charge carriers also depends on the trapping species. In the hopping model charge transport, a hopping site with a lower total energy for the hole acts as a trap. Life time of the trapped carriers will be determined by the depth of the trap compared to thermal energy. A deep hole trap is one that can be subjected to thermal detrapping at the rate of  $10^{-4}$  per second. For shallow traps, the detrapping rate is of the order of 1 per sec [54]. Oh. *et al.* studied the dependence of hole mobility on trap density and enabled detailed understanding on how trap density influences the space charge formation [55]. For photorefractive polymer systems, deep traps are generally observed, when the HOMO level of the polymer is above the HOMO level of the transport molecule. Impurities, defects and orientational effects generally produce shallow traps [56,57]. It is observed that, systems with deep traps have slower response time and faster chromophore systems are those in which the energy levels of chromophore molecule and charge transport molecule are similar and number of deep traps are minimized [58]. Another study shows that, to obtain a large space charge electric field in a high resolution environment (large grating vector), trap density should be high.

### 1.5.4 Sensitizers

Sensitizers are essential part of photorefractive polymer composite, since they intensely assist photoinduced charge generation. The conducting polymers usually used for the photorefractive composites exhibit absorption in the ultraviolet region or in the higher frequencies of the visible spectrum. This limits the utility of the polymer for visible and infrared holographic applications. By doping/blending these conducting polymers with suitable molecules (sensitizers) having absorption in the desired wavelength, spectral response can be considerably extended.

Depending on the nature of the majority charge carriers, the sensitizer can be an electron donating moiety (p-type) or electron accepting moiety (n-type). Most of the photoconducting polymer materials are hole conducting (p-type). So all most all sensitizers are n-type electron acceptor molecules. A good electron acceptor should have a HOMO level well below the charge transporting matrix. If the sensitizer molecule forms a charge transfer complex with the charge transporting matrix, the spectral sensitivity is extended to the red region along with the enhanced photogeneration [59].

Organic molecules/dyes and semiconductor nanocrystals are usually used as sensitizers for the photogeneration in the visible and infrared region [60–62]. Earlier, fullerene ( $C_{60}$ ) has served as a leading acceptor molecule with many of the photoconducting polymers for efficient charge separation during photoexcitation [63]. In addition, TNF is another sensitizer widely used in polymer photorefractive systems, mostly in PVK based systems [64].

### 1.5.5 Mechanism of exciton dissociation at the donor-acceptor interface

Usually, conjugated polymers exhibit large absorption coefficients, so that a thin polymer layer can provide enough light harvesting. But, efficient light absorption alone cannot generate free carriers. In conjugated polymers, the absorption of light will create bound electron-hole pairs called excitons, which need to be dissociated for generating photocurrent in the material. Dissociation of the excitons created immediately after the absorption of light is the crucial process determining the photocurrent generated in the sample. However, in order to dissociate the excitons, the Coulombic binding energy of the electron-hole pair need to be overcome. This Coulombic energy is given by,

$$E_C = \frac{e^2}{4 \pi \epsilon_r \epsilon r}, \quad (6)$$

$r$  is the electron-hole pair separation distance. For inorganic crystals,  $\epsilon_r > 10$ , and the Coulomb binding energy is nearly 10 meV. In the case of organic materials, the dielectric constant is in between 2 and 4, thereby binding energy is of the order of 1 eV. Thus, the thermal energy ( $KT \approx 25 \text{ meV}$ ) cannot provide the driving force for the effective dissociation of the Frenkel type excitons in organic materials.

The photocurrent in the conjugated polymer:fullerene/fullerene derivative composite is dominated by the high exciton dissociation efficiency at the donor-acceptor interface [65]. There are many suggestions in literature regarding the basic physics behind the exciton dissociation. Some report state that, once the excitons are generated, they

diffuse to the polymer-acceptor interface and the electrons are captured by the acceptor molecule and the holes are left behind in the polymer material [66]. Also some reports inform that, an energy transfer from polymer to acceptor molecule occurs so that, the excitons initially generated in the polymer material is transferred to the acceptor molecule and holes are returned to the polymer via polymer-acceptor interface [67]. Whatever be these two reports on that, once the exciton gets dissociated, electrons remaining in the acceptor molecule and holes residing on the polymer material are still bound by the Coulomb potential [68–70]. To obtain free charge carriers, these bound electron-hole pairs have to be separated. Due to the low dielectric constant of the polymers, the Coulomb binding energy is much large compared to the thermal energy. Then the natural question is, how they acquire the driving force for the charge separation.

Arkhipov *et al.* proposed that, a dipolar layer was formed in the dark at the polymer-acceptor interface which resulted in an efficient dissociation [71]. This model was criticized severely because, the model was valid for very small effective masses of holes. It is not possible in organic materials with small electronic band width [72,73]. Deibel *et al.* argued that, no dark dipoles were necessary for the efficient exciton dissociation at the polymer-acceptor interface. The delocalization of the holes in the polymer back bone carried the holes to distant locations with respect to the electron captured in the fullerene, which reduced the Coulomb energy of the dissociating electron-hole pair [74]. A. V. Nanashev *et al.* also showed that, delocalization of charge carriers along

the polymer back bone could help the carriers to overcome the Coulomb potential barrier [75].

Monishka Rita Narayan and Jai Singh proposed a mechanism explaining the exciton dissociation at the interface [76]. According to this, absorption of photons having energy greater than or equal to the band gap of the donor polymer results in the excitation of an electron to the LUMO level by leaving a hole in the HOMO level. These excited charges immediately form a Frenkel type exciton-the bound electron-hole pair within the donor polymer due to their strong Coulomb attraction. These excitons diffuse to the donor-acceptor interface through Forster energy transfer mechanism and get dissociated. The excitons dissociate at the interface through two steps-(1) since the energy of the LUMO level of the acceptor is lower than the LUMO of the donor molecule, the exciton first relaxes to the charge transfer exciton (CT exciton) state by transferring the electron to the LUMO level of the acceptor [77]. Still the electron and hole are bound until an external energy, at least equal to the binding energy, acts on the CT exciton [78]. Here, the external energy comes from the excess vibrational energy released during the formation of excitons. If this excess vibrational energy is enough, this energy may impact back to the CT exciton and dissociate it into free electron and hole. Fig. 1.3 explains this mechanism schematically. The increase in LUMO offset between donor and acceptor molecule increases the rate of dissociation of the exciton at the interface. This is because, larger offset results in a higher excess vibrational energy available for the exciton dissociation.

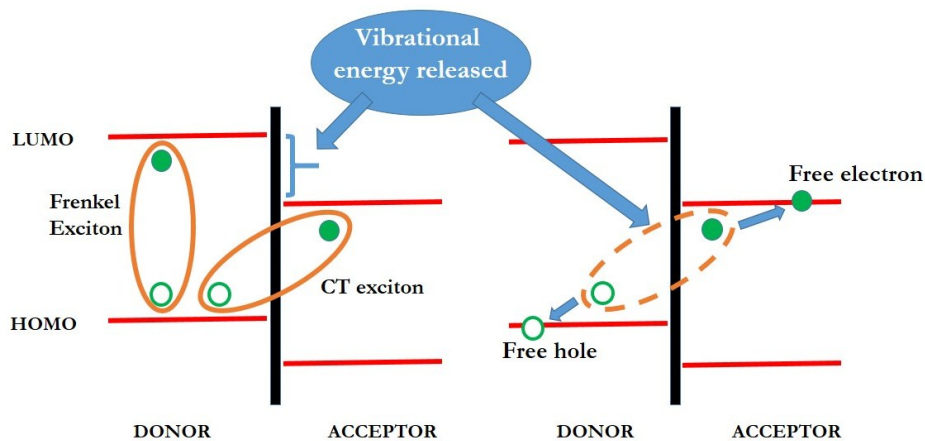


**Fig. 1.3** The Frenkel exciton initially formed at the donor polymer, immediately after the light absorption is relaxed to CT exciton by moving the electron to the LUMO of the acceptor molecule. The excess vibrational energy released lead to the dissociation of CT exciton into free charges.

### 1.5.6 Photoconductivity

Steady state photocurrent generated in a conductor as a result of optical illumination is,  $J_{ph} = \sigma_{ph}E$ ,  $\sigma_{ph}$  is the photoconductivity and  $E$  is the applied electric field. Photoconductivity in polymers depends on several physical mechanisms that are not usually operative in the inorganic crystals. Photoconductivity can simply be expressed as

$$\sigma_{ph} = n_c e \mu \quad (7)$$

where  $\sigma_{ph}$  is the photoconductivity,  $n_c$  is the density of charge carriers,  $e$  is the electronic charge,  $\mu$  is the mobility of carriers.

The internal photocurrent efficiency ( $\Phi$ ) of the photogeneration is defined as the number of measured charge carriers and can be calculated from the photocurrent measurement as [46,47,79]

$$\phi(E) = \frac{J_{ph}h\nu}{eI\alpha L} = \frac{\sigma_{ph}Eh\nu}{eI\alpha L} \quad (8)$$

where,  $\alpha$  is the absorption coefficient,  $I$  is the incident optical intensity,  $h$  is Planck's constant,  $\nu$  is the frequency of the light.  $L$  is the sample thickness. The internal photocurrent efficiency can be related to the photogeneration efficiency ( $\phi$ ), which is the number of generated carriers per absorbed photon as,

$$\phi(E) = G\phi = \frac{\epsilon_0\epsilon_r E}{eLT_i} \phi \quad (9)$$

$G$  is the photoconductivity gain factor [80], where  $T_i$  is the initial trap density in Schildkraut model [54].

Photoconductivity per unit light intensity is termed as photoconductive sensitivity which is another parameter usually calculated for a photorefractive system. This can be obtained as,

$$\frac{\sigma_{ph}}{I} = \frac{I_{ph}L}{PAV} \quad (10)$$

where  $I_{ph}$  is the photocurrent generated,  $L$  is the sample thickness,  $P$  is the power density,  $A$  is the active area and  $V$  is the applied voltage.

The response time of grating formation,  $\tau$  (the inverse of which is called response rate of grating formation) is an essential feature for the performance of photorefractive polymers. The rate of grating formation is significantly related to the photoconductivity of the composite. Kukhtarev *et al.* and Yeh studied the formation of light induced grating theoretically and proposed a limit for the response time  $\tau$  of the grating formation in inorganic crystals as,

$$\tau = \frac{2\epsilon_0\epsilon_r E_{sc}\hbar\omega}{e\Lambda \alpha\phi I} \quad (11)$$

Where  $E_{sc}$  is the space charge field,  $\hbar$  is the Planks constant,  $\omega$  is the angular frequency,  $\phi$  is the photogeneration efficiency and I is the incident intensity.

Alternatively, the grating growth time can be defined as the time needed to fill the traps by the holes and can be expressed as,

$$\tau = \frac{\alpha\phi I}{\hbar\omega} T_i \quad (12)$$

Here,  $T_i$  can be obtained from trap-limited space-charge electric field ( $E_q$ ) as,

$$E_q = \frac{e\Lambda}{2\pi\epsilon_0\epsilon_r} T_i \quad (13)$$

Thus the growth time can be expressed as [80]

$$\tau = \frac{2\pi\epsilon_0\epsilon_r E_q\hbar\omega}{e\Lambda \alpha\phi I} \quad (14)$$

Using above mentioned relations, response rate ( $1/\tau$ ) of grating formation can be expressed as

$$\frac{1}{\tau} = \frac{\sigma_{ph}}{\epsilon_0\epsilon_r} \quad (15)$$

In this way, the response rate can be related to photoconductivity and dielectric constant of the composite. Response rate depends linearly on photoconductivity. But there are suggestion in literature that, large photocurrent may limit the formation of effective space charge electric field [46].

## 1.6 NLO chromophores

The photoconductors along with sensitizer molecules enable a space charge distribution within the photorefractive system when it is exposed to an interference pattern. This involves the carrier generation immediately after the absorption of light, transport of the generated carriers through the charge transport agent (mostly, charge transport through the polymer backbone) and finally the localization of mobile carriers within the trap (which are intrinsic or extrinsic). The second demand of the photorefractive effect is the alternation of refractive index of the photorefractive composite in accordance with the space charge electric field (Pockel's effect). The linear electro-optic effect in the photorefractive media is ensured by the uniform distribution of NLO chromophores throughout the composite. For achieving bulk second order nonlinearity in the polymeric composite, non-centrosymmetric nonlinear molecules must be arranged in the bulk such that the bulk material does not exhibit centrosymmetry [81].

Organic NLO chromophores are used in a variety of photonic applications [82]. In 1980s and 1990s, numerous research efforts have been there on to develop organic NLO molecules based on  $\pi$  conjugation for optimizing nonlinear optical properties of electro-optic polymers [83]. In such  $\pi$  conjugated molecules, the first hyperpolarizability  $\beta$  (second order molecular polarizability) and permanent dipole moment  $\mu$  (ground state dipole moment) are the two major parameters determining the second order nonlinearity of these molecules. Figure of merit (FOM) of these molecules is defined as,

$$FOM = \frac{1}{M_w} \left[ 9\mu\beta + 2 \frac{\mu^2 \Delta\alpha}{kT} \right] \quad (16)$$

where  $M_w$  is the molecular weight,  $\Delta\alpha$  is the anisotropy of the linear polarizability,  $k$  is the Boltzmann constant and  $T$  is the temperature. For NLO chromophores,  $\beta$  can be calculated from the two state model approximation [84]. Large charge separation in organic molecules is associated with a series of delocalized  $\pi$ -conjugated bonds. Delocalization of  $\pi$ -conjugated bridge allow rapid electronic redistribution in the presence of an applied electric field. To exhibit second order nonlinear effects, the molecule should have non-centrosymmetry. By attaching a donor (electron rich) group and an acceptor (electron deficient) group on either side of the  $\pi$ -bridge, the charge asymmetry can be obtained and the molecules acquire a permanent dipole moment. Such type of molecules are known as push-pull chromophores [85]. The degree of charge separation (ie., the degree of ground state polarization) depends on the structure of the  $\pi$ -conjugated system or the strength of the donor and acceptor moieties. Though the presence of large dipole moment provides high electro-optic properties, it will inhibit the charge carrier mobility owing to the increase in the dipolar disorder of the charge transporting agent. In the case of push-pull chromophores, it is reported that, the major contribution of the electro-optic effect originates from the polarizability anisotropy term ( $\Delta\alpha$ ) compared to the second order polarizability term in the expression for FOM [6]. This supports the relevance of orientational enhancement effect.

Large dipole moment of the chromophore molecules leads to crystallization which results in inhomogeneity and scattering of the light

within the composite. The attachment of the bulky alkyl chains on ends of the chromophore molecules can reduce the crystallization. However, it decreases the FOM due to increased molecular weight [86]. Also, higher chromophore concentration and large dipole moment also disturb the orientational effect through intermolecular interactions between the chromophore molecules [87].

Following the demand of FOM, various successful NLO chromophore molecules were designed and synthesized such as azo-dye derivatives (like DMNPAA) [88], dicyanostyrene derivative (like DCST) [39] and oxopyridone dyes (like ATOP) [89].

## **1.7 Plasticizers**

Plasticizers are inert molecules used to reduce the glass transition temperature ( $T_g$ ) of a composite. At or above the glass transition temperature, the polymer is changed to a glassy/rubber like state. At this stage, dipolar molecules can be oriented by applying moderate electric field. For most of the polymers, the glass transition temperature lies above the room temperature, in the range 100 °C to 200 °C [90]. 70 to 80% of the nonlinear optical response in a nonlinear system is obtained from the reorientation of the NLO chromophore in response to a biasing field, which is called poling [91]. To achieve this, the operating temperature should be increased or the glass transition temperature should be reduced to operating temperature (in most of the cases, room temperature). Fixing a higher operating temperature results in the degradation of the polymer, which severely affects the photorefractive performance of the sample. So the practical solution is fixing a low operating temperature and reduce the

glass transition temperature towards the operating region by using plasticizers.

The plasticizer molecules disperse within the composite material and disturb the long range order of the polymer chains, which increases the free volume within the composite. This will increase the fluidity [92]. In plasticized photorefractive systems, photorefractive response is correlated with photoconductivity [93]. 9-Ethyl carbazole (ECZ) [45], benzyl butyl phthalate (BBP) [94], triphenylamine (TPA) [95], 2,4,6-trimethylphenyldiphenylamine (TAA) [47], carbazolyethylpropionate (CzEPA) [96], (4-(diphenylamino)phenyl)methanol (TPAOH) [97], 9-(2-ethylhexyl)carbazole (EHCz) [98], tricresylphosphate (TCP) [99] and dicyclohexyl phthalate (DCP) [100] are commonly used plasticizer molecules and a concentration of 15 to 30% by weight is used [59]. But, in highly plasticized systems, aggregation of the components occur due to high degree of freedom to move and cause failure of the device [101]. Plasticizer molecule does not have direct functionality contribution to the photorefractive performance of the composite. However, inert plasticizer molecule may deteriorate the charge transport properties. Monomer units of charge transport polymers can also be used as plasticizers, since they can take part in charge transport. Carbazole based plasticizers are such type of plasticizers.

## 1.8 Outline of the thesis

Aim of the present work was to develop potential polymer systems: both non-conjugated and conjugated for photorefractive applications. As photoconductivity and electro-optic effect are the basic requirements of a photorefractive system, this work mainly explores the details of

photoconductive properties of a series of non-conjugated and conjugated polymer systems. The polymers described in this thesis are newly synthesized and characterized by the group and the experimental setup for the different studies was assembled in the lab.

The second chapter describes the photoconductivity studies of three non-conjugated polymers based on polybenzoxazine. As the pristine films of these polymers did not show photoconductivity, PCBM was used as the sensitizer and thereby achieved photoconductivity. The photoconductive sensitivity and internal photocurrent efficiency of the polymers systems are comparable with many of the typical photorefractive polymer systems. In Chapter 3, the photorefractive device preparation and the two beam coupling experiments are discussed.

Chapter 4 describes the photoconductive properties of low band gap conjugated copolymers based on ethylenedioxythiophene and fluorene. This conjugated polymer exhibited photoconductivity in pristine form. In order to achieve higher photocarrier generation, PCBM was used as an acceptor along with this polymer. An internal photocurrent efficiency of 0.86 was achieved in this system.

In Chapter 5, the photoconductive properties of three donor-acceptor conjugated polymers are discussed in which benzothiadiazole acted as acceptor moiety. Triphenylamine, 3-hexylthiophene and 3,4-dihexyloxythiophene were used as donor moieties. Out of these, poly(benzothiadiazole-3,4-dihexyloxythiophene) exhibited the lowest band gap of 1.65 eV. Poly(benzothiadiazole-triphenylamine):PCBM exhibited high photoconductive properties. Chapter 6 summarizes the main results of this work and discusses the future scope.

## References

- [1] A. Ashkin, G.D. Boyd, J.M. Dziedzic, R.G. Smith, A.A. Ballman, J.J. Levinstein, K. Nassau, Optically induced refractive index inhomogeneities in  $\text{LiNbO}_3$  and  $\text{LiTaO}_3$ , *Appl. Phys. Lett.* 9 (1966) 72–74.
- [2] W.E. Moerner, S.M. Silence, Polymeric photorefractive materials, *Chem. Rev.* 94 (1994) 127–155.
- [3] F.S. Chen, J.T. Lamacchia, D.B. Fraser, F.S. Chen, J.T. Lamacchia, D.B. Fraser, Holographic storage in lithium niobate, *Appl. Phys. Lett.* 13 (1968) 223–225.
- [4] J. Thomas, C.W. Christenson, P. Blanche, M. Yamamoto, R.A. Norwood, N. Peyghambarian, Photoconducting polymers for photorefractive 3D display applications, *Chem. Mater.* 23 (2011) 416–429.
- [5] S. Ducharme, J.C. Scott, R.J. Twieg, W.E. Moerner, Observation of the photorefractive effect in a polymer, *Phys. Rev. Lett.* 66 (1991) 6–9.
- [6] O. Ostroverkhova, W.E. Moerner, Organic photorefractives: mechanisms, materials and applications, *Chem. Rev.* 104 (2004) 3267–3314.
- [7] B. Lynn, P.A. Blanche, N. Peyghambarian, Photorefractive polymers for holography, *J. Polym. Sci. Part B Polym. Phys.* 52 (2014) 193–231.
- [8] Q. Wang, L. Wang, L. Yu, Development of fully functionalized photorefractive polymers, *Macromolecules.* 21 (2000) 723–745.
- [9] B. Kippelen, K. Meerholz, N. Peyghambarian, An introduction to photorefractive polymers, CRC press, 1997.
- [10] H.J. Eichler, P. Günter, D.W. Pohl, *Laser-induced dynamic gratings*, Springer-Verlag Berlin Heidelberg, 1986.
- [11] G.H. Brown, *Techniques of chemistry, Vol. III: photochromism*, Wiley-Interscience, New York, 1971.
- [12] W.E. Moerner, A. Grunnet-Jepsen, C.L. Thompson, Photorefractive polymers, *Annu. Rev. Mater. Sci.* 27 (1997) 585–623.

- 
- [13] J. Thomas, R.A. Norwood, N. Peyghambarian, Nonlinear optical polymers for photorefractive applications, *J. Mater. Chem.* 19 (2009) 7476–7489.
- [14] P. Gunter, Holography, coherent light amplification and optical phase conjugation with photorefractive materials, *Phys. Rep.* 93 (1982) 199–299.
- [15] R.A. Fisher, *Optical phase conjugation*, Academic press, New York, 2012.
- [16] P. Günter, J.-P. Huignard, *Photorefractive materials and their applications I*, Springer-Verlag Berlin Heidelberg, 2005.
- [17] G.C. Valley, M.B. Klein, R.A. Mullen, D. Rytz, B. Wechsler, *Photorefractive materials*, *Annu. Rev. Mater. Sci.* 18 (1988) 165–188.
- [18] M.P. Petrov, S.I. Stepanov, A. V. Khomenko, *Photorefractive crystals in coherent optical systems*, Springer, 2013.
- [19] L. Solymar, D.J. Webb, A. Grunnet-Jepsen, *The physics and applications of photorefractive materials*, Clarendon Press, 1996.
- [20] Günter Peter, H.J. Pierre, *Photorefractive materials and their applications 2*, Springer-Verlag Berlin Heidelberg, New York, 2007.
- [21] P.C. Yeh, *Introduction to photorefractive nonlinear optics*, Wiley, New York, 1993.
- [22] D.S. Chemla, J. Zyss, *Nonlinear optical properties of organic molecules and crystals*, Academic press: Orlando, 1987.
- [23] K. Sutter, P. Gunter, Photorefractive gratings in the organic crystal 2-cyclooctylamino-5-nitropyridine doped with 7,7,8,8-tetracyanoquinodimethane, *J. Opt. Soc. Am. B.* 7 (1990) 2274–2278.
- [24] C.W. Tang, S.A. Vanslyke, Organic electroluminescent diodes, *Appl. Phys. Lett.* 51 (1987) 913–915.
- [25] J.H. Burroughes, D.D.C. Bradley, A.R. Brown, R.N. Marks, K. Mackay, R.H. Friend, A.B. Holmes, Light-emitting diodes based on conjugated polymers, *Nature.* 341 (1990) 539–541.
- [26] R.H. Friend, R.W. Gymer, A.B. Holmes, J.H. Burroughes, R.N. Marks, C. Taliani, D.D.C. Bradley, M. Lo, W.R. Salaneck, D.A. Dos Santos, J.L. Bre, Electroluminescence in conjugated polymers, *Nature.* 397 (1999) 121–128.

- 
- [27] K. Meerholz, B.L. Volodin, Sandalphon, B. Kippelen, N. Peyghambarian, A photorefractive polymer with high optical gain and diffraction efficiency near 100 %, *Nature*. 371 (1994) 497–500.
- [28] E. Hendrickx, D. Van Steenwinckel, Photorefractive polysilanes functionalized with a nonlinear optical chromophore, *Macromolecules*. 32 (1999) 2232–2238.
- [29] D. Haarer, S. Schloter, U. Hofmann, K. Hoechstetter, G. Ba, Permanently poled fully functionalized photorefractive polyesters, *J. Opt. Soc. Am. B*. 15 (1998) 2560–2565.
- [30] B. Kippelen, K. Tamura, N. Peyghambarian, A.B. Padias, J. H. K. Hall, Photorefractivity in a functional side-chain polymer, *Phys. Rev. B*. 48 (1993) 10710–10718.
- [31] S.J. Zilker, Materials design and physics of organic photorefractive systems, *Chemphyschem*. 1 (2000) 72–87.
- [32] C.K. Chiang, C.R. Fincher, Y.W.P. Jr., A.J. Heeger, H. Shirakawa, E.J. Louis, S.C. Gau, A.G. MacDiarmid, Electrical conductivity in doped polyacetylene, *Phys. Rev. Lett.* 39 (1977) 1098.
- [33] T.A. Skotheim, Handbook of conducting polymers, Vol-1 & 2, Marcell Dekker, New York, 1986.
- [34] C.C. Ku, R. Liepins, Electrical properties of polymers, Hanser publishers, New York, 1987.
- [35] J.R. Ferraro, J.M. Williams, Introduction to synthetic electrical conductors, Academic press, New York, 1987.
- [36] M. Thakur, A class of conducting polymers having nonconjugated backbones, *Macromolecules*. 21 (1988) 661–664.
- [37] Y. Zhang, T. Wada, H. Sasabe, Carbazole photorefractive materials, *J. Mater. Chem.* 8 (1998) 809–828.
- [38] Y. Zhang, Y. Cui, P.N. Prasad, Observation of photorefractivity in a fullerene-doped polymer composite, *Phys. Rev. B*. 46 (1992) 9900–9902.

- [39] D. Wright, M.A. Diaz-Garcia, J.D. Casperson, M. Declue, W.E. Moerner, R.J. Twieg, High-speed photorefractive polymer composites, *Appl. Phys. Lett.* 73 (1998) 1490–1492.
- [40] N. Tsutsumi, A. Dohi, A. Nonomura, W. Sakai, Enhanced performance of photorefractive poly(N-vinyl carbazole) composites, *J. Polym. Sci. Part B Polym. Phys.* 49 (2011) 414–420.
- [41] J. Choi, S. Ji, C. Choi, J. Oh, F.S. Kim, N. Kim, Enhanced photorefractive performance of polymeric composites through surface plasmon effects of gold nanoparticles, *Optical Lett.* 39 (2014) 4571–4574.
- [42] B.J. Thomas, C. Fuentes-hernandez, M. Yamamoto, K. Cammack, K. Matsumoto, G.A. Walker, S. Barlow, B. Kippelen, G. Meredith, S.R. Marder, Bistriaryamine polymer-based composites for photorefractive applications, *Adv. Mater.* 16 (2004) 2032–2034.
- [43] K. Sebastian, F. Gallego-gomez, M. Salvador, F.B. Kooistra, J.C. Hummelen, K. Aleman, K. Meerholz, Influence of the sensitizer reduction potential on the sensitivity of photorefractive polymer composites, *J. Mater. Chem.* 20 (2010) 6170–6175.
- [44] K. Ogino, T. Nomura, T. Shichi, S. Park, H. Sato, Synthesis of polymers having tetraphenyldiaminobiphenyl units for a host polymer of photorefractive composite, *Chem. Mater.* 9 (1997) 2768–2775.
- [45] K. Kinashi, H. Shinkai, W. Sakai, N. Tsutsumi, Photorefractive device using self-assembled monolayer coated indium-tin-oxide electrodes, *Org. Electron.* 14 (2013) 2987–2993.
- [46] N. Tsutsumi, K. Kinashi, K. Masumura, K. Kono, Photorefractive dynamics in poly(triarylamine)-based polymer composites, *Opt. Express.* 23 (2015) 25158–25170.
- [47] N. Tsutsumi, K. Kinashi, K. Masumura, K. Kono, Photorefractive performance of poly(triarylamine)-based polymer composites: an approach from the photoconductive properties, *J. Polym. Sci. Part B Polym. Phys.* 53 (2015) 502–508.

- 
- [48] V.I. Arkhipov, H. Bässler, Exciton dissociation and charge photogeneration in pristine and doped conjugated polymers, *Phys. Status Solidi*. 201 (2004) 1152–1187.
- [49] T.J. Hall, R. Jaura, L.M. Connors, The photorefractive effect-a review, *Prog. Quantum Electron.* 10 (1985) 11–146.
- [50] G.P. J. Mort, *Electronic properties of polymers*, Wiley, New York, 1982.
- [51] P. Taylor, Comparison of charge transport models in molecularly doped polymers, *Philos. Mag. Part B.* (2006) 795–810.
- [52] G. Pfister, Hopping transport in a molecularly doped organic polymer, *Phys. Rev. B.* 16 (1977) 3676–3687.
- [53] H. Bassler, Charge transport in disordered organic photoconductors a Monte Carlo simulation study, *Phys. Status Solidi*. 175 (1993) 15–56.
- [54] J.S. Schildkraut, A. V Buettner, Theory and simulation of the formation and erasure of space-charge gratings in photoconductive polymers, *J. Appl. Phys.* 72 (1992) 1888–1892.
- [55] J. Oh, C. Lee, N. Kim, J. Oh, C. Lee, N. Kim, Influence of chromophore content on the steady-state space charge formation of poly[methyl-3-(9-carbazolyl) propylsiloxane]-based polymeric photorefractive composites, *J. Appl. Phys.* 104 (2008).
- [56] J.H. Slowik, I. Chen, J.H. Slowik, I. Chen, Effect of molecular rotation upon charge transport between disordered carbazole units, *J. Appl. Phys.* 54 (1983) 4467.
- [57] P.S.F. Cacialli, *Functional supramolecular architectures*, Wiley- VCH Verlag & Co. KGaA, 2011.
- [58] O. Ostroverkhova, K.D. Singer, Space-charge dynamics in photorefractive polymers, *J. Appl. Phys.* 92 (2002) 1727–1743.
- [59] J. Thomas, R.A. Norwood, N. Peyghambarian, Nonlinear optical polymers for photorefractive applications, *J. Mater. Chem.* 19 (2009) 7476–7489.

- [60] E. Hendrickx, Y. Zhang, K.B. Ferrio, J.A. Herlocker, J. Anderson, P. Persoons, N. Peyghambarian, N.R. Armstrong, E.A. Mash, Photoconductive properties of PVK-based photorefractive polymer composites doped with fluorinated styrene chromophores, *J. Mater. Chem.* 9 (1999) 2251–2258.
- [61] C. Svanberg, D. Apitz, F. Gallego-gomez, K.G. Jespersen, Dynamics of organic holographic materials, *SPIE–Int. Soc. Opt. Eng.* 4802 (2002) 95–102.
- [62] J.G. Winiaz, L. Zhang, M. Lal, C.S. Friend, P.N. Prasad, Observation of the photorefractive effect in a hybrid organic-inorganic nanocomposite, *J. Am. Chem. Soc.* 121 (1999) 5287–5295.
- [63] D. Wright, B. Smith, M.S. Bratcher, M.S. Declue, J.S. Siegel, W.E. Moerner, Spectroscopic determination of trap density in C60-sensitized photorefractive polymers, *Chem. Phys. Lett.* 291 (1998) 553–561.
- [64] N. Tsutsumi, Molecular design of photorefractive polymers, *Polym. J.* 48 (2016) 571–588.
- [65] V.D. Mihailetschi, L.J.A. Koster, J.C. Hummelen, P.W.M. Blom, Photocurrent generation in polymer-fullerene bulk heterojunctions, *Phys. Rev. Lett.* 93 (2004) 216601.
- [66] L.W. Barbour, R.D. Pensack, M. Hegadorn, S. Arzhantsev, J.B. Asbury, Excitation transport and charge separation in an organic photovoltaic material: watching excitations diffuse to interfaces, *J. Phys. Chem.* 112 (2008) 3926–3934.
- [67] M.T. Lloyd, Y. Lim, G.G. Malliaras, M.T. Lloyd, Y. Lim, G.G. Malliaras, Two-step exciton dissociation in poly(3-hexylthiophene)/fullerene heterojunctions, *Appl. Phys. Lett.* 92 (2008) 143308.
- [68] C. Deibel, V. Dyakonov, Polymer–fullerene bulk heterojunction solar cells, *Reports Prog. Phys.* 73 (2010) 96401.
- [69] J.-L. Bredas, J.E. Norton, J. Cornil, V. Coropceanu, Molecular understanding of organic solar cells: the challenges., *Acc. Chem. Res.* 42 (2009) 1691–1699.
- [70] T.M. Clarke, J.R. Durrant, Charge photogeneration in organic solar cells, *Chem. Rev.* 110 (2010) 6736–6767.

- 
- [71] V.I. Arkhipov, P. Heremans, H. Bässler, Why is exciton dissociation so efficient at the interface between a conjugated polymer and an electron acceptor?, *Appl. Phys. Lett.* 82 (2003) 4605–4607.
- [72] P. Peumans, S.R. Forrest, Separation of geminate charge-pairs at donor–acceptor interfaces in disordered solids, *Chem. Phys. Lett.* 398 (2004) 27–31.
- [73] M. Wiemer, A. V Nenashev, F. Jansson, S.D. Baranovskii, On the efficiency of exciton dissociation at the interface between a conjugated polymer and an electron acceptor, *Appl. Phys. Lett.* 99 (2011) 13302.
- [74] C. Deibel, T. Strobel, V. Dyakonov, Origin of the efficient polaron-pair dissociation in polymer-fullerene blends, *Phys. Rev. Lett.* 103 (2009) 36402.
- [75] A. V Nenashev, S.D. Baranovskii, M. Wiemer, F. Jansson, R. Osterbacka, A. V Dvurechenskii, F. Gebhard, Theory of exciton dissociation at the interface between a conjugated polymer and an electron acceptor, *Phys. Rev. B.* 84 (2011) 35210.
- [76] M.R. Narayan, J. Singh, Study of the mechanism and rate of exciton dissociation at the donor-acceptor interface in bulk-heterojunction organic solar cells, *J. Appl. Phys.* 114 (2013) 73510.
- [77] X.Y. Zhu, Q. Yang, M. Muntwiler, Charge-transfer excitons at organic semiconductor surfaces and interfaces, *Acc. Chem. Res.* 42 (2009) 1779–1787.
- [78] M.C. Scharber, D. Mühlbacher, M. Koppe, P. Denk, C. Waldauf, A.J. Heeger, C.J. Brabec, Design rules for donors in bulk-heterojunction solar cells-towards 10% energy-conversion efficiency, *Adv. Mater.* 18 (2006) 789–794.
- [79] P. Chantharasupawong, C.W. Christenson, R. Philip, L. Zhai, M. Yamamoto, L. Tetard, R.R. Nair, J. Thomas, Photorefractive performances of a graphene doped PATPD/7-DCST/ECZ composite, *J. Mater. Chem. C.* 2 (2014) 7639–7647.
- [80] T. Däubler, R. Bittner, K. Meerholz, V. Cimrová, D. Neher, Charge carrier photogeneration, trapping, and space-charge field formation in PVK-based photorefractive materials, *Phys. Rev. B.* 61 (2000) 13515–13527.

- [81] S.R. Marder, B. Kippelen, A.K. Jen, N. Peyghambarian, Design and synthesis of chromophores and polymers for electro-optic and photorefractive applications, *Nature*. 388 (1997) 845–851.
- [82] P. Gunter, *Nonlinear optical effects and materials*, Springer-V, Berlin, 2000.
- [83] T. Van Nguyen, H.N. Giang, K. Kinashi, W. Sakai, N. Tsutsumi, Photorefractivity of perylene bisimide-sensitized poly(4-(diphenylamino) benzyl acrylate), *Macromol. Chem. Phys.* 217 (2016) 85–91.
- [84] V.C. Kishore, R. Dhanya, K. Sreekumar, R. Joseph, C. Sudha Kartha, On the dipole moments and first-order hyperpolarizability of N,N-bis(4-bromobutyl)-4-nitrobenzenamine, *Spectrochim. Acta - Part A Mol. Biomol. Spectrosc.* 70 (2008) 1227–1230.
- [85] H.S. Nalwa, S. Miyata, *Nonlinear optics of organic molecules and polymers*, CRC Press, Boca Raton, 1997.
- [86] H. Chun, I.K. Moon, D. Shin, N. Kim, Preparation of highly efficient polymeric photorefractive composite containing an isophorone-based NLO chromophore, *Chem. Mater.* 13 (2001) 2813–2817.
- [87] W. Frank, R. Wortmann, K. Meerholz, Chromophore design for photorefractive organic materials, *Chemphyschem.* 3 (2002) 17–31.
- [88] G. Büiuml, S. Schloter, U. Hofmann, D. Haarer, Determination of the density of recombination centers in a photorefractive guest-host polymer, *Syn.* 97 (1998) 165–169.
- [89] K. Meerholz, Y. De Nardin, R. Bittner, R. Wortmann, F. Würthner, K. Meerholz, Y. De Nardin, R. Bittner, F. Wu, Improved performance of photorefractive polymers based on merocyanine dyes in a polar matrix, *Appl. Phys. Lett.* 73 (1998) 4–6.
- [90] J.K. Fink, *High performance polymers*, William Andrew, United States, 2008.
- [91] S. Köber, M. Salvador, K. Meerholz, Organic photorefractive materials and applications, *Adv. Mater.* 23 (2011) 4725–4763.
- [92] S.L.R. Christopher S. Brazel, *Fundamental principles of polymeric materials*, Wiley, New York, 1993.

- [93] M.A. Diaz-Garcia, D. Wright, J.D. Casperson, B. Smith, E. Glazer, W.E. Moerner, Photorefractive properties of poly(N-vinyl carbazole)-based composites for high-speed applications, *Chem. Mater.* 11 (1999) 1784–1791.
- [94] N. Tsutsumi, W. Miyazaki, Photorefractive performance of polycarbazoleethylacrylate composites with photoconductive plasticizer, *J. Appl. Phys.* 106 (2009) 083113-.
- [95] S. Tsujimura, K. Kinashi, W. Sakai, N. Tsutsumi, Recent advances in photorefractivity of poly(4-diphenylaminostyrene) composites: wavelength dependence and dynamic holographic images, *Jpn. J. Appl. Phys.* 53 (2014) 119202.
- [96] K. Kinashi, Y. Wang, W. Sakai, N. Tsutsumi, Optimization of photorefractivity based on poly(N-vinylcarbazole) composites: an approach from the perspectives of chemistry and physics, *Macromol. Chem. Phys.* 214 (2013) 1789–1797.
- [97] H.N. Giang, K. Kinashi, W. Sakai, N. Tsutsumi, Triphenylamine photoconductive polymers for high performance photorefractive devices, *J. Photochem. Photobiol. A Chem.* 291 (2014) 26–33.
- [98] S. Tsujimura, T. Fujihara, T. Sassa, K. Kinashi, W. Sakai, Enhanced photoconductivity and trapping rate through control of bulk state in organic triphenylamine-based photorefractive materials, *Org. Electron.* 15 (2014) 3471–3475.
- [99] N. Tsutsumi, Y. Shimizu, Asymmetric two-beam coupling with high optical gain and high beam diffraction in external-electric-field-free polymer composites, *Jpn. J. Appl. Phys.* 43 (2004) 3466–3472.
- [100] N. Tsutsumi, J. Eguchi, W. Sakai, Asymmetric energy transfer and optical diffraction in novel molecular glass with carbazole moiety, *Opt. Mater. (Amst).* 29 (2006) 435–438.
- [101] O. Kwon, S. Lee, G. Montemezzani, P. Gu, Highly efficient photorefractive composites based on layered photoconductive polymers, *J. Opt. Soc. Am. B.* 20 (2003) 2307–2312.



# Photoconductivity studies on Polybenzoxazine based polymers

### Abstract

The present chapter deals with the photophysical and photoconductive properties of three non-conjugated, benzoxazine polymers, poly(6-tert-butyl-3-phenyl-3,4-dihydro-2H-1,3-benzoxazine) labelled as PBZ, poly([4-(6-tert-butyl-4H-benzo[e][1,3]oxazin-3-yl) phenyl] phenyldiazene) labelled as AZO-PBZ and poly(4-tert-butyl-2-{{ethyl(4-nitrophenyl)amino}methyl}6{{methyl(4-phenylazophenyl)-amino}methyl}phenol) labelled as AZO-PNA. These polymers were synthesized via thermally activated cationic ring opening polymerization method without using a catalyst or solvent. The polymers exhibited good thermal stability. Experiments were carried out to explore their optical, electrochemical, and photoconducting properties. The polymers showed optical absorption in the visible region and exhibited good fluorescence emission. Influence of typical photosensitizer [6, 6]-phenyl-C<sub>61</sub>-butyric acid methyl ester labelled as PCBM on photoconductivity was investigated by preparing PBZ/AZO-PBZ/AZO-PNA: PCBM blend films, with polymer to PCBM weight ratios of 1:0.5 and 1:1. Photoinduced charge transfer nature of the polymer:PCBM blend films were studied by analyzing the fluorescence spectra. Incorporation of PCBM into the polymer led to quenching of the fluorescence intensity and a significant increase in photoconductivity. The photocurrent through the PCBM blend films was measured as a function of electric field to recognize the field dependence on carrier generation. Internal photocurrent efficiencies of the order of  $10^{-6}$ ,  $10^{-5}$  and  $10^{-4}$  were achieved in the PBZ:PCBM, AZO-PBZ:PCBM and AZO-PNA:PCBM blend films, respectively. Also the films showed photoconductive sensitivities of the order of  $10^{-11}$  and  $10^{-11}$  SW<sup>-1</sup>cm for PBZ:PCBM and AZO-PBZ:PCBM and of the order of  $10^{-10}$  SW<sup>-1</sup>cm for AZO-PNA:PCBM.

## **2.1 Introduction**

In the past few decades, macromolecules with unique combination of both electronic and optical properties have gained considerable attention in the field of optical storage media, dynamic holography, photorefractive composites, photovoltaic and photoconducting devices due to increasing need for low cost materials with structural flexibility [1–4]. There are a handful of reports discussing synthesis, photoconductive properties and various applications of conjugated polymers [5–7], only a few reports are available in literature regarding the non-conjugated polymers. Photogeneration of charge carriers and carrier mobility are the two important requirements of photorefractivity. Charge carrier mobility directly influences the response time of the photorefractive composites [8]. Photoconductivity in polymeric systems is a complex process involving absorption of radiation, generation of charge carriers, transport, recombination and trapping. The charge transport and photoconducting properties of these materials mainly depend on the structure and morphology of the polymer chains and conjugated, non-conjugated categorizations stick to these parameters[9,10].

Polybenzoxazine is one of the most important class of polymers among the non-conjugated conducting polymers, due to its good mechanical, thermal and optical properties. These polymers exhibit excellent adhesion with different substrates [11]. The benzoxazine polymers exhibit unique properties such as, low cost, low water absorption, ease of synthesis, absence of byproducts, no need of catalysts etc. Hence they are highly attractive for future applications and are used in various fields like aerospace, automotive industries, optical storage etc [12–14]. However, they possess some disadvantages such as high brittleness,

requirement of high temperature for synthesis, difficulties in preparing neat films or complex structures [15]. Also, polybenzoxazine exhibits wide molecular design flexibility [12]. Exploring these design possibilities, the properties of polybenzoxazine can be enhanced by using suitable functional species. However, the conducting and photoconductive aspects of this class of polymers is less discussed in literature. Kishore *et al.* conducted the photoconductivity studies on a series of polybenzoxazine systems and reported that the incorporation of  $C_{60}$  resulted in an enhancement of photoconductivity [16].

The present chapter discusses the photoconductive properties of three benzoxazine polymers. Benzoxazine polymers were synthesized using inexpensive precursors such as phenol or its derivative, formaldehyde and primary amine or its derivatives [17]. The polymers were synthesized by solventless ring opening polymerization method. Fig. 2.1 shows the synthesis route of the benzoxazine polymers. The polymers were synthesized by modifying the primary amine derivatives. Photoconductive properties of the polymers were analyzed along with the photosensitizer PCBM.

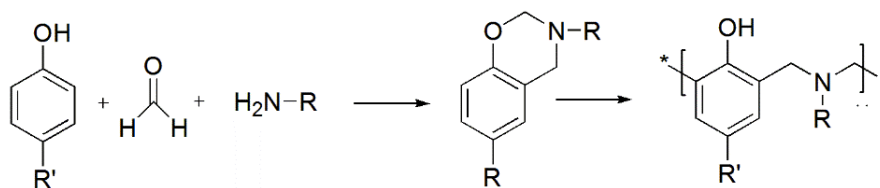


**Fig. 2.1:** Schematic representation of the synthesis route of polybenzoxazine. Here (a) phenol or its derivative, (b) formaldehyde and (c) primary amine or its derivative which are the precursors for the synthesis of benzoxazine polymer. (d) the general structure of polybenzoxazine.

## 2.2 Sample preparation

Optical and photoconductive studies were performed on spin coated thin films, prepared on ITO coated glass substrates, having thickness of typically  $1 \mu\text{m}$ . A spin coating unit of model SPIN 150 (SPS Euorope) was used. Spin coating process includes the deposition of optimized solution over a levelled surface and spinning it at required spinning conditions (speed, acceleration) for a fixed duration. Here, 10 wt% solutions with polymer to PCBM ratios of 1:0 (pristine) 1:0.5 and 1:1 were initially prepared in spectroscopic grade chloroform and spin coated to get uniform films. For spin coating, the ITO coated glass substrate of dimension 1 cm x 2 cm, was initially kept over the vacuum chuck and a fixed volume of the polymer: PCBM blend solution (0.3 ml) was placed over the ITO film. Films were prepared by spinning the substrate at a speed of 800 rpm for 60 s. The acceleration of the spinning was fixed to 800 rpm/s. After spin coating, films were carefully removed from the chuck and kept on a neat levelled surface. The films were kept in ambient condition for 6 h for the evaporation of the solvent. It was transferred to a vacuum desiccator for 48 h for the complete removal of the solvent. Higher concentration of the PCBM above the ratio of 1:1 resulted in the formation of films with less optical clarity. For electrical measurements, a sandwich cell structure ITO/Polymer:PCBM/Ag was used. Silver electrodes of thickness  $\approx 50 \text{ nm}$  were deposited using thermal evaporation. The active area of the device was  $3 \text{ mm}^2$ .

### 2.3 Poly(6-tert-butyl-3-phenyl-3,4-dihydro-2H-1,3-benzoxazine)

Initially, studies were focused on optical and photoconductive properties of poly(6-tertiary-butyl-3-phenyl-3,4-dihydro-2H-1,3-benzoxazine), labelled as PBZ, in which aniline was used as primary amine derivative. Aniline is an electron rich group, widely used in photoconducting polymers. The structure of this non-conjugated polymer is shown in Fig. 2.2. Also, tertiary butyl phenol was used, instead of phenol. Presence of this group avoids the possibilities of cross-linking of the benzoxazine polymer. This increases the film forming properties of the benzoxazine polymer systems for optical and electrical applications. In addition, tertiary butyl phenol increases the electron donor strength of the polymer back bone.

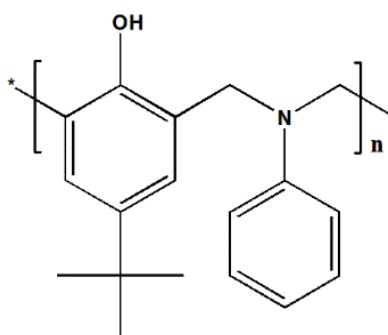


**Fig. 2.2:** Structure of poly(6-tertiary-butyl-3-phenyl-3,4-dihydro-2H-1,3-benzoxazine)

The molecule is soluble in common organic solvents such as chloroform, toluene, dichlorobenzene and chlorobenzene. The polymer has good film forming properties and the films are highly transparent. The number average molecular weight ( $\bar{M}_n$ ) of PBZ is 1012 and weight average

molecular weight ( $\bar{M}_w$ ) of PBZ is 974, obtained by performing Gel Permeation Chromatography (GPC). The calculated value of the polydispersity index ( $\bar{M}_w/\bar{M}_n$ ) is 0.96.

### 2.3.1 Electrochemical properties

Electrochemical properties of PBZ were investigated using cyclic voltammetry (CV). CV was performed at 25 °C in a solution of tetrabutylammonium hexafluorophosphate ( $\text{Bu}_4\text{NPF}_6$ ) (0.1 M) in dry acetonitrile at 100 mV/s under nitrogen atmosphere. The experimental set up includes a three electrode configuration with Ag/AgCl reference electrode, a platinum working electrode ( $0.08 \text{ cm}^2$ ) coated with the thin polymer film and a platinum wire as counter electrode. The highest occupied molecular orbital (HOMO) and lowest unoccupied molecular orbital (LUMO) energy levels of the PBZ polymer can be estimated from the onset of oxidation ( $E_{\text{onset}}^{\text{ox}}$ ) and reduction ( $E_{\text{onset}}^{\text{red}}$ ) potentials. From the value of  $E_{\text{onset}}^{\text{ox}}$  and  $E_{\text{onset}}^{\text{red}}$ , the HOMO and LUMO as well as the electrochemical band gap ( $E_g$ ) of the polymer were calculated by the following equation [18].

$$\text{HOMO} = - (E_{\text{onset}}^{\text{ox}} + 4.71) \text{ eV} \quad (1)$$

$$\text{LUMO} = - (E_{\text{onset}}^{\text{red}} + 4.71) \text{ eV} \quad (2)$$

$$E_g = (E_{\text{onset}}^{\text{ox}} - E_{\text{onset}}^{\text{red}}) \text{ eV} \quad (3)$$

HOMO and LUMO levels of the polymer obtained from the electrochemical measurement were -6.27 eV and -3.87 eV respectively. Therefore, band gap of the polymer is calculated to be 2.40 eV which was

much lower than the band gap of poly(vinylcarbazole) ( $E_g = 4.10 \text{ eV}$ ), a well-known photoconductor [19].

The band gap values estimated from CV should be interpreted to have many interfering factors, such as those arising from physical and surface status of electrodes. The redox potentials could be different in different media and critically depend on the quality of electrode surface, pre-adsorbed gases, and status of electrolyte. While the optical band gap refers to the energy required to form a bound electron hole pair by exciting an electron from the HOMO level to LUMO level. So there is always the chances for a difference between the electrochemical band gap and optical band gap.

## **2.3.2 Optical properties of PBZ**

### **2.3.2.1 Absorption spectra and fluorescence spectra**

The UV-vis absorption spectra of PBZ in solution and films prepared on ITO coated glass substrates were taken using JASCO V 570 UV-vis spectrophotometer. Fig. 2.3 shows the absorption spectra of PBZ. The PBZ films showed an absorption in the higher frequencies of the visible region. Absorption onset of the polymer thin film was found at 475 nm and the corresponding optical band gap is  $2.61 \text{ eV}$ . The longer wavelength absorption is attributed to intermolecular charge transfer (ICT) band [20,21]. The polymer chains have electron rich t-butyl substituted phenol rings. So the formation of the charge transfer complex (CT) was possible.

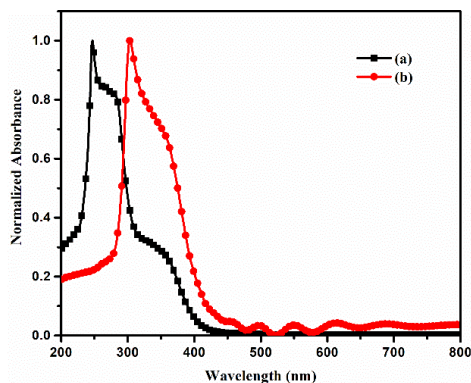


**Fig. 2.3:** Absorption spectra of PBZ (a) dissolved in chloroform and (b) PBZ thin films on ITO coated glass plates.

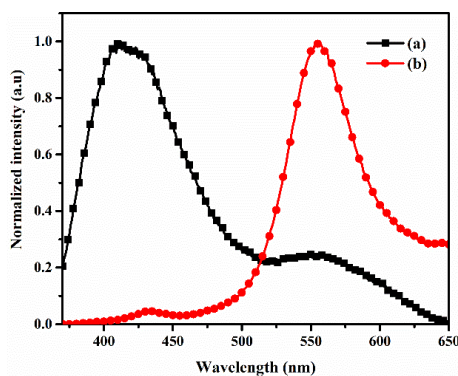


**Fig. 2.4:** Fluorescence spectra of (a) PBZ dissolved in chloroform and (b) PBZ thin film prepared on ITO coated glass plates

The PBZ molecule exhibited fluorescence emission when excited with photons of energy greater than the optical band gap. The fluorescence spectrum of the polymer was recorded using Horiba Fluoromax-3 spectrometer. The sample was excited with photons of wavelength 360 nm. The fluorescence spectrum of PBZ dissolved in chloroform and PBZ films prepared on ITO coated glass substrates are shown in Fig. 2.4. In both the cases, emission shows two distinct peaks, 420 nm and 555 nm. In solution,

the PL spectrum has a prominence around 420 nm, while the emission from the thin film exhibited a prominent peak at 555 nm.

### 2.3.3 Temperature dependence of electrical conductivity

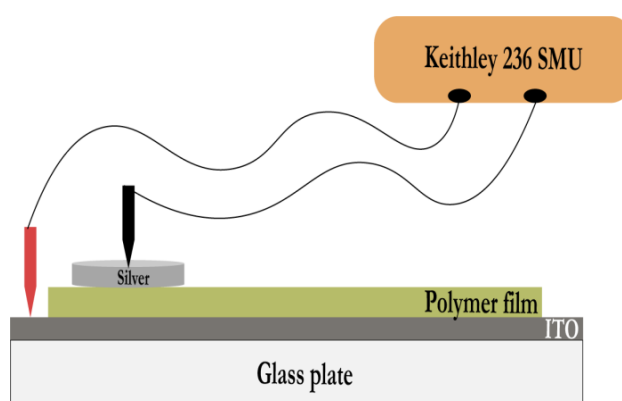


Fig. 2.5: Sandwich cell structure

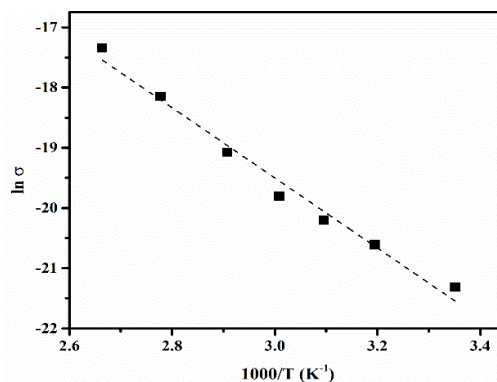


Fig. 2.6: Temperature dependence of dark conductivity of PBZ. Dotted lines are linear fit to the data.

Dark conductivity of the PBZ was measured by preparing sandwich cells (Fig. 2.5). Electrical conductivity was measured for various temperatures above the room temperature at a biasing electric field of  $5 \text{ V}/\mu\text{m}$ .

Dark current through the film was measured using Keithley 236 Source Measure Unit. The Arrhenius plot showing the variation in electrical conductivity with temperature of PBZ is shown in Fig. 2.6. The activation energy is calculated by assuming that the variation in electrical conductivity with temperature follows the relation  $\sigma = \sigma_0 e^{-E_a/kT}$ , where  $\sigma$  is the electrical conductivity,  $\sigma_0$  is the proportionality factor,  $E_a$  is the activation energy,  $k$  is the Boltzmann constant and  $T$  is the absolute temperature. The activation energy of the polymer above room temperature is 50 meV.

### **2.3.4 Steady state photocurrent measurement in PBZ film**

Photoconductivity measurements were done in the pristine PBZ films. Steady state photocurrent measurement involves the measurement of the DC current through the sample, with and without illumination on the sample. For this, dark current was measured as a function of the electric field. Also, current was measured after illuminating the sample through the ITO side. This is called, illuminated current. The difference between the illuminated current and dark current gives the photocurrent. In this case, the sample was illuminated using 488 nm laser beam. None of the samples exhibited photoconductivity in the pristine form.

### **2.3.5 PCBM as an acceptor**

Fig. 2.4 revealed the intense fluorescence emission from the PBZ film. This could be due to the recombination of excitons [22]. Also, the pristine films did not exhibit photoconductivity. This could be due to the inefficient exciton dissociation in the PBZ films. To obtain photoconductivity, the charge separation in the polymer film should be increased to a sufficient regime. This can be done by introducing a suitable acceptor

molecule along with the conducting polymer. Here, phenyl- $C_{61}$ -butyric-acid methyl ester (PCBM) is selected as the acceptor molecule, which is a derivative of  $C_{60}$ . One of the main advantages of PCBM is, its solubility. Due to the spherical symmetry, the molecule can make a good contact with surrounding molecules almost independent of the orientation of the fullerene. On the other hand, this structural symmetry forbids low energy transitions, which results in inadequate absorption in the higher wavelength region of the visible spectrum [23]. PCBM exhibits large electron affinities and high electron mobilities [24].

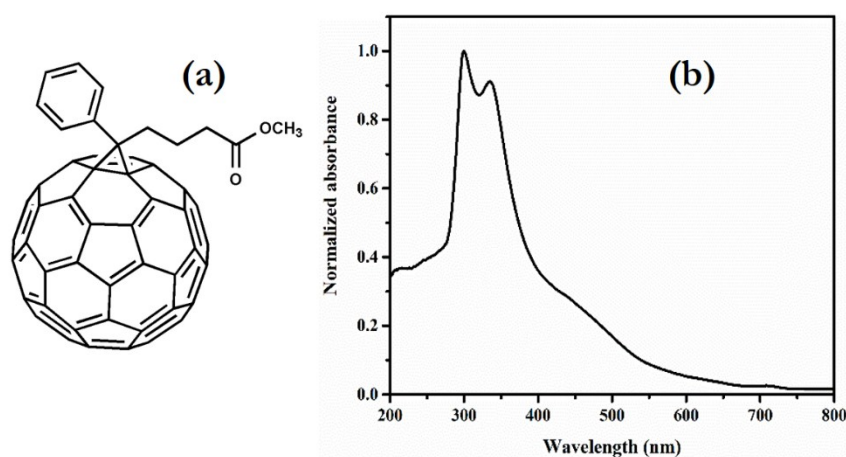


**Fig. 2.7:** (a) Structure of PCBM and (b) absorption spectrum of PCBM thin film which was spin coated over the ITO coated glass substrate.

In literature, the LUMO level of PCBM was reported to have values in between  $-3.7 eV$  to  $-4.3 eV$ , and the widely accepted value is  $-4.3 eV$  [25,26]. The absorption spectra of PCBM thin film spin coated over the ITO coated glass plate is shown in Fig. 2.7. The absorption is much less in the higher wavelength region.

### 2.3.6 Optical properties of PBZ:PCBM blend

The optical properties of the PBZ:PCBM blend was studied in thin film form. Fig. 2.8 shows the absorption spectra of PBZ:PCBM blend films for PBZ to PCBM weight ratios of 1:0.5 and 1:1. The films of PBZ:PCBM blend exhibited an enhanced absorption in the higher frequencies of visible region compared to that of pristine film. There was no additional features observed in the absorption of the blend films compared to absorption of the pristine film, which suggests that there is no ground state interaction between PBZ and PCBM. This was confirmed by measuring electrical conductivity in pristine and blend films. The absorption spectrum of the films of PBZ: PCBM could be considered as a superposition of the optical absorption spectra of PBZ and PCBM.

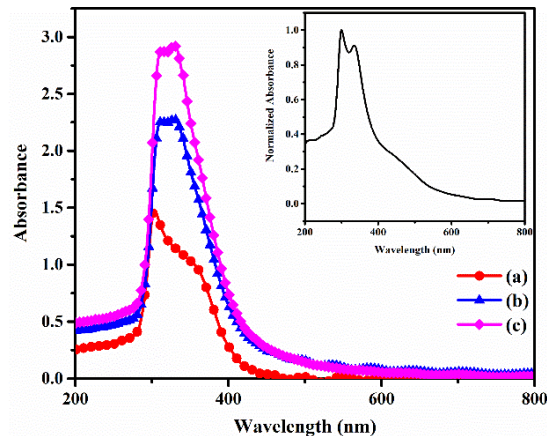


**Fig. 2.8:** Absorption spectra of PBZ:PCBM blend for a ratio of (a) 1:0, (b) 1:0.5 and (c) 1:1. Figure inset present the absorption spectrum of PCBM thin film.

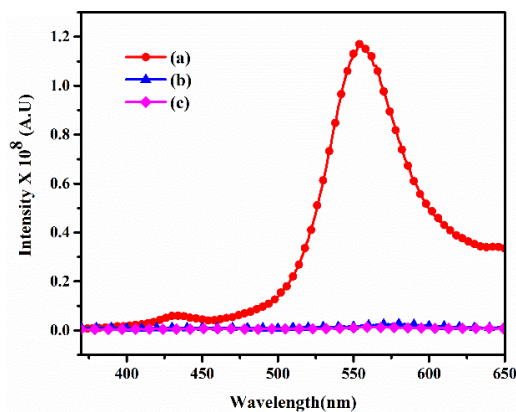


**Fig. 2.9:** Fluorescence spectra of PBZ:PCBM blend films for a ratio of (a) 1:0, (b) 1:0.5 and (c) 1:1.

The emission from the molecule was quenched in the presence of sensitizer molecule. The quenching of fluorescence intensity when PBZ was doped with PCBM at different ratios, is shown in Fig. 2.9. The quenching of the fluorescence emission from these blend films could be either due to an energy transfer reaction or due to a charge transfer reaction. The strength of the energy transfer reaction depends on the Forster radius, which is determined by the relative overlap between the absorption band of the acceptor molecule and emission band of the polymer film [27]. Here, there was negligible overlap between the absorption of PCBM and emission spectrum of PBZ and thereby ruled out the possibility of energy transfer reaction. So the reason for quenching is entirely assigned to a charge transfer reaction between polymer and PCBM. In this case, the bound exciton gets dissociated at the polymer:PCBM interface and electron is transferred to PCBM and thus resulted in quenching. This can be confirmed by observing photoconductivity in the blend films.

## 2.3.7 Steady state photocurrent measurements

### 2.3.7.1 Photocurrent action spectra

The photocurrent action spectra is measured to understand spectral dependence of the steady state photocurrent generated in the blend films. For this, measurements were carried out by illuminating the sample with different wavelengths and measured the current for each wavelength. A 150 W Xenon lamp was used as excitation source. The excitations have 30 nm band width. The sample was illuminated for a fixed interval of time to achieve a steady state. The intensity of exciting wavelengths was measured initially using a power meter (Coherent) and is shown in Fig. 2.10. Normalization of the collected data was done by dividing the obtained photocurrent with the intensity of excitations measured under similar conditions.

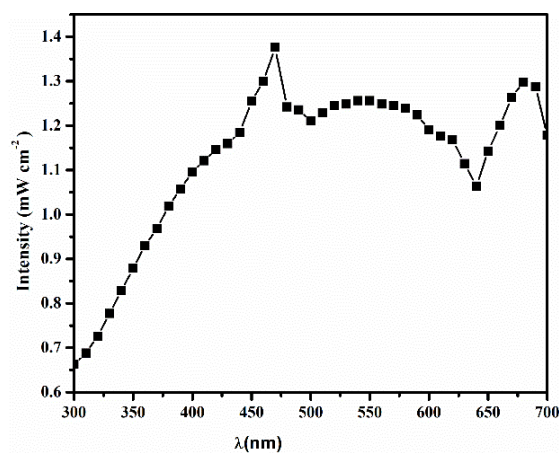
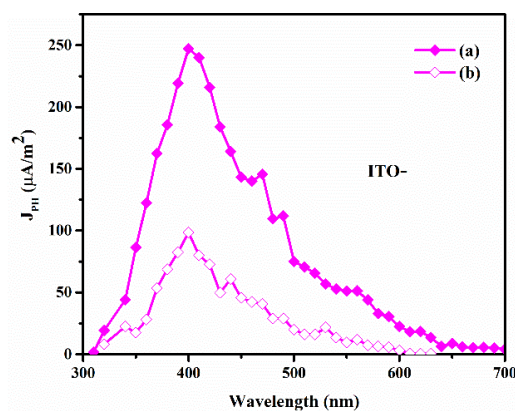


Fig. 2.10 Intensity distribution of Xenon lamp

The photocurrent action spectrum was measured for two different biasing electric fields of 10 V/ $\mu\text{m}$  and 20 V/ $\mu\text{m}$ . Also the action spectrum

was measured for two different polarities of ITO+ and ITO-, and is depicted in Fig. 2.11, Fig. 2.12, Fig. 2.13 and Fig. 2.14.



**Fig. 2.11** Action spectra of PBZ: PCBM blend films for a weight ratio of 1:1 by applying an electric field of (a)  $10 V/\mu m$  and (b)  $20 V/\mu m$ , by maintaining ITO electrode at negative polarity.

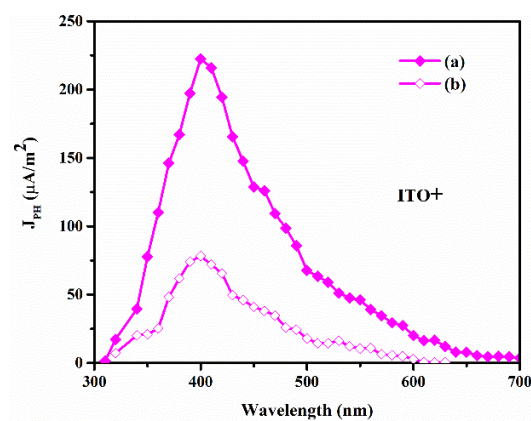


**Fig. 2.12** Action spectra of PBZ: PCBM blend films for a weight ratio of 1:1 by applying an electric field of (a)  $10 V/\mu m$  and (b)  $20 V/\mu m$ , by maintaining ITO electrode at positive polarity.

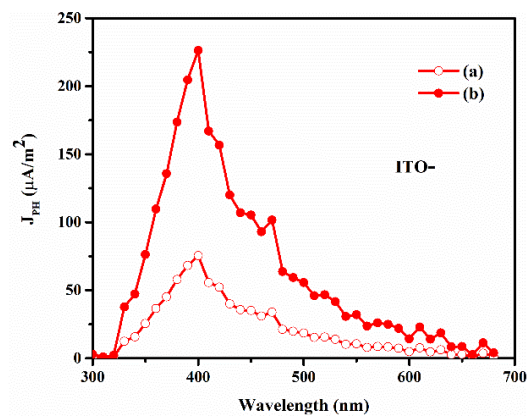


**Fig. 2.13** Action spectra of PBZ:PCBM blend films for a weight ratio of 1:0.5 by applying an electric field of (a)  $10 \text{ V}/\mu\text{m}$  and (b)  $20 \text{ V}/\mu\text{m}$ , by maintaining ITO electrode at negative polarity.

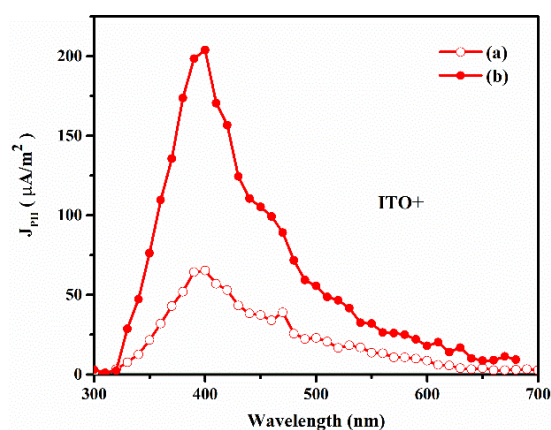


**Fig. 2.14** Action spectra of PBZ:PCBM blend films for a weight ratio of 1:0.5 by applying an electric field of (a)  $10 \text{ V}/\mu\text{m}$  and (b)  $20 \text{ V}/\mu\text{m}$ , by maintaining ITO electrode at positive polarity.

The blend films exhibited a good photoresponse in the entire visible region. The maximum photoresponse was obtained around 400 nm. Photocurrent was slightly higher, when ITO electrode was negatively biased. The probable explanation of this could be done by considering the

absorption spectrum. The absorption coefficient of the blend films were significantly high compared to pristine films. So, during illumination, the exciton formation is not uniform throughout the film. The excitons are more near to ITO and much less near to silver electrode. The hole injection effect from ITO and silver remained the same. So the number of dissociated excitons near ITO in the ITO+ case was smaller than the number of dissociated excitons near silver electrode. This was reflected in the photocurrent action spectrum.

The photoconductivity studies of PBZ polymer blended with sensitizer TNP (2,4,6-trinitrophenol) was already reported previously [16]. The photocurrent was significantly improved (by two orders) when the polymer was blended with PCBM. Since polymers have a low dielectric constant, the photogeneration efficiency for carrier generation strongly depends on the applied field. This could be clearly seen in the action spectrum of the blended film taken for two different electric fields. Also, more photocurrent was obtained for the films with blend ratio 1:1. This is because, higher concentration of PCBM molecules substantially increases the exciton encounter at the acceptor interface and cause more charge separation.

### 2.3.7.2 Intensity dependence of photocurrent

The dependence of photocurrent on intensity of illumination was studied using a laser beam of 488 nm at a biasing field of  $10 \text{ V}/\mu\text{m}$  and is shown in Fig. 2.15. For the measurements ITO was kept at negative polarity. The intensity of the laser beam was varied using a polarizer. The variation of photocurrent with the intensity of the incident beam followed a power law dependence of the form  $J_{PH} \propto I^\beta$ , where  $I$  is the incident

intensity and  $\beta$  is the power index. Here the value of  $\beta$  are 0.45 and 0.51 respectively for films with polymer to PCBM ratios of 1:0.5 and 1:1. Hence  $J_{PH} \propto \sqrt{I}$ . This sub linear intensity dependence on photocurrent suggests the existence of bimolecular recombination in the PBZ:PCBM blend films [28,29]. Presence of this bimolecular recombination limits the generation of photocurrent in the PBZ:PCBM.

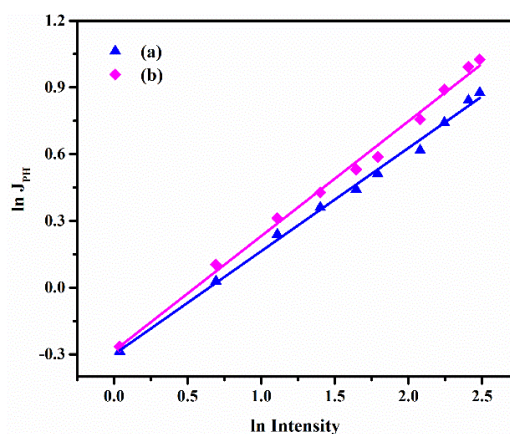
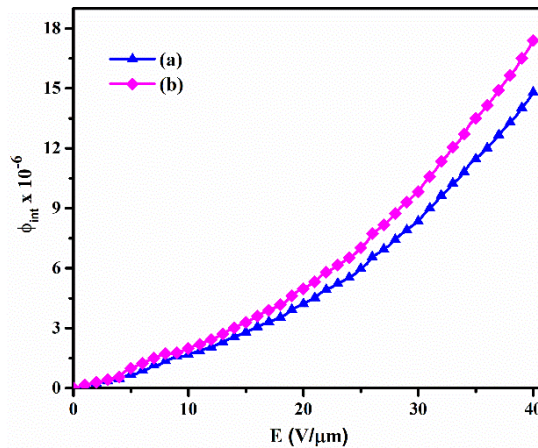


Fig. 2.15: Dependence of photocurrent on the intensity of illumination of PBZ:PCBM blend films for a weight ratio of (a) 1:0.5 and (b) 1:1. The solid lines present the linear fit to the data.

### 2.3.7.3 Internal photocurrent efficiency and photoconductive sensitivity

Internal photocurrent efficiency ( $\phi$ ) and photoconductive sensitivity ( $\sigma_{ph}/I$ ) of PBZ:PCBM blend films were calculated from the measured photocurrent using the formula as discussed in section 1.5.6 of Chapter 1. For this, photocurrent was measured in blend films with PBZ to PCBM weight ratios of 1:0.5 and 1:1, as a function of electric field, by keeping ITO at negative polarity. Laser beam of 488 nm with intensity  $125 \text{ mW/cm}^2$  was used to illuminate the sample. It was observed that the PBZ :

PCBM blend films could withstand an electric field upto  $40 \text{ V}/\mu\text{m}$ . Internal photocurrent efficiency and photoconductive sensitivity were calculated from the measured photocurrent. The results are plotted as a function of the electric field and is shown in Fig. 2.16 and Fig. 2.17.



**Fig. 2.16:** Electric field dependence of internal photocurrent efficiency of PBZ:PCBM blend films for a weight ratio of (a) 1:0.5 and (b) 1:1, by irradiating with laser beam of wavelength of 488 nm.

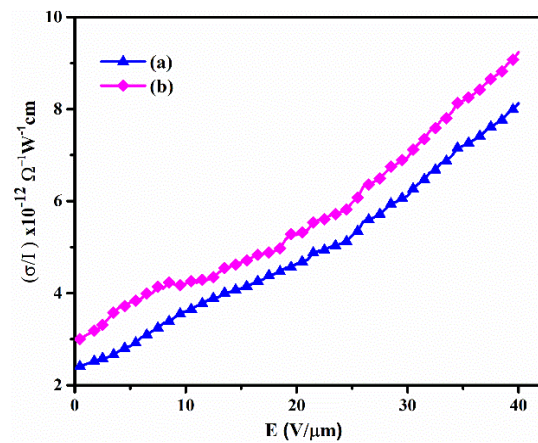


**Fig. 2.17:** Dependence of photoconductive sensitivity on electric field of PBZ:PCBM blend films for a weight ratio of (a) 1:0.5 and (b) 1:1, by irradiating with laser beam of wavelength of 488 nm.

It was observed that, in both the blend films, at low electric fields, the photocurrent and the photogeneration efficiency exhibited a linear power law dependence with the electric field and at higher electric fields it was super-linear ( $E^{1.9}$ ). This strong dependence of photogeneration on the electric field suggests the relevance of Onsager's theory of geminate ion pair dissociation [30,31]. The calculated values of the photoconductive sensitivity are of the order of  $10^{-12}$  and photogeneration efficiency was of the order of  $10^{-5}$  at  $40 \text{ V}/\mu\text{m}$  and the results are summarized in Table 2.1.

**Table 2.1:** Internal photocurrent efficiency and photoconductive sensitivity of the PBZ:PCBM blend films for the weight ratios of 1:0.5 and 1:1 at the biasing electric field of  $40 \text{ V}/\mu\text{m}$ . Sample was illuminated with 488 nm laser beam at a fixed intensity of  $125 \text{ mW}/\text{cm}^2$ .

PBZ:PCBM	$\phi$	$\frac{\sigma_{PH}}{I}$ ( $\text{SWcm}^{-1}$ )
1:0.5	$1.4 \times 10^{-5}$	$6.15 \times 10^{-12}$
1:1	$1.74 \times 10^{-5}$	$8.14 \times 10^{-12}$

These values are comparable with the results obtained from previous reports [32,33]. PBZ:PCBM composite therefore can be a good photoconducting host matrix for photorefractive applications.

## 2.4 Poly([4-(6-tert-butyl-4H-benzo[e][1,3]oxazin-3-yl)phenyl]-phenyldiazene)

Poly([4-(6-tert-butyl-4H-benzo[e][1,3]oxazin-3-yl)phenyl]-phenyldiazene), labelled as "AZO-PBZ" is a p-aminoazobenzene based non-conjugated benzoxazine polymer. Here, p-aminoazobenzene is used as primary amine derivative. The structure of the polymer is shown in Fig. 2.18. The large value

of photoinduced birefringence, photoinduced isomerization, nonlinear absorption and molecular re-orientation, makes azo polymeric systems important candidates for optical storage and processing applications [34]. The synthesis and characterization of benzoxazines, prepared by incorporating azobenzene chromophoric groups into benzoxazines was reported earlier [35]. The p-aminoazobenzene exhibits high electron delocalization, which can enhance the photoconductive properties of the benzoxazine polymer system. The synthesis route and structural characterizations of p-aminoazobenzene based benzoxazine polymer is detailed in reference 17.

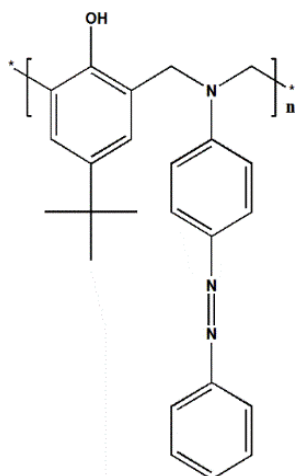


**Fig. 2.18:** Structure of poly([4-(6-tert-butyl-4H-benzo[e][1,3]oxazin-3-yl)phenyl]-phenyldiazene)

AZO-PBZ is soluble in common organic solvents such as chloroform, toluene, dichlorobenzene and chlorobenzene. The polymer has good film forming properties and the films are highly transparent. The number average molecular weight ( $\bar{M}_n$ ) of PBZ is 1716 and weight average molecular weight ( $\bar{M}_w$ ) of PBZ is 3124, which are determined by GPC (gel permeation chromatography). The calculated value of the polydispersity index ( $\bar{M}_w/\bar{M}_n$ ) is 1.82.

### **2.4.1 Electrochemical properties**

In order to understand the HOMO and LUMO energy levels of AZO-PBZ, cyclic voltammetry experiment was performed as discussed in section 2.3.1. The onset of oxidation of AZO-PBZ was found to occur at 0.88 V corresponding to ionization potential value of -5.58 eV. HOMO and LUMO levels of the polymer obtained from the electrochemical measurement were -5.58 eV and -3.56 eV respectively. Therefore, band gap of the polymer was calculated to be 2.02 eV. The incorporation of azo group resulted in a slight increase of HOMO level, which might be due to the contribution of electron rich units in its structure.

### **2.4.2 Optical properties of AZO-PBZ**

The UV-vis absorption spectra of AZO-PBZ in solution and as thin film, which is prepared on ITO coated glass substrates, are shown in Fig. 2.19. The band below 350 nm correspond to  $\pi - \pi^*$  transition of the aromatic ring present in the structure of the polymer. The polymer backbone has electron rich t-butyl substituted phenyl ring which acts as a donor and p-aminoazobenzene acts as an electron acceptor. The peak at higher wavelength region was attributed to the formation of intramolecular charge transfer complex. The absorption onset of the polymer film was at 555 nm, corresponding to an optical band gap of 2.23 eV so that AZO-PBZ could be loosely defined as a narrow band gap polymer. Absorption spectrum of the polymer film was slightly red shifted as a result of inter-chain interactions in the solid film.

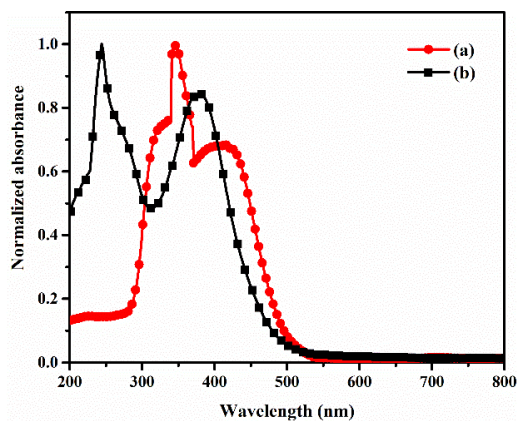


**Fig. 2.19:** Absorption spectra of (a) AZO-PBZ thin films on ITO coated glass plates and (b) AZO-PBZ dissolved in chloroform.

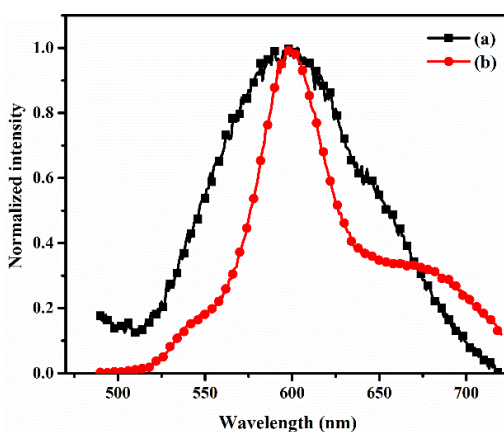


**Fig. 2.20:** Fluorescence spectra of (a) AZO-PBZ dissolved in chloroform and (b) AZO-PBZ thin films prepared on ITO coated glass substrate.

The fluorescence spectrum of the AZO-PBZ was studied, by exciting with photons of wavelength 380 nm, in solution and as film. The fluorescence spectra of AZO-PBZ dissolved in chloroform and as thin film prepared on ITO coated glass substrates are shown in Fig. 2.20. The

emission maximum occurs at 597 nm. Emission spectrum of AZO-PBZ in solution is much broadened than the emission from AZO-PBZ thin film.

### 2.4.3 Temperature dependence of electrical conductivity

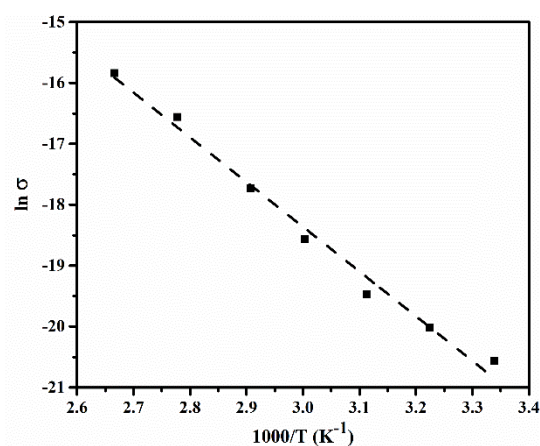


**Fig. 2.21:** Temperature dependence of dark conductivity of AZO-PBZ. Dotted lines are linear fit to the data.

Spin coating of 10 wt% solution of AZO-PBZ in chloroform can produce neat films of 1  $\mu\text{m}$  thickness. Dark conductivity of the AZO-PBZ film was measured by preparing sandwich cells. Variation of dark conductivity with temperature was studied as discussed in section 2.3.3. Fig. 2.21 presents  $\ln \sigma$  vs  $1/T$  plot of AZO-PBZ, which gave a linear fit. The measurements were carried out for a biasing electric field of 5 V/ $\mu\text{m}$ . The activation energy was calculated from the slope of the curve. Thus, activation energy of AZO-PBZ was calculated to be 56 meV.

#### **2.4.4 Steady state photocurrent measurement in AZO-PBZ film**

Photoconductivity measurements were done in the pristine AZO-PBZ films as mentioned in section 2.3.4. For this, the sample was illuminated using 488 nm laser beam. None of the sample exhibited photoconductivity in the pristine form.

#### **2.4.5 Optical properties of AZO-PBZ:PCBM blend**

To obtain charge transfer properties in AZO-PBZ films, AZO-PBZ:PCBM blend films were prepared with polymer to PCBM ratios of 1:0.5 and 1:1. The absorption spectra of the blend films along with the absorption of pristine AZO-PBZ films is shown in Fig. 2.22. Incorporation of sensitizer PCBM with AZO-PBZ resulted in a significant enhancement in the absorption coefficient of the blend film. The optical absorption spectrum of the AZO-PBZ: PCBM blend films could be considered as the simple superposition of the absorption spectra of these two components. There is no indication of the substantial interaction between the polymer and sensitizer in its ground state. This can be confirmed by measuring the dark electrical conductivity of the pristine and blend films. Both the samples possessed the same value of electrical conductivity which confirmed this statement. Thus, the AZO-PBZ:PCBM blend films form a neutral electron donor-acceptor complex in which the overlapping of the electronic wave function in the ground state is negligible.

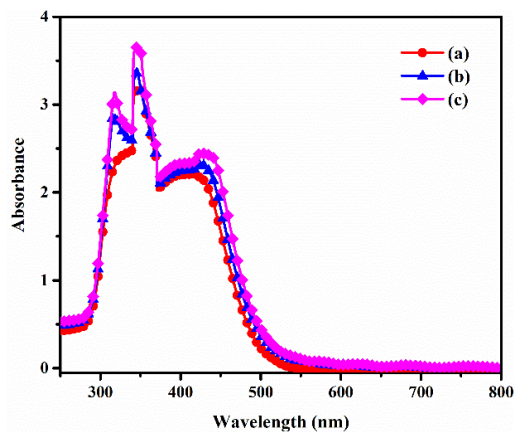


**Fig. 2.22:** Absorption spectra of AZO-PBZ:PCBM blend films for a ratio of (a) 1:0, (b) 1:0.5 and (c) 1:1.

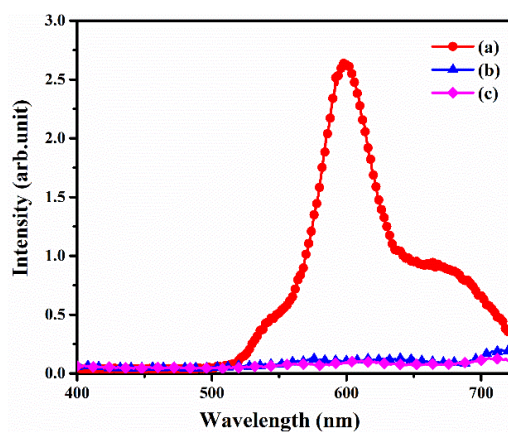


**Fig. 2.23:** Fluorescence spectra of AZO-PBZ:PCBM blend films for a weight ratio of (a) 1:0 (b) 1:0.5 and (c) 1:1.

Incorporation of PCBM molecules leads to a drastic quenching of the fluorescent intensity of the blend films. The absorption onset of PCBM in solid state is at 425 nm. There is no significant overlap between the emission band of AZO-PBZ and absorption band of PCBM which ruled out the possibility of energy transfer process leading to the quenching of the

fluorescence intensity. AZO-PBZ:PCBM blend films exhibited enhanced conductivity during irradiation. So the quenching of the fluorescence intensity can be attributed to the photoinduced intermolecular charge transfer of electrons from AZO-PBZ to the sensitizer, PCBM.

## 2.4.6 Steady state photocurrent measurements

### 2.4.6.1 Photocurrent action spectrum

The spectral dependence of the steady state photocurrent was measured as explained in the previous section. AZO-PBZ sandwich cell was found to be a poor conductor of electricity in its intrinsic state and the observed dark current was much low. The incorporation of PCBM molecules resulted in a considerable increase in the optical absorption which lead to a considerable change in the photocurrent through the sample.

The photocurrent action spectrum was measured for the blend films in which AZO-PBZ to PCBM ratio was 1:0.5 and 1:1, by irradiating with photons of wavelength from 300 nm (4.14 eV) to 700 nm (1.77 eV) at an applied electric field of 10V/ $\mu\text{m}$ . The action spectrum measured for both the positive and negative polarities of ITO, is shown in Fig. 2.23, Fig. 2.24, Fig. 2.25 and Fig. 2.26. When the ITO electrode was negatively biased, the AZO-PBZ:PCBM films exhibited an enhanced photocurrent over the entire spectral range. Slightly higher photocurrent was observed for blend films with a polymer to PCBM ratio of 1:1 compared to the blend films of polymer to PCBM ratio of 1:0.5.

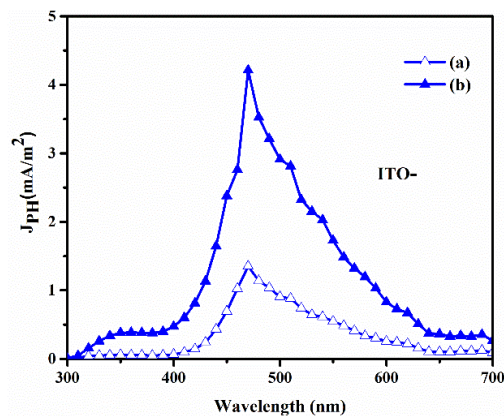


**Fig. 2.24:** Action spectra of AZO-PBZ:PCBM blend films for a weight ratio of 1:0.5 by applying an electric field of (a) 10 V/ $\mu$ m and (b) 20 V/ $\mu$ m, by maintaining ITO electrode at negative polarity.

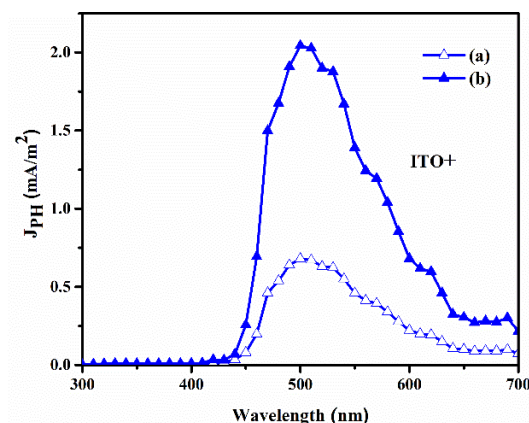


**Fig. 2.25:** Action spectra of AZO-PBZ:PCBM blend films for a weight ratio of 1:0.5 by applying an electric field of (a) 10 V/ $\mu$ m and (b) 20 V/ $\mu$ m, by maintaining ITO electrode at positive polarity.

The onset of action spectrum is at 1.90 eV (653 nm). Photocurrent increases with photon energy and a maximum photoresponse was obtained for 2.66 eV (470 nm). For photons with energy greater than 2.66 eV, photocurrent

was found to be decreasing. The photocurrent gradually decreased for energy greater than 3 eV (414 nm). The maximum spectral response was obtained at the onset of the optical absorption of the pristine AZO-PBZ film. The blend films exhibited an increase in photocurrent at 430 nm, which corresponded to the onset absorption of PCBM thin film

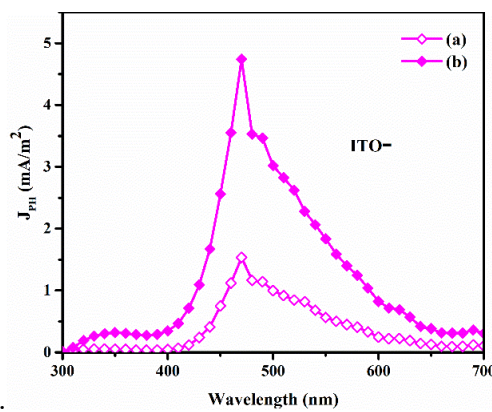


**Fig. 2.26:** Action spectra of AZO-PBZ:PCBM blend films for a weight ratio of 1 : 1 by applying an electric field of (a) 10 V/ $\mu$ m and (b) 20 V/ $\mu$ m, by maintaining ITO electrode at negative polarity.

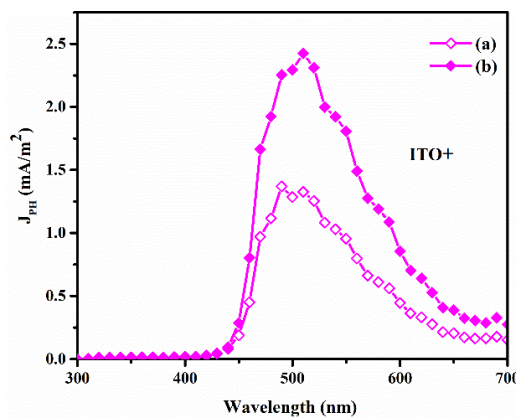


**Fig. 2.27:** Action spectra of AZO-PBZ:PCBM blend films for a weight ratio of 1 : 1 by applying an electric field of (a) 10 V/ $\mu$ m and (b) 20 V/ $\mu$ m, by maintaining ITO electrode at positive polarity.

### 2.4.6.2 Intensity dependence of photocurrent

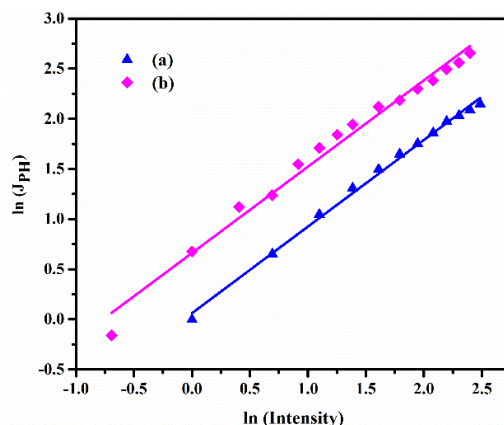


**Fig. 2.28:** Intensity dependence of photocurrent of AZO-PBZ:PCBM blend films with polymer to PCBM ratio of (a) 1:0.5 and (b) 1:1 by irradiating with laser beam of wavelength 488 nm at an applied electric field of 10 V/ $\mu$ m

The dependence of photocurrent on intensity of illumination was studied using a laser beam of wavelength 488 nm by applying an electric field of 10 V/ $\mu$ m. Fig. 2.28 shows the variation of photocurrent with the variations in intensity of illumination. The power law dependence of the photocurrent on the intensity of the incident light beam was found to be slightly sub linear;  $J_{PH} \propto I^{0.87}$ , in both the polymer films with polymer to PCBM ratio of 1:0.5 and 1: 1. This sub linear intensity dependence is the general behavior of most of the amorphous semiconducting materials [36,37].

### 2.4.6.3 Internal photocurrent efficiency and photoconductive sensitivity

The photogeneration efficiency and photoconductive sensitivity of the PCBM blend films were calculated as a function of the electric field by measuring the photocurrent through the sample. The photocurrent measurements were carried out on PCBM blend thin films by varying the

electric field through the samples at an illumination intensity of  $125 \text{ mWcm}^{-2}$ . The samples could withstand electric fields up to  $30 \text{ V}/\mu\text{m}$  and beyond this the samples underwent dielectric breakdown. Photoconductive sensitivity and photogeneration efficiency were calculated and was plotted as a function of the electric field (Fig. 2.29 and Fig. 2.30) and the results are summarised in Table 2.2. It was observed that, at low electric fields, the photocurrent and the photogeneration efficiency exhibited a linear power law dependence with the electric field and at higher electric fields it is super linear ( $E^{1.7}$ ). This strong dependence of photogeneration on the electric field again suggests the relevance of Onsager's theory of geminate ion pair dissociation. The calculated values of the photoconductive sensitivity are of the order of  $10^{-11}$  and photogeneration efficiency is of the order of  $10^{-5}$ .

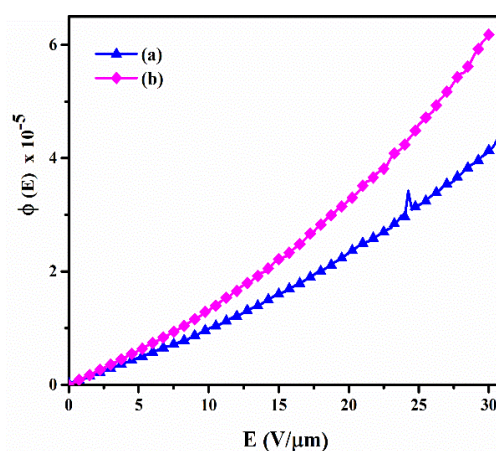


**Fig. 2.29:** Electric field dependence of photogeneration efficiency of AZO-PBZ:PCBM blend films with polymer to PCBM ratio of (a) 1:0.5 and (b) 1:1 by irradiating with laser beam of wavelength 488 nm with intensity of  $125 \text{ mW}/\text{cm}^2$

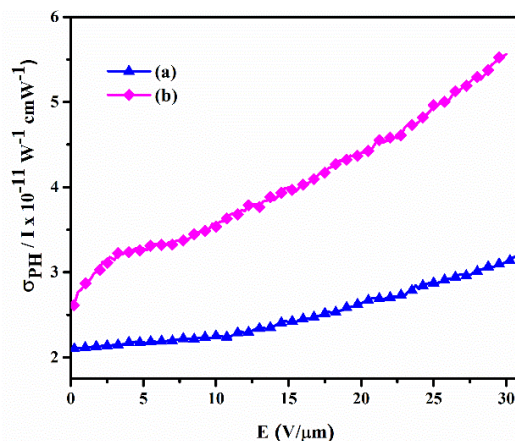


**Fig. 2.30:** Electric field dependence of photoconductive sensitivity of AZO-PBZ:PCBM blend films with polymer to PCBM ratio of (a) 1:0.5 and (b) of 1:1 by irradiating with laser beam of wavelength 488 nm with intensity of 125 mW/cm<sup>2</sup>

**Table 2.2:** Internal photocurrent efficiency and photoconductive sensitivity of the AZO-PBZ:PCBM blend films for the weight ratios of 1:0.5 and 1:1 at the biasing electric field of 30 V/μm. Samples were illuminated with 488 nm laser beam at a fixed intensity of 125 mW/cm<sup>2</sup>.

AZO-PBZ:PCBM	$\phi$ at 30 V/μm	$\sigma_{PH}/I$ at 30 V/μm (SWcm <sup>-1</sup> )
1:0.5	$4.15 \times 10^{-5}$	$3.13 \times 10^{-11}$
1:1	$6.2 \times 10^{-5}$	$5.57 \times 10^{-11}$

## 2.5 Poly(4-tert-butyl-2-[[ethyl(4-nitrophenyl)amino]methyl]6[[methyl(4-phenylazophenyl)-amino]methyl]phenol)

An attempt was made to study the photoconductive properties of poly(4-tert-butyl-2-[[ethyl(4-nitrophenyl)amino]methyl]6[[methyl(4-phenylazophenyl)-amino]methyl]phenol), labeled as AZO-PNA. It was a polymer of p-amino-azobenzene and p-nitroaniline.

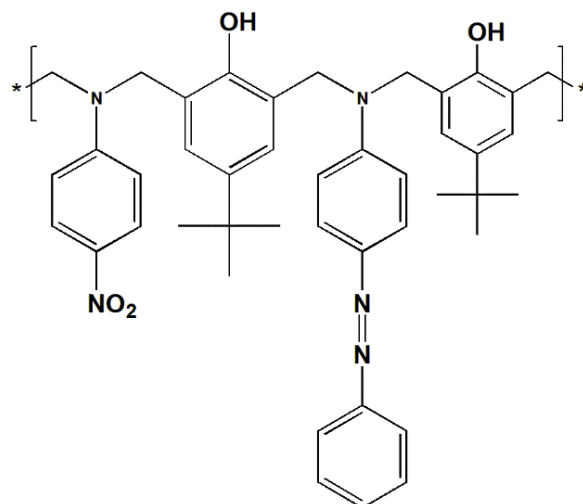


**Fig. 2.31:** Structure of poly(4-tert-Butyl-2-[[ethyl(4-nitrophenyl) amino] methyl]6[[methyl-(4-phenylazo-phenyl)-amino] methyl]phenol)

In this case, p-aminoazobenzene is directly linked to one side of t-butylphenol and p-nitroaniline is attached to other side of the tertiary butyl phenol. The structure of the molecule is shown in Fig. 2.31. p-Nitroaniline is an electron deficient molecule.

The polymer has good film forming properties and the films are highly transparent. The number average molecular weight ( $\bar{M}_n$ ) of AZO-PNA is 951 and weight average molecular weight ( $\bar{M}_w$ ) of PBZ is 1450, which are calculated by GPC (gel permeation chromatography). The calculated value of the polydispersity index ( $\bar{M}_w/\bar{M}_n$ ) is 1.52.

### 2.5.1 Electrochemical properties

Electrochemical properties of AZO-PNA were investigated using cyclic voltammetry. The highest occupied molecular orbital (HOMO) and lowest unoccupied molecular orbital (LUMO) energy levels of the AZO-PNA

polymer was estimated as discussed in section 2.3.1. The onset of oxidation of AZO-PNA was found to occur at 1.41 V and the onset of the reduction potential is -1.01 V. HOMO and LUMO levels of the polymer obtained from the electrochemical measurement were -6.12 eV and -3.69 eV respectively. Therefore, band gap of the polymer is calculated to be 2.43 eV.

## 2.5.2 Optical properties of AZO-PNA

The UV-vis absorption spectra of AZO-PNA in solution and as thin film, which was prepared on ITO coated glass substrates, are shown in Fig. 2.32. The band below 350 nm correspond to  $\pi - \pi^*$  transition of the aromatic ring present in the structure of the polymer. The polymer backbone has electron rich t-butyl substituted phenyl ring which acted as a donor and p-aminoazobenzene acted as an electron acceptor. The peak at higher wavelength region is attributed to the formation of intramolecular charge transfer complex. The absorption edge of the polymer film is at 500 nm, corresponding to an optical band gap of 2.48 eV.

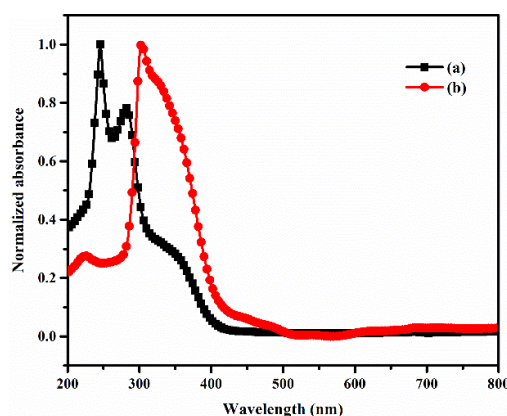


**Fig. 2.32:** Absorption spectra of (a) AZO-PNA dissolved in chloroform and (b) AZO-PNA films on ITO coated glass plates.

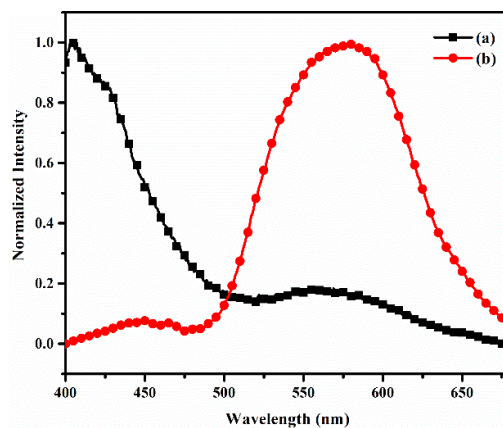


**Fig. 2.33:** Fluorescence emission spectra of (a) AZO-PNA dissolved in chloroform and (b) AZO-PNA thin films prepared on ITO coated glass substrates.

The fluorescence spectrum of the AZO-PNA was studied, by exciting with photons of wavelength 380 nm, in solution and in film. The fluorescence spectra of AZO-PNA dissolved in chloroform and as thin film prepared on ITO coated glass substrates are shown in Fig. 2.32. The emission maximum occurs at 575 nm. Emission spectrum of AZO-PNA in solution is much broadened than the emission from AZO-PNA thin film.

### 2.5.3 Temperature dependence of electrical conductivity

Spin coating of 10 wt% solution of AZO-PNA in chloroform could produce neat films of 1  $\mu\text{m}$  thickness. Dark conductivity of the AZO-PNA film was measured by preparing sandwich cells. Variation of dark conductivity with temperature was studied as discussed in section 2.3.3. Fig. 2.34 shows the Arrhenius plot for the variation of dark conductivity with temperature. The measurements were carried out for a biasing electric field of 5 V/ $\mu\text{m}$ . The activation energy was calculated from the slope of the curve. Thus, activation energy of AZO-PNA was calculated to be 60 meV.

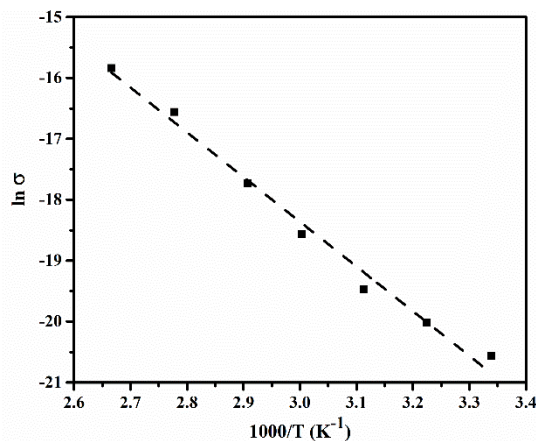


**Fig. 2.34:** Temperature dependence of dark conductivity of AZO-PNA. Dotted lines are linear fit to the data.

#### 2.5.4 Steady state photocurrent measurement in AZO-PNA film

Photoconductivity measurements were done in the pristine AZO-PNA films as mentioned in section 2.3.4. For this, the sample was illuminated using 488 nm laser beam. None of the samples exhibited photoconductivity in the pristine form.

#### 2.5.5 Optical properties of AZO-PNA:PCBM blend

To obtain charge transfer properties in AZO-PNA films, AZO-PNA:PCBM blend films were prepared with polymer to PCBM ratios of 1:0.5 and 1:1. The absorption spectra of the blend films along with the absorption of pristine AZO-PNA films is shown in Fig. 2.35. Incorporation of sensitizer PCBM with AZO-PNA resulted in a significant enhancement in the absorption coefficient of the blend film. The optical absorption spectrum of the AZO-PNA:PCBM blend films could be considered as a superposition of the absorption spectra of these two components. There is no indication of the substantial interaction between the polymer and sensitizer in its ground state.

Thus, the AZO-PNA:PCBM blend films form a neutral electron donor-acceptor complex in which the overlapping of the electronic wave function in the ground state is negligible.

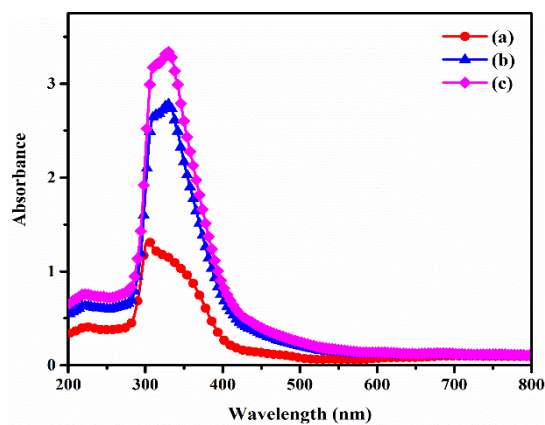


**Fig. 2.35:** Absorption spectra of AZO-PNA:PCBM blend films for a weight ratio of (a) 1:0 (b) 1:0.5 and (c) 1:1. All films were prepared on ITO coated glass substrates.

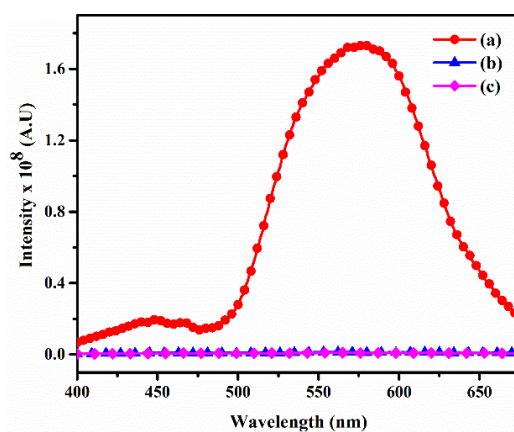


**Fig. 2.36:** Fluorescence emission spectra of AZO-PNA:PCBM films for a weight ratio of (a) 1:0 (b) 1:0.5 and (c) 1:1

Incorporation of PCBM molecules led to a drastic quenching of the fluorescent intensity of the blend films (Fig. 2.36). The absorption onset of PCBM in solid state is at 425 nm. There is no significant overlap between the emission band of AZO-PNA and absorption band of PCBM which ruled out the possibility of energy transfer process leading to the quenching of the fluorescence intensity. As discussed in the two previous cases, this significant fluorescent quenching can be considered as a strong evidence to the efficient charge transfer from the photoexcited AZO-PNA units to the PCBM.

## **2.5.6 Steady state photocurrent measurements**

### **2.5.6.1 Photocurrent action spectrum**

The spectral dependence of the steady state photocurrent was measured as explained in the previous cases. The photocurrent action spectrum was measured for the blend films in which AZO-PNA to PCBM ratio was 1:0.5 and 1:1, by irradiating with photons of wavelength from 300 nm (4.14 eV) to 700 nm (1.77 eV) at an applied electric field of 10 V/ $\mu\text{m}$ . The action spectrum measured for both the positive and negative polarities of ITO, is shown in Fig. 2.37, Fig. 2.38, Fig. 2.39 and Fig. 2.40. When the ITO electrode was negatively biased, the AZO-PNA:PCBM films exhibited an enhanced photocurrent over the entire spectral range. Slightly higher photocurrent was observed for blend films with a ratio of 1:1.

The maximum spectral response was obtained at the onset of the optical absorption of the pristine AZO-PNA film. The blend films exhibited an increase in photocurrent at 400 nm.

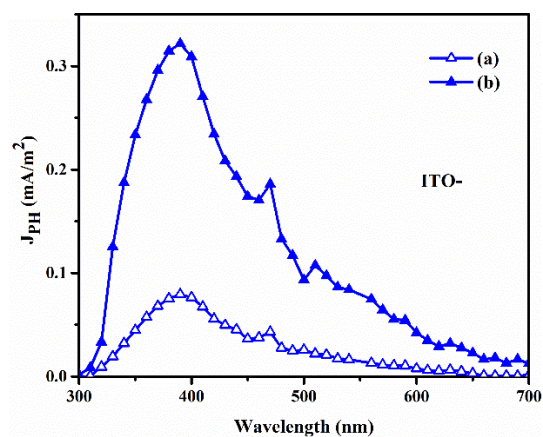


Fig. 2.37: Photocurrent action spectra of AZO-PNA:PCBM blend films for a weight ratio of 1:0.5. The ITO electrode was maintained at negative polarity.

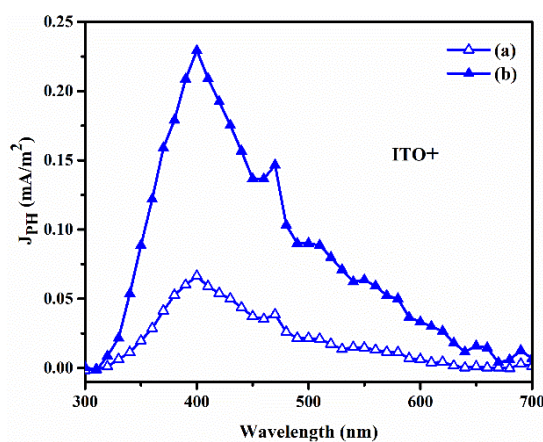
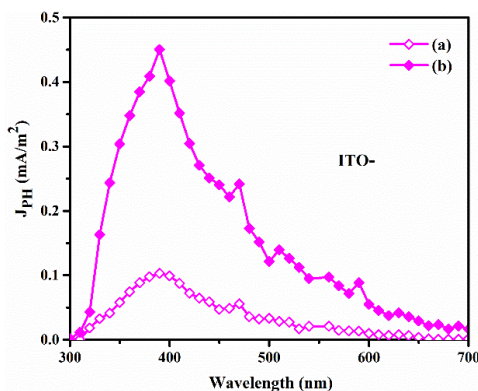
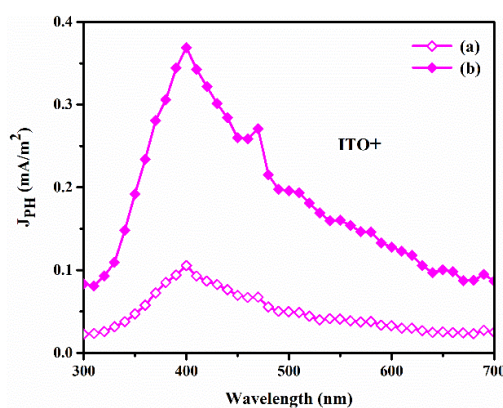


Fig. 2.38: Photocurrent action spectra of AZO-PNA:PCBM blend films for a weight ratio of 1:0.5. The ITO electrode was maintained at positive polarity.



**Fig. 2.37:** Photocurrent action spectra of AZO-PNA:PCBM blend films for a weight ratio of 1:1. The ITO electrode was maintained at negative polarity.



**Fig. 2.38:** Photocurrent action spectra of AZO-PNA:PCBM blend films for a weight ratio of 1:1. The ITO electrode was maintained at positive polarity.

### 2.5.6.2 Intensity dependence of photocurrent

The dependence of photocurrent on intensity of illumination was studied using a laser beam of wavelength 488 nm by applying an electric field of 10 V/ $\mu\text{m}$  (Fig 2.41). A linear power law dependence of photocurrent with intensity of illumination was obtained, i.e.,  $J_{PH} \propto I$ . This revealed the absence of bimolecular recombination in the AZO-PNA:PCBM blend films.

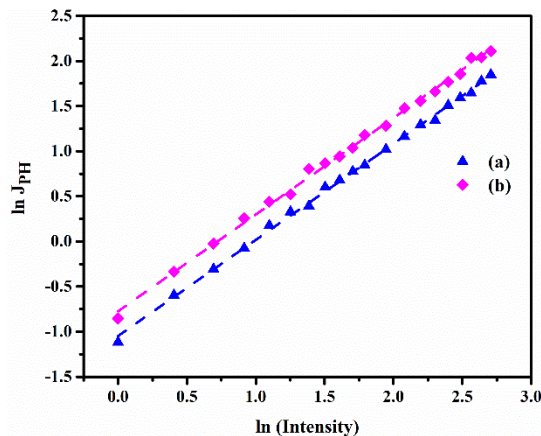


**Fig. 2.41:** Intensity dependence of photocurrent of AZO-PNA:PCBM blend films with polymer to PCBM ratio of (a) 1:0.5 and (b) 1:1 by irradiating with laser beam of wavelength 488 nm at an applied electric field of 10 V/ $\mu\text{m}$

### 2.5.6.3 Internal photocurrent efficiency and photoconductive sensitivity

The photogeneration efficiency and photoconductive sensitivity of the PCBM blend films were calculated as a function of the electric field by measuring the photocurrent through the sample. The photocurrent measurements were carried out on PCBM blend thin films by varying the electric field through the samples at an illumination intensity of 125 mWcm<sup>-2</sup>. The AZO-PNA:PCBM films could withstand electric fields up to 55 V/ $\mu\text{m}$  and beyond this the samples underwent dielectric breakdown. Photoconductive sensitivity and photogeneration efficiency were calculated and is plotted as function of the electric field (Fig. 2.42 and Fig. 2.43). The important results are summarized in Table 2.3. It was observed that, at low electric fields, the photocurrent and the photogeneration efficiency exhibited a linear power law dependence with the electric field

and at higher electric fields it was super linear ( $E^{1.7}$ ). The calculated values of the photoconductive sensitivity are of the order of  $10^{-10}$  and photogeneration efficiency was of the order of  $10^{-4}$ .

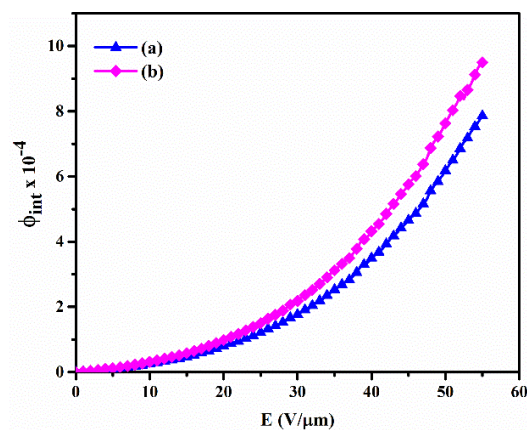


**Fig. 2.42:** Dependence of internal photocurrent efficiency on applied electric field of AZO-PNA:PCBM blend films for a weight ratio of (a) 1:0.5 and (b) 1:1, by illuminating with 488 nm laser wavelength.

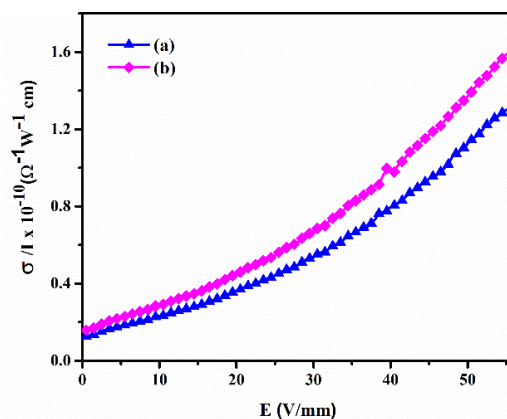


**Fig. 2.43:** Dependence of Photoconductive sensitivity on applied electric field of AZO-PNA:PCBM blend films for a weight ratio of (a) 1:0.5 and (b) 1:1, by illuminating with 488 nm laser wavelength.

**Table 2.3:** Internal photocurrent efficiency and photoconductive sensitivity of the AZO-PNA:PCBM blend films for the weight ratios of 1:0.5 and 1:1 at the biasing electric field of  $55 \text{ V}/\mu\text{m}$ . Sample are illuminated with 488 nm laser beam at a fixed intensity of  $125 \text{ mW}/\text{cm}^2$ .

AZO-PNA:PCBM	$\phi$ at $55 \text{ V}/\mu\text{m}$	$\sigma_{PH}/I$ at $55 \text{ V}/\mu\text{m}$ ( $\text{SWcm}^{-1}$ )
1:0.5	$7.9 \times 10^{-4}$	$1.31 \times 10^{-10}$
1:1	$9.52 \times 10^{-4}$	$1.59 \times 10^{-10}$

## 2.7 The band diagram

On comparing with PBZ, AZO-PNA showed two orders of increment in the internal photocurrent efficiency and photoconductive sensitivity. Several factors can affect the photoconductivity in the blend films. The initial process in photoconductivity is the dissociation of the exciton at the polymer-PCBM interface. For PCBM to act as an acceptor, the LUMO level of the PCBM should be below the LUMO level of the polymers. The LUMO-LUMO difference of the polymer and PCBM determines the efficiency of the exciton dissociation. The energy level band diagram of benzoxazine polymers and PCBM is shown in Fig. 2.44. It is seen that LUMO-LUMO offset is minimum for PBZ:PCBM interface and maximum for PCBM:AZO-PBZ interface. But the performance of the AZO-PNA:PCBM composite is better. On comparing with AZO-PBZ, the HOMO level of AZO-PNA is lower, suggesting that the donor strength of AZO-PNA is high. This higher donor strength may provide the better charge transfer during excitation.

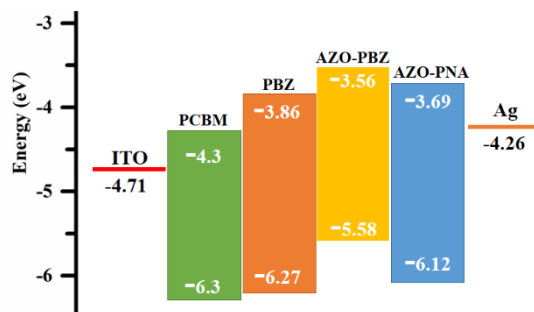


**Fig. 2. 44:** The energy band diagram of benzoxazine polymers along with PCBM. The work functions of ITO and silver electrodes are also presented.

## 2.8 Summary

Detailed photoconductivity studies were carried out on three non-conjugated benzoxazine polymers in conjugation with efficient photosensitizer PCBM. The HOMO and LUMO energy levels were estimated from cyclic voltammetry experiment. The synthesized polymers exhibited absorption in the higher frequencies of the visible spectrum. The polymers also exhibited good fluorescence emission.

The photoconductivity experiments were performed by preparing sandwich cells. The polymers did not exhibit photoconductivity in pristine films. The incorporation of PCBM resulted drastic quenching of the fluorescence. The quenching of fluorescence is considered as the strong evidence of the photoinduced charge transfer reaction. The electron transfer from polymer to PCBM happens in an ultrafast time scale. This time span is much less than the average life of the excited states. The PCBM blended films exhibited good photoresponse in the entire visible region.

Internal photocurrent efficiency and photoconductive sensitivity were determined as a function of the electric field. Both internal photocurrent efficiency and photoconductive sensitivity strongly depended on the external electric field. The estimated values are sufficient to observe photorefractive effect, based on literature reports. AZO-PNA:PCBM blend films exhibited high values of internal photocurrent efficiency and photoconductive sensitivity.

## References

- [1] H.J. Bolink, C. Arts, V. V Krasnikov, G.G. Malliaras, G. Hadziioannou, Novel bifunctional molecule for photorefractive materials, *Chem. Mater.* 9 (1997) 1407–1413.
- [2] J. Maldonado, V. Herrera-ambriz, M. Rodríguez, Reversible holography and optical phase conjugation for image formation / correction using highly efficient organic photorefractive polymers, *Rev. Mex. Trastor. Aliment.* 13 (2015) 537–542.
- [3] R. Xu, Y. Li, J. Tang, Recent advances in flexible organic light-emitting diodes, *J. Mater. Chem. C.* 4 (2016) 9116–9142.
- [4] Y. Su, S. Lan, K. Wei, Organic photovoltaics, *Mater. Today.* 15 (2012) 554–562.
- [5] L. Smilowitz, N.S. Sariciftci, R. Wu, C. Gettinger, A.J. Heeger, F. Wudl, Photoexcitation spectroscopy of conducting-polymer-C60 composites: Photoinduced electron transfer, *Phys. Rev. B.* 47 (1993) 13835–13842.
- [6] A. Abbas, J.J. Pillai, S. Narayanan, K. Sreekumar, R. Joseph, Study on the photoconductive properties of charge carriers in donor- acceptor copolymer P(EDOT-FL) and P(EDOT-FL): PCBM blend, *Synth. Met.* 233 (2017) 52–57.
- [7] S. Narayanan, A. Abbas, S.P. Raghunathan, K. Sreekumar, C.S. Kartha, R. Joseph, Theoretical and experimental investigations on the photoconductivity and nonlinear optical properties of donor–acceptor  $\pi$  conjugated copolymer, poly(2,5-(3,4-ethylenedioxythiophene)-alt-2,7-(9,9-dioctylfluorene)), *RSC Adv.* 5 (2015) 8657–8668.

- 
- [8] J.D. Shakos, A.M. Cox, D.P. West, K.S. West, F.A. Wade, T.A. King, R.D. Blackburn, Processes limiting the rate of response in photorefractive composites, *Opt. Commun.* 150 (1998) 230–234.
- [9] A.C. Arango, S.A. Carter, P.J. Brock, Charge transfer in photovoltaics consisting of interpenetrating networks of conjugated polymer and TiO<sub>2</sub> nanoparticles, *Appl. Phys. Lett.* 74 (1999) 1698–1700.
- [10] O. Ostroverkhova, W.E. Moerner, Organic photorefractives : Mechanisms , materials and applications, *Chem. Rev.* 104 (2004) 3267–3314.
- [11] A. Hariharan, M. Kesava, M. Alagar, K. Dinakaran, K. Subramanian, Optical, electrochemical, and thermal behavior of polybenzoxazine copolymers incorporated with tetraphenylimidazole and diphenylquinoline, *Polym Adv Technol.* 29 (2018) 355–363.
- [12] Y. Yagci, B. Kiskan, N.N. Ghosh, Recent advancement on polybenzoxazine — a newly developed high performance thermoset, *J. Polym. Sci. Part A Polym. Chem.* 47 (2009) 5565–5576.
- [13] B.T.T. Akeichi, A.T.K. Awauchi, T.A. Gag, High performance polybenzoxazines as a novel type of phenolic resin, *Polym. J.* 40 (2008) 1121–1131.
- [14] X. Wang, L. Lv, W. Gu, X. Wang, T. Dong, Z. Yang, H. Cao, H. Huang, Novel triphenylamine-based copolymers for all-polymer solar cells, *Dyes and Pigments.* 140 (2017) 141–149.
- [15] B. Kiskan, N.N. Ghosh, Y. Yagci, Polybenzoxazine-based composites as high-performance materials, *Polym. Int.* 60 (2011) 167–177.
- [16] V.C. Kishore, R. Dhanya, K. Sreekumar, R. Joseph, C.S. Kartha, Spectral distribution of photocurrent in poly(6-tert-butyl-3-methyl-3,4-dihydro-2H-1,3-benzoxazine), *Synth. Met.* 158 (2008) 676–680.
- [17] J.J. Pillai, A. Abbas, S. Narayanan, K. Sreekumar, C.S. Kartha, R. Joseph, Synthesis and experimental investigations on the photoconductivity of p - aminoazobenzene based non-conjugated polybenzoxazine system, *Polymer* 137 (2018) 330–337.

- [18] Z.K. Chen, W. Huang, L.H. Wang, E.T. Kang, B.J. Chen, C.S. Lee, S.T. Lee, A family of electroluminescent silyl-substituted poly(p-phenylenevinylene)s: synthesis, characterization, and structure–property relationships, *Macromolecules*. 33 (2000) 9015–9025.
- [19] J. Sworakowski, J. Ulanski, Electrical properties of organic materials, *Annu. Rep. Prog. Chem., Sect. C*. 99 (2003) 87–125.
- [20] A.M. Mehranpour, S. Hashemnia, Solvatochromism in binary solvent mixtures by means of a penta-tert-butyl pyridinium N-phenolate betaine dye, *J. Chinese Chem. Soc.* 53 (2006) 759–765.
- [21] A.S. Studies, N.C. Dyes, Synthesis, absorption spectra studies and biological activity of some novel conjugated dyes, *J. Chinese Chem. Soc.* 47 (2000) 389–395.
- [22] V.I. Arkhipov, H. Bässler, Exciton dissociation and charge photogeneration in pristine and doped conjugated polymers, *Phys. Status Solidi*. 201 (2004) 1152–1187.
- [23] C.S. Cheng, Y. J. Yang, S. H. Hsu, Synthesis of conjugated polymers for organic solar cell applications, *Chem. Rev.* 109 (2009) 5868–5923.
- [24] X. Qian, P. Umari, N. Marzari, First-principles investigation of organic photovoltaic materials C60, C70, [C60] PCBM, and bis-[C 60] PCBM using a many-body G0W0-Lanczos approach, *Phys. Rev. B*. 91 (2015) 1–8.
- [25] P. Hudhomme, An overview of molecular acceptors for organic solar cells, *EPJ Photovoltaics*. 4 (2013) 4401.
- [26] B.W. Larson, J.B. Whitaker, X. Wang, A.A. Popov, G. Rumbles, N. Kopidakis, S.H. Strauss, O. V Boltalina, Electron affinity of phenyl-C61-butyric acid methyl ester (PCBM), *J. Phys. Chem. C*. 117 (2013) 14958–14964.
- [27] J. Cabanillas-Gonzalez, T. Virgili, G. Lanzani, S. Yeates, M. Ariu, J. Nelson, D.D.C. Bradley, Photophysics of charge transfer in a polyfluorene/violanthrone blend, *Phys. Rev. B-Condens. Matter Mater. Phys.* 71 (2005) 014211–014219.
- [28] J.C. Scott, L.T. Pautmeier, W.E. Moerner, Photoconductivity studies of photorefractive polymers, *J. Opt. Soc. Am. B*. 9 (1992) 2059.

- [29] H.B. M. Gailberger, DC and transient photoconductivity of poly(2-phenyl-1,4-phenylenevinylene), *Phys. Rev. B.* 44 (1991) 8643–8651.
- [30] J.P. Osaheni, J.A. Osaheni, S.A. Jenekhe, N. York, J. Perlstein, Photogeneration of charge carriers in bilayer assemblies of conjugated rigid-rod polymers, *J. Phys. Chem.* 98 (1994) 12727–12736.
- [31] L. Onsager, Initial recombination of ions, *Phys. Rev.* 54 (1938) 554–557.
- [32] T. Däubler, R. Bittner, K. Meerholz, V. Cimrová, D. Neher, Charge carrier photogeneration, trapping, and space-charge field formation in PVK-based photorefractive materials, *Phys. Rev. B.* 61 (2000) 13515–13527.
- [33] T.K. Däubler, L. Kulikovskiy, D. Neher, Photoconductivity and charge-carrier photogeneration in photorefractive polymers, *Proc. SPIE.* 4462 (2002) 206–216.
- [34] Y. Zhang, T. Wada, L. Wang, H. Sasabe, Main-chain polymers with nonlinear optical chromophores as a slipped shoulder-to-shoulder arrangement, *Polym. J.* 29 (1997) 685–692.
- [35] P. Taylor, B. Kiskan, F. Dogan, Y.Y. Durmaz, Y. Yagci, Synthesis, characterization and thermally-activated curing of azobenzene-containing benzoxazines, *Designed Monomers and Polymers* (2008) 473–482.
- [36] V.C. Kishore, R. Dhanya, C.S. Kartha, K. Sreekumar, R. Joseph, Photoconductivity in molecularly doped poly(methylmethacrylate) sandwich cells, *J. Appl. Phys.* 101 (2007).
- [37] G. Bäuml, S. Schlöter, U. Hofmann, D. Haarer, Correlation between photoconductivity and holographic response time in a photorefractive guest host polymer, *Opt. Commun.* 154 (1998) 75–78.

# Photorefractive effect in PBZ composite

### Abstract

Photorefractive devices based on poly(6-tert-butyl-3-phenyl-3,4-dihydro-2H-1,3-benzoxazine) was prepared by guest-host approach. In this device PCBM was used as a sensitizer, disperse red 1 (DR 1) was used as nonlinear chromophore and 9-ethylcarbazole (ECZ) was used as plasticizer molecule. The concentrations of each component was optimized and the photorefractive devices were prepared by sandwiching the composite between two patterned ITO glass plates. Optical and photoconductivity studies were carried out on the devices and two beam coupling experiment was performed to check whether they were photorefractive.

### 3.1 Introduction

Photorefractive effect is the combined effect of photoconductivity and electro-optics [1]. Photorefractive materials have versatile applications in areas of high density optical data, optical limiting, phase conjugation, storage and simulations of neural network [2]. Earlier works of photorefractive materials were mainly focused on inorganic crystals [3]. But these inorganic crystals suffered a lot of disadvantages such as phase separation during doping, high dielectric constant: reduced the strength of space charge electric field. Also, noncentrosymmetric crystals constitute a small class, which could provide the second order optical nonlinearity. On

the other hand, polymer materials offer flexibility during doping and a non-zero Pockel's effect can be obtained by orienting the chromophore molecules under an external electric field. In polymers, externally applied electric field is a requirement for the formation of the space charge electric field. The external electric field reduces the binding energy of excitons and thus facilitates the charge separation. Also, carrier mobility also predominantly depends on the external electric field. These field dependent properties in polymers is the apparent difference with inorganic crystals [4]. Nowadays, the studies are mainly concentrated on polymer based photorefractive systems. 100% diffraction efficiency was reported in PVK based guest-host system with a gain coefficient of  $200 \text{ cm}^{-1}$  [5]. Also, erasable holographic displays were demonstrated in photorefractive polymer composites [6–9].

Many photorefractive systems are reported in literature and most of them belong to guest-host polymer systems due to their wide flexibility for device fabrication. In guest-host approach, the required components such as sensitizers, chromophores and plasticizer molecules were physically mixed with a photoconducting host matrix. There are reports in literature describing electro-optic polymers as the host matrix and charge transport molecules were used as guests. Other polymeric photorefractive systems are the fully functionalized photorefractive polymers in which the required functional species were directly attached to the polymer backbone. These polymer systems are reliable for their stability against phase separation. However, the synthesis of this type of polymers includes complicated procedure and the synthesis is highly time consuming [4,10].

This chapter discusses the validity of the benzoxazine polymers for achieving photorefractivity. From the discussions in Chapter 2, it was obvious that benzoxazine polymers exhibited excellent photoconducting properties. Photorefractive devices were prepared through guest-host approach in which these benzoxazine polymers acted as photoconducting host matrix. The discussions in the previous chapter also suggested that PCBM was a good sensitizer for benzoxazine polymers for obtaining photoconductivity. The nonlinear optical molecule (DR 1) and plasticizer molecule, ECZ selected from literature were added for preparing the photorefractive composite. The samples were analyzed by taking the absorption spectra, performing the photoconductivity experiments and two beam coupling experiment.

### **3.2 Poly(6-tert-butyl-3-phenyl-3-4-dihydro-2H-1,3-benzoxazine) based guest-host photorefractive composite**

Photorefractive composite was prepared through guest-host approach. In guest-host approach, all the required functional species to exhibit photorefractive effect are physically mixed to form the photorefractive composite. A photoconducting host matrix, electro-optic molecules and plasticizers are the essential part of a photorefractive composite. Poly(6-tert-butyl-3-phenyl-3-4-dihydro-2H-1,3-benzoxazine) labelled as PBZ, along with PCBM showed photoconductive properties enough to exhibit photorefractive effect. So, PBZ:PCBM was selected as photoconducting host matrix. In order to bring electro-optic effect, NLO chromophores can be used. In this case, a well-established NLO molecule N-Ethyl-N-(2-hydroxyethyl)-4-(4-nitrophenylazo)aniline commonly named as Disperse Red I (DR I) was

selected to fulfill the second demand of the photorefractive system. DR 1 is widely used for many of the electro-optic applications [11–13]. Also, 9-ethylcarbazole (ECZ) molecule was used as plasticizer. ECZ is a widely used in photorefractive polymer composites as plasticizer especially in PVK based composites [14]. Presence of plasticizer decreases the glass transition temperature of the photorefractive composite. If the glass transition temperature is near to room temperature, the NLO molecules get aligned in the direction of the applied electric field. This process is called poling. The orientation of the chromophore molecules provides a bulk asymmetry to the photorefractive composite and thereby enhances the photorefractive performance of the composite[15,16]. The structure of the molecules used are shown in Fig. 3.1.

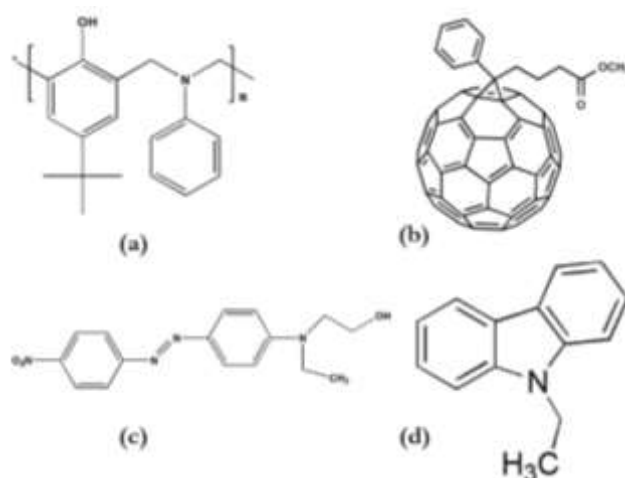


**Fig. 3.1:** Structure of (a) PBZ, (b) PCBM, (c) DR 1 and (d) 9-ethyl carbazole

### 3.3 Photorefractive device fabrication

Usually the photorefractivity is confirmed by doing the two beam coupling experiment in which the intensity of the transmitted light beams is

analyzed. So the sample should have good optical clarity. Phase separation of the components, aggregation of the components, non-uniform distribution of the components during mixing, formation of air gaps during film formation, etc. will result in scattering of the incident beams with in the photorefractive device. The sample preparation is very important and care should be taken during every steps.

The process for preparing photorefractive devices includes three steps.

- 1) Patterning or etching of transparent electrode (ITO) on glass substrates.
- 2) Preparation of the photorefractive polymer composite.
- 3) Device fabrication.

### 3.3.1 Patterning of ITO electrodes

This section discusses the basic procedure for etching of ITO for a required pattern. The ITO used have 20 Ohm sheet resistance and high transmittance in the visible region. Initially, ITO coated glass substrates were cut in a square shape of size  $2\text{ cm} \times 2\text{ cm}$ . The ITO was covered with a sheet of parafilm having the same dimension of the glass substrate, by applying pressure to confirm the complete removal of air bubbles. The parafilm covering was gently heated by supplying hot air over it to improve adhesion. Supply of the hot air was continued until, the parafilm covering became uniformly clear. When the parafilm was cooled, standard mask of desired shape was placed over the parafilm and parafilm was removed from the area to be etched. Care should be taken to avoid the formation of rough edges otherwise dielectric breakdown will occur in the presence of high electric field.

For etching the ITO, 50 ml of aqua regia solution was prepared by mixing concentrated HCl and HNO<sub>3</sub> for a ratio of HCl : HNO<sub>3</sub> =1:3 and then diluted by adding water such that HCl : HNO<sub>3</sub> : H<sub>2</sub>O =1:3:5. The prepared ITO glass plates were immersed in this solution. The glass slides were kept in the solution for nearly 10 minutes for the complete etching of exposed ITO.

The glass slides were rinsed with adequate amount of distilled water to eliminate the residual solution used for etching. Again the glass slides were thoroughly dried by hot air. After drying, the remaining parafilm present in the masked area were removed carefully.

The ITO etched glass plates were sonicated in distilled water for 30 minutes. Then it was cleaned using soap solution and water.

### **3.3.2 Preparation of the photorefractive polymer composite**

The photorefractive polymer composite was prepared by taking the necessary components in an appropriate ratio, so that, the composite should ensure good optical clarity, photoconductivity and electro-optic response. In this case, the components were taken in a proportion, PBZ (56%), PCBM (11%), ECZ (23%) and DR1 (10%). These components were dissolved in 25 ml HPLC grade chloroform by bath sonication method. After the uniform mixing of these components, the solution was filtered using 0.45 $\mu$ m PTFE filter. Then it was allowed to solidify and ensured the complete solvent removal by keeping it in a hot air oven kept at 60 °C for 48 h. The dried solid material was crushed into fine powder using a mortar.

### 3.3.3 Device fabrication

For photorefractive device fabrication, ITO glass cells were assembled initially. Two ITO glass plates patterned in T shape were used for making the ITO cell. One of the ITO was flipped over the other and Teflon sheets of  $24\ \mu\text{m}$  thickness were used in between them to produce an inter electrode separation of  $24\ \mu\text{m}$ . Thermally stable glues were used to fix the arrangement. Thus an ITO cell was made for device fabrication. The arrangement also have electrode areas to take two contacts.

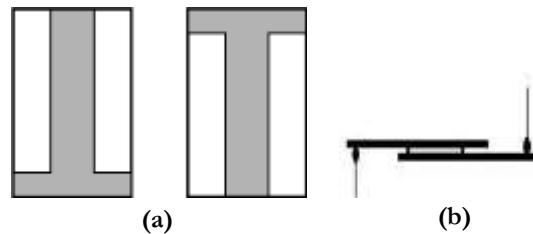


**Fig 3.2:** (a) Patterned (etched) ITO and  
(b) Schematic representation of ITO glass cell.

Finally, a clean glass plate was placed over a hot plate and sufficient quantity of the fine powder of the composite was placed on the top of the glass plate. The temperature of the hot plate was raised until the fine powder got melted. When the entire powder was melted, the opening of the glass cell was made in contact with the melt. This enabled the melt to get into the ITO cell due to capillary action. The process was continued till the spacing between the electrode areas was completely filled. Care was taken to avoid formation of bubbles inside the cell. The device was suddenly cooled by placing it over ice bags. The device was kept around 24 h for setting.

### 3.4 Optical absorption

The absorption spectrum of photorefractive device was taken using Jasco V-570 spectrophotometer. Fig. 3.3 shows the absorption spectrum of the device. The device showed absorption in the entire visible region of the spectrum. The absorption in the higher wavelength region is due to the intermolecular charge transfer (ICT) of the dye during excitation [17].

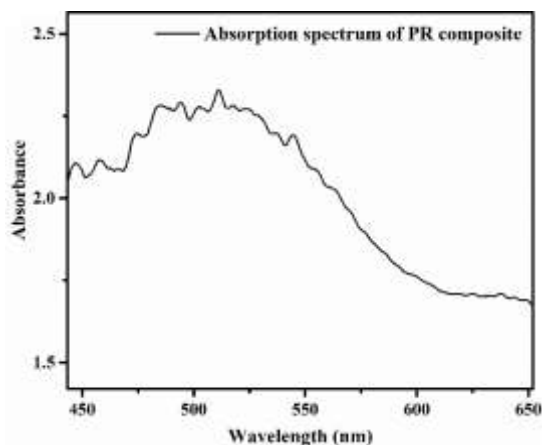


Fig. 3.3: Absorption spectrum of photorefractive composite

### 3.5 Photoconductivity in photorefractive device

Photoconductivity experiments were performed on the prepared device to check whether it exhibited photoconductivity. For this, the sample was biased at 50 V and current through the device was measured using a Keithely 236 Source Measure Unit, with and without illumination. The dark current at the room temperature was obtained as  $8 \times 10^{-10}$  A. The sample was illuminated using 632 nm laser beam. When the sample was illuminated, the current through the device was increased to  $1.9 \times 10^{-7}$  A. The intensity of illumination was  $5 \text{ mW/cm}^2$ .

## 3.6 Two beam coupling experiment

Even if a polymer matrix exhibits photoconductivity and electro-optic effect, it need not always exhibit photorefractivity. The interference of two coherent laser beams in the polymer composite may generate non-photorefractive gratings. This may originate from some physical or chemical changes during illumination. Presence of this type of gratings can be identified by analyzing the intensity of the writing beams. A simultaneous change in the intensity (increase or decrease) of both the writing beams due to the change in absorption coefficient of the composite, which is in phase with the intensity distribution of the incident beams, indicates the presence of such gratings. Two beam coupling experiment only could confirm the photorefractive nature of the composite. Photorefractive gratings lead to asymmetric energy transfer between the two writing beams. In two beam coupling experiment, the intensities of the writing beams after passing through the sample is monitored.

### 3.6.1 Theory

As outlined in Chapter 1, photorefractive grating exhibits a phase shift,  $\varphi$  with the intensity distribution of the incident beam. This phase shift is the unique property of the photorefractive effect due to the nonlocal mechanism of grating formation. Once the grating is generated, both the writing beams are inevitably Bragg-matched to the grating. Thus, a component of each beam diffracts in the direction of the counter beam. Due to the phase shift, superposition of one of the writing beam with the diffracted one happens constructively and for the other writing beam, superposition occurs destructively. Thus the phase shift leads to an

asymmetric energy transfer between two mutually coherent optical beams inside a photorefractive medium [16]. This energy transfer confirms the photorefractive nature of the composite.

From the coupled wave theory, the change in intensity of each beam along the z-axis can be represented by the following relations [18],

$$\frac{\partial I_1^{0.5}}{\partial z} = -\left(\frac{\pi \Delta n}{\lambda}\right) (I_2)^{0.5}$$

$$\frac{\partial I_2^{0.5}}{\partial z} = -\left(\frac{\pi \Delta n}{\lambda}\right) (I_1)^{0.5}$$

The energy transfer in the photorefractive medium is characterized by calculating the gain coefficient,  $\Gamma$  as [19],

$$\Gamma = \frac{4\pi}{\lambda} (\hat{e}_1 \cdot \hat{e}_2) \Delta n \sin \phi$$

Where  $\hat{e}_1$  and  $\hat{e}_2$  are the polarization vectors of the two writing beams and  $\Delta n$  is the refractive index modulation.

### 3.6.2 Experiment and results

The experimental setup for the two beam coupling experiment is similar to the experimental setup for recording hologram. Here the coherent laser beam is split into two beams of almost same intensity and allowed to interfere in the sample. A DC electric field is applied across the sample using a high voltage power supply. Also, the geometry is tilted from the normal. This is to achieve one component of electric field in the direction of grating vector. After the sample, two detectors are used to collect the light emerging from the sample. The detectors are connected to a digital oscilloscope.

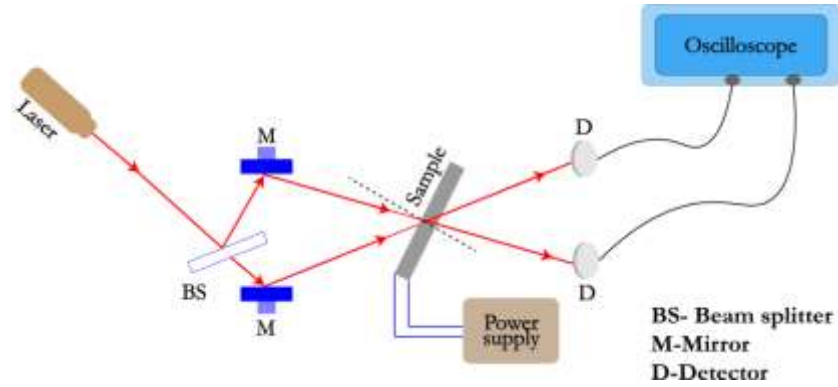


**Fig. 3.4:** Schematic representation of two beam coupling experiment.

Fig. 3.4 shows the experimental setup used for the two beam coupling experiment in the present study. The experiment was conducted using He-Ne laser. S-polarized light beam from the laser was split into two beams of almost same intensity and allowed to interfere in the sample. The intensities of the writing beams were nearly  $4 \text{ mW/cm}^2$ . The inter-beam angle was  $40^\circ$ . The angle made by the writing beams with the sample normal were  $20^\circ$  and  $60^\circ$ . The intensities of the transmitted beams were monitored after applying DC electric field of  $35 \text{ V}/\mu\text{m}$ .

Fig. 3.5 shows the screen shots of the digital oscilloscope display corresponding to the intensities of the signals monitored after passing through device. The screen shots were taken at three instants of time,  $t_1 < t_2 < t_3 \text{ s}$ . Here the yellow signal indicate the intensity of the first writing beam and orange signal corresponds to the second writing beam. It was clear that, as time passed the yellow signal was amplified and orange signal became weakened simultaneously. From this, it was obvious that, while passing through the device, a part of the energy from the second writing beam got transferred to the first writing beam. This asymmetric energy

transfer observed in the two beam coupling experiment establishes the presence of photorefractive gratings developed in the device.

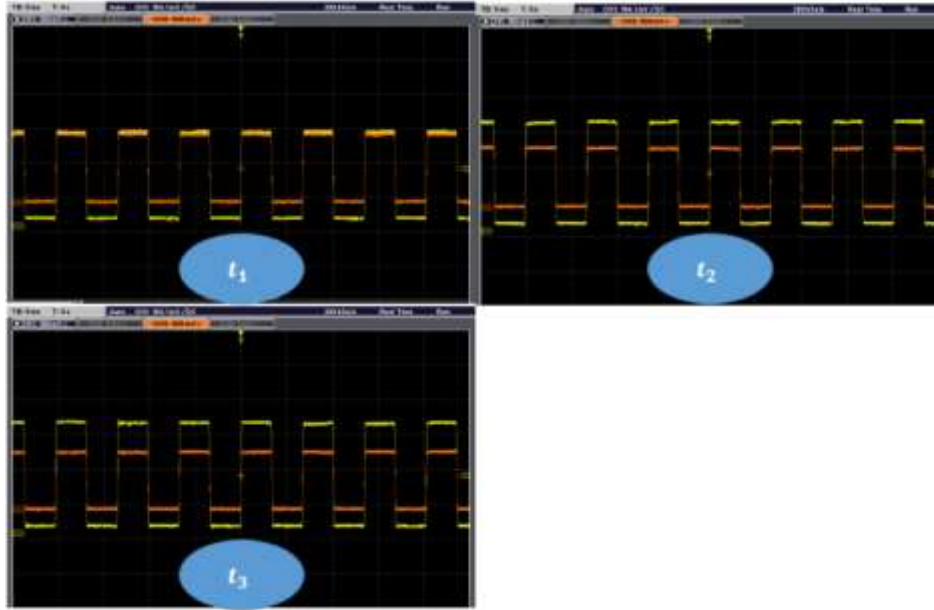


**Fig. 3.5:** Screen shots from the digital oscilloscope showing the signal intensities of the two beams after passing through the sample at three instants of time ( $t_1 < t_2 < t_3$ ), after applying the DC field. Yellow indicate beam 1 and red indicate beam 2. The asymmetric energy transfer from beam 1 to beam 2 can be clearly seen.

In order to characterize the energy transfer between two beams, gain coefficient was calculated. Gain is the increase in energy that one beam obtain from another beam. The following expression is used for the quantitative measurement of photorefractive gain [20],

$$\Gamma = \left\{ \frac{1}{D} \left[ \ln \frac{I_{12}}{I_1} - \ln \left( 2 - \frac{I_{12}}{I_1} \right) \right] \right\} - \alpha$$

where  $I_{21}$  is the transmitted intensity of the second beam with beam 1 applied,  $I_{12}$  is the transmitted intensity of the first beam with beam

2 applied,  $I_2$  is the transmitted intensity with beam 2 alone,  $I_1$  is the transmitted intensity with beam 1 alone,  $D$  is the optical path length through the sample and  $\alpha$  is the absorption coefficient. Here the beam ratios were calculated as  $I_{12}/I_1 = 1.22$  and  $I_{21}/I_2 = 0.92$ . The beam ratios depict the asymmetric energy transfer between the two interfering beams. Using these, the photorefractive gain was calculated as  $87.45 \text{ cm}^{-1}$ .

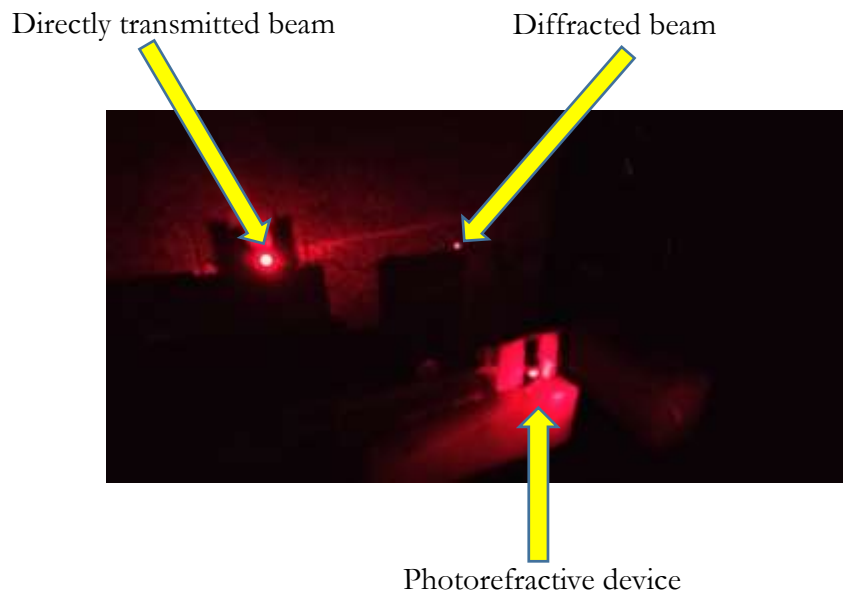


**Fig. 3.6:** Photograph showing the diffraction of the incident beam from the photorefractive device after recording the grating.

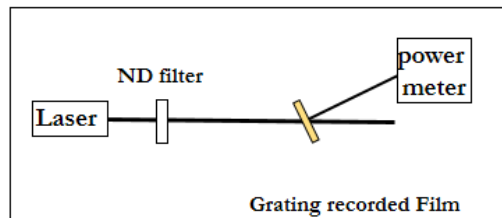


**Fig. 3.7:** Schematic representation of diffraction through grating

After the grating development, the sample was illuminated with a single beam without applying the DC field. Fig. 3.6 shows the diffraction observed from the grating. The diffraction efficiency of the grating was calculated as the ratio of the intensity of the diffracted beam to the intensity of the incident beam. The diffraction efficiency calculated in this way also included the contributions of non-photorefractive gratings. Here the diffraction efficiency obtained was 11.4%.

### 3.7 Summary

Poly(6-tert-butyl-3-phenyl-3-4-dihydro-2H-1,3-benzoxazine) based photorefractive composite was developed, which showed a photorefractive gain of  $87.45 \text{ cm}^{-1}$  at an electric field of  $35 \text{ V}/\mu\text{m}$ . The obtained gain coefficient is good enough for using the photorefractive composite for photorefractive applications. The other two benzoxazine polymers, poly([4-(6-tert-butyl-4H-benzo[e][1,3]oxazin-3-yl)phenyl]phenyldiazene) (AZO-PBZ) and poly(4-tert-butyl-2-{{ethyl(4-nitrophenyl)amino}methyl}6{{methyl(4-phenylazophenyl)amino}methyl}phenol) (AZO-PNA) developed exhibited higher photoconductive performance than the PBZ. But, the device fabrication with these two polymers could not be done successfully. It is envisaged that on successful fabrication of a photorefractive device using the above two polymers it may be possible to achieve higher gain than the PBZ:PCBM polymer composite.

### References

- [1] W.E. Moerner, S.M. Silence, Polymeric photorefractive materials, Chem. Rev. 94 (1994) 127–155.
- [2] W.E. Moerner, A. Grunnet-Jepsen, C.L. Thompson, Photorefractive

- polymers, *Mater. Sci.* 27 (1997) 585–623.
- [3] B.Y. Zhang, R. Burzynski, S. Ghosal, M.K. Casstevens, Photorefractive polymers and composites, *Adv. Mater.* 8 (1996) 111–125.
- [4] S.J. Zilker, Materials design and physics of organic photorefractive systems, *Chemphyschem.* 1 (2000) 72–87.
- [5] K. Meerholz, B.L. Volodin, Sandalphon, B. Kippelen, N. Peyghambarian, A photorefractive polymer with high optical gain and diffraction efficiency near 100 %, *Nature.* 371 (1994) 497–500.
- [6] J.W. Perry, Update on 3D displays, *Nature.* 451 (2008) 636–637.
- [7] W. Lin, S. Rokutanda, T. Gu, D. Flores, P. Wang, G. Li, P.S. Hilaire, J. Thomas, R.A. Norwood, M. Yamamoto, N. Peyghambarian, An updatable holographic three-dimensional display, *Nature.* 451 (2008) 694–698.
- [8] J. Thomas, R.A. Norwood, N. Peyghambarian, Non-linear optical polymers for photorefractive applications, *J. Mater. Chem.* 19 (2009) 7476–7489.
- [9] J. Thomas, C.W. Christenson, P.A. Blanche, M. Yamamoto, R.A. Norwood, N. Peyghambarian, Photoconducting polymers for photorefractive 3D display applications, *Chem. Mater.* 23 (2011) 416–429.
- [10] N. Tsutsumi, Molecular design of photorefractive polymers, *Polym. J.* 48 (2016) 571–588.
- [11] P. Wu, D.V.G.L.N. Rao, B.R. Kimball, M. Nakashima, B.S. Decristofano, Transient optical modulation with a disperse-red-1 – doped polymer film, *Appl. Opt.* 39 (2000) 814–817.
- [12] K.U.K.R.O. Yoon, S. Lee, Synthesis and characterization of nonlinear optical polymers containing carbazole and disperse red dye, *J. Macromol. Sci. Part B.* 45 (2006) 859–870.
- [13] W.O.H. Eni, C.H.H. Affner, D.E.L.E. Lder, A. Ndreas, F.T. Illack, Y.U.F. Edoryshyn, R.A.C. Ottier, Y. Annick, S. Alamin, C.L.H. Oessbacher, U.E.L.I.K. Och, B.O.C. Heng, B.R.R. Obinson, L.A.R.D. Alton, J.U.L. Euthold, Nonlinearities of organic electro-optic materials in nanoscale slots and implications for the optimum modulator design, *Opt. Express.* 25

- (2017) 2627–2653.
- [14] Y. Zhang, T. Wada, H. Sasabe, Carbazole photorefractive materials, *J. Mater. Chem.* 8 (1998) 809–828.
- [15] O. Ostroverkhova, W.E. Moerner, Organic photorefractives: mechanisms, materials and applications, *Chem. Rev.* 104 (2004) 3267–3314.
- [16] S. Köber, M. Salvador, K. Meerholz, Organic photorefractive materials and applications, *Adv. Mater.* 23 (2011) 4725–4763.
- [17] C. Toro, A. Thibert, L. De Boni, E. Masunov, Fluorescence emission of disperse red 1 in solution at room temperature, *J. Phys. Chem. B.* 112 (2008) 929–937.
- [18] A. V Vannikov, A.D. Grishina, The photorefractive effect in polymeric systems, *Russ. Chem. Rev.* 72 (2003) 471–488.
- [19] H.S. Nalwa, S. Miyata, *Nonlinear optics of organic molecules and polymers*, CRC Press, Boca Raton, 1997.
- [20] G.P. Wiederrecht, B.A. Yoon, M.R. Wasielewski, High photorefractive gain in nematic liquid crystals doped with electron donor and acceptor molecules, *Science.* 270 (1995) 1794–1797.

.....✂.....

## Photoconductive Properties of P(EDOT-FL)

### Abstract

The photoinduced charge transfer properties of low band gap donor-acceptor  $\pi$ -conjugated copolymer poly(2,5-(3,4-ethylenedioxythiophene)-alt-2,7-(9,9-dioctylfluorene)) labelled as P(EDOT-FL) was investigated through solvatochromic and photoconductivity studies. The effect of strong acceptor, phenyl-C<sub>61</sub>-butyric acid methyl ester (PCBM) on the photogeneration of free carriers was studied by comparing the fluorescence spectra and photoconductive properties of the polymer-PCBM blend [P(EDOT-FL):PCBM] films with the pristine polymer films. The positive solvatochromism exhibited by the P(EDOT-FL) revealed its photoinduced charge transfer nature of the absorption and emission bands. The blend films exhibited quenching of the fluorescence intensity and showed increased photoconductivity. Internal photocurrent efficiency and photoconductive sensitivity of the pristine P(EDOT-FL) films and P(EDOT-FL):PCBM blend films were calculated as a function of electric field, by measuring the photocurrent generated in the sample. Blend films exhibited higher internal photocurrent efficiency of 86% and photoconductive sensitivity of  $5.44 \times 10^{-7} \text{ SW}^{-1} \text{ cm}$  at  $70 \text{ V}/\mu\text{m}$ .

## 4.1 Introduction

Photorefractive composites prepared through guest-host approach are liable to phase separation, due to the presence of multiple components [1,2]. The elimination of the required components such as sensitizers or NLO chromophore will decrease the chances of phase separation during device fabrication. If the polymer molecule itself is photoconducting, phase separation can be reduced in the multicomponent environment. Stability can be improved in such systems. Also, if the band gap of the polymer is in the low energy region, spectral sensitivity can be improved in the low energy region. This chapter addresses a low band gap conjugated copolymer which itself acts as a photoconductor. Conjugated polymers, have emerged as an important class due to the potential applications in the development and construction of advanced devices such as sensors [3], photovoltaic devices such as polymer solar cells/plastic solar cells [4,5] and displays [6,7] as a consequence of the combined effect of mechanical, electrical and optoelectronic properties of these polymers. They can be easily synthesized by low cost processing techniques [5,8]. The advancement of band gap engineering results in the development of new organic polymers with desired photon absorption and efficient photoinduced charge separation. The concept of donor-acceptor alternation along the polymer backbone has received a great deal of interest among current researchers owing to its large intramolecular charge transfer and its capability of band gap tuning to the desired photon energies [9,10]. However, most of the polymer devices exhibited low photogeneration efficiency due to the high recombination rate of photoexcited electron and hole. Realization of efficient charge transfer at the interface of

conjugated polymer and fullerene occurred as a breakthrough in the design of optoelectronic and photovoltaic devices [5,7,11].

This chapter discusses the results of investigations carried out to explore the photoconducting behavior of poly(2,5-(3,4-ethylenedioxythiophene)-alt-2,7-(9,9-dioctylfluorene)) labelled as P(EDOT-FL) in which EDOT acts as the donor moiety and FL acts as the acceptor moiety. Donor-acceptor architecture of the P(EDOT-FL) polymer has tuned its band gap to optical regime and this enables photon harvesting in the wide range of the optical spectrum. Also, the structure consisting of electron rich group and electron deficient group facilitates inter-chain charge transfer in the polymer backbone [9]. The extended  $\pi$ - conjugation and donor-acceptor scheme provides photoconductivity to the pristine film. In order to enhance photoconductivity of the P(EDOT-FL), a soluble fullerene derivative, PCBM was used as sensitizer. Efficient and ultrafast photoinduced charge transfer at the interface of conjugated polymer and PCBM is reported in literature [12,13].

Nonlinear optical properties in organic NLO chromophores originate from effective donor-acceptor intermolecular interaction and  $\pi$  electron delocalization [14]. So the NLO properties can be tuned by selecting the suitable donor and acceptor moieties. The polymer backbone of P(EDOT-FL) has typical D-A structure, intramolecular charge transfer happens effectively. So this synthesized polymer may also fulfill the second requirement (electro-optic effect) to exhibit photorefractivity. Photoconductivity studies carried out in P(EDOT-FL) and P(EDOT-FL):PCBM blend films reveal higher photogeneration efficiency of the polymer which throw some light into the validity of this polymer for photorefractive applications [15].

## 4.2 Experimental

Preparation of P(EDOT-FL):PCBM blend films involved physical mixing of host matrix, P(EDOT-FL) and sensitizer, PCBM at 1:0 (pristine), 1:1 and 1:2 weight ratios in distilled chloroform and spin coating of this solution on to an ITO coated glass substrate. Both polymer and sensitizer were dissolved by bath sonication method. The blend solution was filtered through 0.45  $\mu\text{m}$  PTFE filter, and the clear solution obtained was spin coated to produce good films. The spin coating was done on the spin coater supplied by SPS Europe (model SPIN 150). The spinning parameters are fixed as rpm=800, rpm/s=800 and time=60 s. The ITO layer has thickness of 200 nm and sheet resistance of 20  $\Omega/\text{cm}^2$  as specified by the manufacturer (GEOMATEC, Japan). After spin coating, the films were kept in ambient conditions for 6 h and then it was transferred into vacuum desiccator for maximum solvent removal. The blend films were uniform as that of the pristine polymer films due to the good solubility of the PCBM and were free from phase separation. The resulting films were having a thickness of approximately 1-1.5  $\mu\text{m}$ . Thickness was determined using a Dektak 6M Stylus profiler. Electrical characterization of these samples were done by depositing silver electrode on the top of the films via thermal evaporation technique (at a typical pressure of  $2 \times 10^{-5}$  milli bar), so that sandwich cell configuration of ITO/P(EDOT-FL):PCBM/Silver was obtained. The silver electrode had a thickness of 50 nm. Active area of the device (defined by the silver contact) was 3  $\text{mm}^2$ .

Photocurrent measurements were performed by illuminating the devices from the ITO side and the photocurrent was measured using Keithley 236 Source Measure Unit. Dark current, measured as a function of

electric field before illumination, was subtracted from current measured under illumination to give the photocurrent ( $J_{\text{photo}} = J_{\text{light}} - J_{\text{dark}}$ ). Photoconductivity in polymers depends both on intensity of illumination and external electric field and these parameters were varied independently in photoconductivity experiments. Optically Pumped Semiconductor Laser (488 nm, Coherent) was used to explore the intensity dependence and electric field dependence of the photoconductivity and internal photocurrent efficiency of the pristine and PCBM blended polymer films.

### 4.3 Poly(2,5-(3,4-ethylenedioxythiophene)-alt-2,7-(9,9-dioctylfluorene))

Poly(2,5-(3,4-ethylenedioxythiophene)-alt-2,7-(9,9-dioctylfluorene)) labelled as P(EDOT-FL) is a donor-acceptor conjugated copolymer synthesized via direct arylation of EDOT with 2,7-dibromo-9,9-dioctylfluorene [16]. Synthesis was done by the copolymerization of two monomers 3,4-ethylenedioxythiophene (EDOT) and fluorene (FL). The structures of EDOT, FL and P(EDOT-FL) are shown in Fig.4.1.

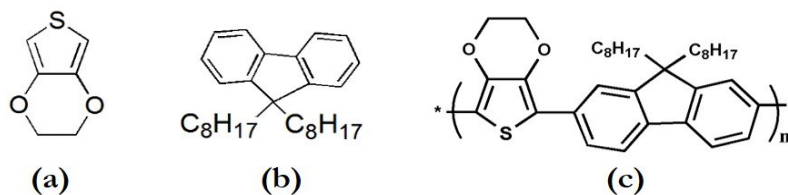


**Fig. 4.1:** Structure of (a) EDOT, (b) FL and (c) P(EDOT-FL)

EDOT based conjugated polymers have been extensively studied due to their low ionization potential, high electrical conductivity during doping and good stability [17,18]. These properties of EDOT based polymers are very useful in different applications such as hole transport layer in light

emitting devices, antistatic coatings, transparent electrodes, electrochromic displays and design and fabrication of chemical and biological sensors [19–23]. Polyfluorenes are widely investigated for LED applications owing to their high photoluminescence efficiency, high hole mobility and good photostability [24–26]. However, polyfluorene polymers exhibited wide band gap in the range of 2.95 eV to 3.68 eV [27,28]. This severely affect the charge transport properties and conducting applications. Copolymerization of fluorene with EDOT aims to overcome these limitations.

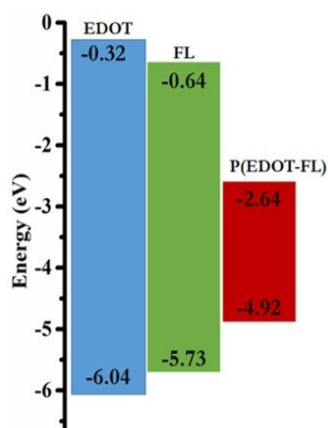


**Fig. 4.2:** Energy band diagram of EDOT, FL and P(EDOT-FL)

Fig. 4.2 shows the energy band diagram of EDOT, FL and P(EDOT-FL). The HOMO and LUMO energy levels of EDOT and FL were estimated theoretically using density functional theory (DFT) methods. The HOMO and LUMO levels of EDOT are -6.04 eV and -0.32 eV respectively. For FL, HOMO and LUMO levels were calculated as -5.73 eV and -0.64 eV respectively. It is obvious that, the LUMO level of FL is below the LUMO level of EDOT. Thus, in this configuration, FL acts as acceptor moiety and EDOT acts as donor moiety. The coupling between these donor and acceptor groups has resulted in a low lying

LUMO level and higher lying HOMO level, so that the band gap of the copolymer is reduced to visible region. The HOMO and LUMO energy levels of the P(EDOT-FL) copolymer was calculated by DFT method and cyclic voltammetry (CV) method. From DFT method, the HOMO and LUMO energy levels of P(EDOT-FL) were determined to be -4.92 eV and -2.64 eV. Thus the band gap of the copolymer is 2.28 eV [16].

Here, two bulky octyl chains were introduced to the fluorene building unit to increase the solubility of the polymer. This synthesized polymer, P(EDOT-FL) exhibited good solubility in organic solvents. The molecular weight of the polymer was calculated by performing gel permeation chromatography in tetrahydrofuran. The number average molecular weight ( $\bar{M}_n$ ) and weight average molecular weight ( $\bar{M}_w$ ) of the polymer were 6994 and 7106 respectively. The polydispersity index was 1.01.

## 4.4 Studies on pristine P(EDOT-FL)

### 4.4.1 Electrochemical properties

Electrochemical methods were used to estimate the HOMO and LUMO energy levels of the synthesized polymer. In this case, cyclic voltammetry (CV) method and differential pulse voltammetry (DPV) methods were used for the calculation of HOMO-LUMO levels. The experimental set up is discussed in section 2.3.1. In CV experiment, HOMO level was calculated by identifying the oxidation onset ( $E_{onset}^{ox}$ ). LUMO level was calculated by using optical band gap. Thus, HOMO and LUMO values of P(EDOT-FL) were -5.19 eV and -2.9 eV respectively. Also, from DPV method, -5.14 eV and -2.86 eV were identified as HOMO and LUMO levels respectively.

## 4.4.2 Optical properties

### 4.4.2.1 Optical absorption

Optical absorption spectra of the samples were recorded at room temperature by measuring the transmission through the sample. The absorption spectrum of the polymer was recorded in both solution and solid state (thin film) form and a redshift of 50 nm in the onset of absorption was observed in the spectra of thin film compared to that of solution (Fig. 4.3). The increased packing of the polymer in solid state resulted in an increased electron delocalization through  $\pi$ - $\pi$  interactions. This has caused the redshift in the spectra [29]. The film exhibited good absorption in the visible region with a peak absorption at a wavelength of 442 nm. The optical band gap corresponding to absorption onset was 2.12 eV. Smaller optical band gap in the solid state revealed its greater intramolecular charge transfer (ICT) [30].

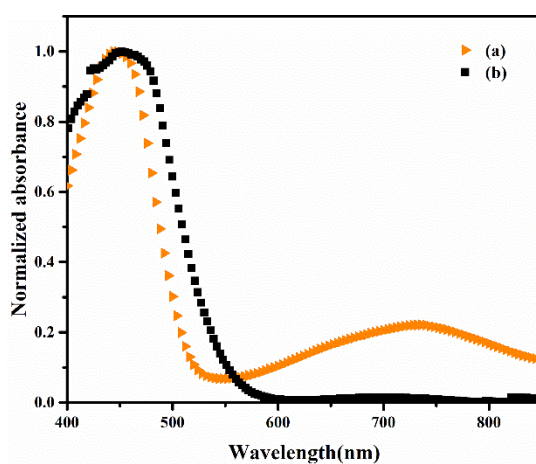


**Fig. 4.3:** Normalized absorption spectra of (a) P(EDOT-FL) dissolved in chloroform and (b) P(EDOT-FL) thin film prepared on ITO coated glass substrate.

#### 4.4.2.2 Fluorescence emission

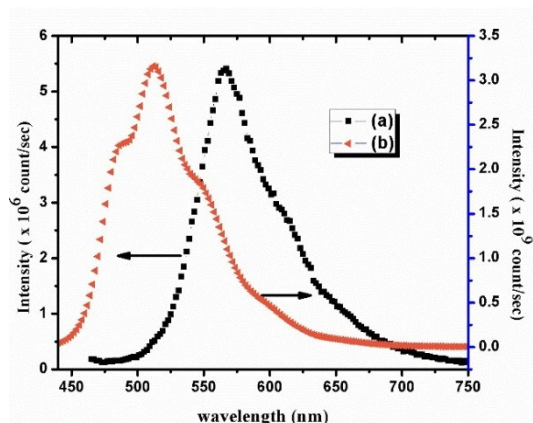


**Fig. 4.4:** (a) Fluorescence spectra of the P(EDOT-FL) polymer dissolved in Chloroform (b) P(EDOT-FL) film prepared on ITO coated glass substrate under the excitation of photons with energy 2.80 eV.

P(EDOT-FL) showed fluorescence when excited with photons of energy greater than the optical band gap. The fluorescence spectra of the P(EDOT-FL) polymer dissolved in chloroform and P(EDOT-FL) film prepared on ITO coated glass substrates were studied, by exciting with photons of energy 2.80 eV and are shown in Fig. 4.4. The emission maximum of P(EDOT-FL) polymer in chloroform was at 512 nm and that of pristine films occurred at 567 nm. The fluorescence maximum occurs at the onset of absorption. Intensity of the fluorescence from pristine film was  $5.5 \times 10^5$  count per second and Stokes shift was 125 nm. This indicated the absence of intermediate triplet states and suggests that singlet transition was responsible for the intense fluorescence emission [31]. The observed spectral shift of absorption and emission bands was attributed to strong electron-phonon interaction [32].

#### 4.4.2.3 Solvatochromic Experiment

Solvatochromism is a tool for understanding the charge transfer nature of the excited state. It is observed that the position, shape and intensity of the absorption and emission bands of an organic molecule get modified when it is dissolved in different solvents. This change in the absorption and emission bands originate from the solute-solvent interaction such as dipole-dipole, dipole-induced dipole, hydrogen bonding, ion-dipole interaction etc. All these interactions could alter the energy difference between ground state and excited state, which is reflected in the absorption and emission spectra [33]. The term solvatochromism is used to refer these changes in the spectral parameters, especially the change in position accompanied by the change in the polarity of the solvent. If a blue shift (hypsochromic shift) is observed with respect to increase in polarity of the solvent, then it is called negative solvatochromism and if there is red shift (bathochromic shift), then it is termed as positive solvatochromism.

The electronic transitions in organic molecules can be  $\sigma \rightarrow \sigma^*$ ,  $n \rightarrow \sigma^*$ ,  $\pi \rightarrow \pi^*$ ,  $n \rightarrow \pi^*$  and charge transfer absorption.  $\pi \rightarrow \pi^*$ ,  $n \rightarrow \pi^*$  (high energy transitions) and charge transfer absorption are generally observed in organic molecules. The charge transfer absorption arises due to formation of charge transfer complex between two moieties and it is commonly seen in systems with electron donor and electron acceptor. It is widely accepted that, the longer wavelength absorption ( $\lambda > 400 \text{ nm}$ ) observed in such systems indicate the transfer of an electron from the donor to acceptor [34]. A positive solvatochromism is expected, if the emission behavior is related to intramolecular charge transfer [35].

P(EDOT-FL) is such type of polymer consisting of a donor (EDOT) and an acceptor (FL) moieties in every repeat unit. So the solvatochromic change of the charge transfer band gives information about the electronic transitions from donor moiety to acceptor moiety.

Here, solvatochromic study was carried out by measuring the absorption and fluorescence spectra of the polymer dissolved in different solvents of varying polarity. Fig. 4.5 depicts the normalized UV-vis absorption spectra and fluorescence spectra of P(EDOT-FL) dissolved in 1,4-dioxane, tetrahydrofuran and 1,2-dichlorobenzene. The polarity of each solvent is indicated by dimension less solvent polarity parameter,  $E_T^N$  parameter proposed by Reichardt [36].  $E_T^N$  parameter corresponding to each solvent is calculated using the charge transfer absorption maximum of standard betaine dye.

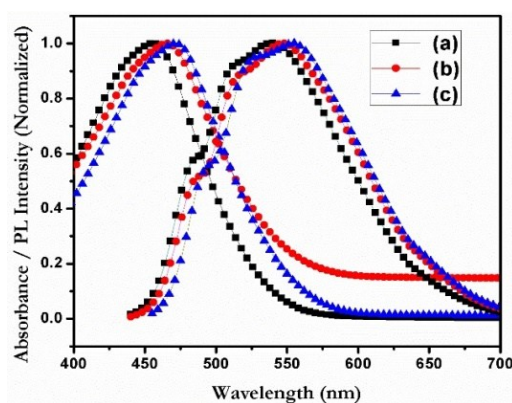


**Fig. 4.5:** Normalized absorption and emission spectra of P(EDOT-FL) in solvents of varying polarity, where (a) 1,4-dioxane, (b) tetrahydrofuran and (c) 1,2-dichlorobenzene

The absorption maxima and emission maxima obtained are shown in Table 4.1 with respect to solvent polarity parameter, [37]. The values corresponding to solvent polarity of each solvent were taken from literature. As the solvent polarity was increased from dioxane to dichlorobenzene, both absorption maxima and emission maxima exhibited a redshift. Thus the polymer exhibited positive solvatochromism, and it was due to the intramolecular charge transfer between donor and acceptor groups [30].

**Table 4.1:** Bathochromic shift of absorption and emission band with the polarity of the solvents

Solvent	$E_T^N$	$\lambda_{max}^{absorption}$ (nm)	■ (nm)
1,4-Dioxane	0.164	462	541
Tetrahydrofuran	0.207	466	548
1,2-Dichlorobenzene	0.225	472	556

#### 4.4.3 Electrical conductivity of P(EDOT-FL) thin films

The charge transport properties in conjugated polymers is a function of mobility, which in turn depends on polymer morphology and applied electric field [38,39]. Usually conjugated polymers exhibit nondispersive hole transport [40]. Presence of traps are a serious issue, which affects the charge transport through the polymer. The slow decay of photocurrent observed in P(EDOT-FL) and P(EDOT-FL):PCBM blend films indicate the presence of traps in the films. The studies on how the trapping-detraping phenomena affects the photoconductive properties of the polymer samples are still going on.

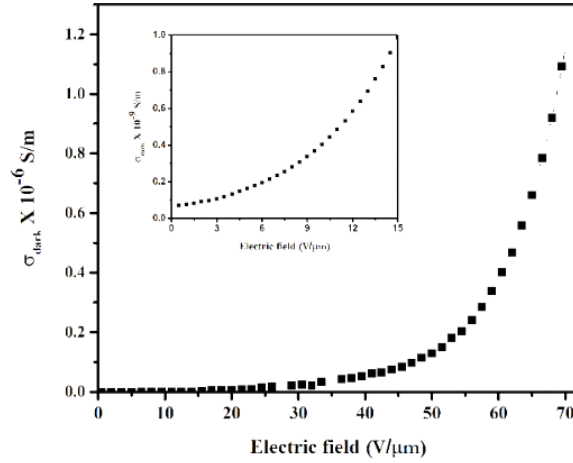


**Fig. 4.6:** Dark conductivity of P(EDOT-FL) films as a function of applied electric field. Inset represents the variation of the dark conductivity at low electric field.

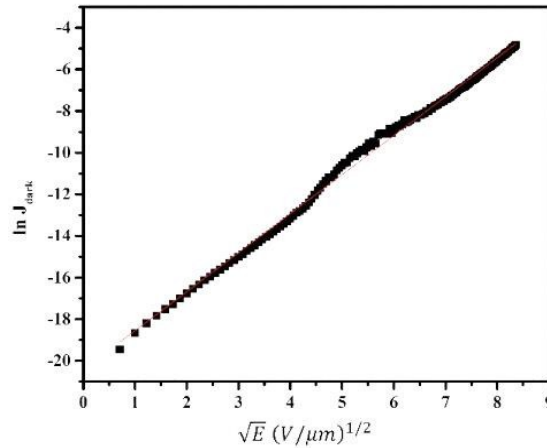


**Fig. 4.7:** Linear correlation between dark current of P(EDOT-FL) films ( $J_{dark}$ ) and applied electric field

It is observed that the dark current ( $J_{dark}$ ) and dark conductivity ( $\sigma_{dark} = J_{dark}/E$ ) of pristine and PCBM blend P(EDOT-FL) films exhibited a pronounced increase at higher electric fields (Fig. 4.6). The samples can withstand electric fields up to  $70 \text{ V}/\mu\text{m}$  and beyond this, the samples undergo dielectric breakdown. A linear correlation between  $\ln J_{dark}$  and  $\sqrt{E}$  was observed (Fig. 4.7). As the field increased to  $70 \text{ V}/\mu\text{m}$ ,

the conductivity in the material exhibited an increment around three orders. In conjugated polymers, the mobility of carriers is a function of electric field and mostly a linear correlation of the form,  $\ln \mu \propto \sqrt{E}$  is observed. This might be the reason for the large dark conductivity at higher electric field, which easily led to dielectric breakdown and limited the applying electric field. This dielectric breakdown is caused by the narrow width between the Fermi level of the ITO -4.80 eV, and the highest occupied molecular orbital of P(EDOT-FL), -5.14 eV [41].

#### 4.4.4 Steady state photocurrent measurements in P(EDOT-FL) films

To study photoconductivity of the samples, steady state photocurrent measurements were carried out on pristine films. Appearance of persistent photoconductivity and very slow decay of the carrier in P(EDOT-FL) limits the accuracy of the steady state photocurrent measurements [42]. In order to increase the accuracy, the measurements were repeated several times in the same sample as well as in other samples prepared at same conditions.

##### 4.4.4.1 Intensity dependence of photocurrent

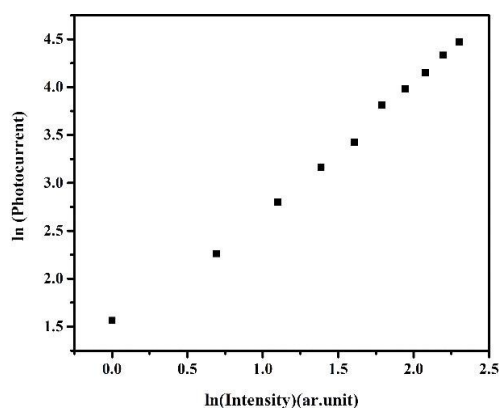


**Fig. 4.8:** The dependence of steady-state photocurrent on the excitation intensity for P(EDOT-FL) films by applying an electric field of  $10\text{V}/\mu\text{m}$ , measured for photons of energy 2.55 eV

Fig. 4.8 illustrates the dependence of photocurrent on the intensity of the laser beam of wavelength 488 nm at an electric field of  $10 \text{ V}/\mu\text{m}$ . Intensity of the light was varied using a polarizer. The power law dependence of the photocurrent with the intensity of the incident photon flux ( $I$ ) was of the form  $J_{PH} \propto I^\beta$ , where  $\beta = 1.26$  for P(EDOT-FL) films. This nearly linear dependence indicates absence of bimolecular recombination of the excitons [31,42].

#### 4.4.4.2 Internal photocurrent efficiency and photoconductive sensitivity

Photoconductive sensitivity is defined as the photoconductivity per unit light intensity. Photogeneration efficiency, defined as the number of carriers generated per absorbed photon, is a significant parameter of a photoconducting device. The traps present in the polymer samples can act as recombination centres which will affect the certainty of the direct calculation of the photogeneration efficiency from the steady state photocurrent measurements. So, the calculation is limited to internal photocurrent efficiency,  $\phi$ , which is defined as the number of measured free charge carriers generated per absorbed photon. This can be calculated from the photocurrent [7] measurements as discussed in Chapter 1. The photogeneration efficiency is always higher than the internal photocurrent efficiency.

The photocurrent measurements were carried out on pristine thin films by varying the electric field through the samples at an illumination intensity of  $125 \text{ mWcm}^{-2}$ . Photoconductive sensitivity and internal photocurrent efficiency of the pristine films were calculated and are plotted as a function of the electric field (Fig. 4.9 and Fig. 4.10). In these pristine

samples, as the electric field increased up to 70 V/ $\mu\text{m}$ , internal photocurrent efficiency increased up to 20% and photoconductive sensitivity was increased up to  $7 \times 10^{-8} \text{ SW}^{-1} \text{ cm}$ . The internal photocurrent efficiency is very large at higher electric fields, which suggest more efficient photogeneration at higher electric field.

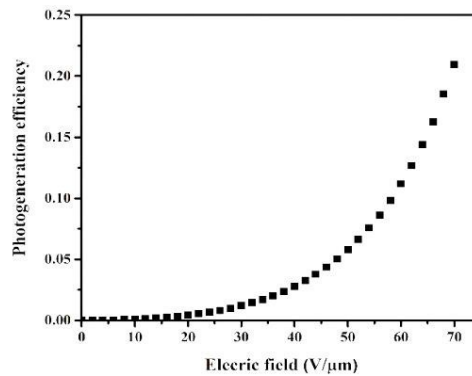


**Fig. 4.9:** The dependence of internal photocurrent efficiency on external electric field for pristine P(EDOT-FL) films measured for photons of energy 2.55 eV and incident intensity of 125 mW/cm<sup>2</sup>

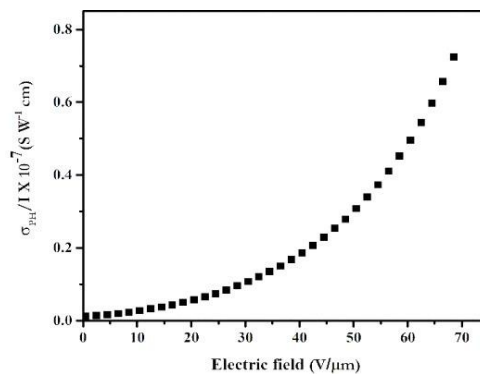


**Fig. 4.10:** The dependence of photoconductive sensitivity on external electric field for pristine P(EDOT-FL) films measured for photons of energy 2.55 eV and incident intensity of 125 mW/cm<sup>2</sup>

## 4.5 Studies on P(EDOT-FL):PCBM blend

In order to enhance the efficiency of photogeneration process, P(EDOT-FL):PCBM blend films were prepared for a polymer to PCBM weight ratios of 1:1 and 1:2. Further increase in concentration of PCBM could not produce neat films. Optical and electrical characterizations were carried out on these blend films and the details are discussed below.

### 4.5.1 Optical Absorption

Optical absorption spectra of pristine and P(EDOT-FL):PCBM blend films prepared on ITO coated glass substrates are shown in Fig. 4.11. P(EDOT-FL):PCBM blend films showed an enhanced absorption in the visible region compared to that of the pristine film. No additional features were observed in the spectra of PCBM blend films indicating negligible overlapping of electronic wave functions of the constituents in the ground state.

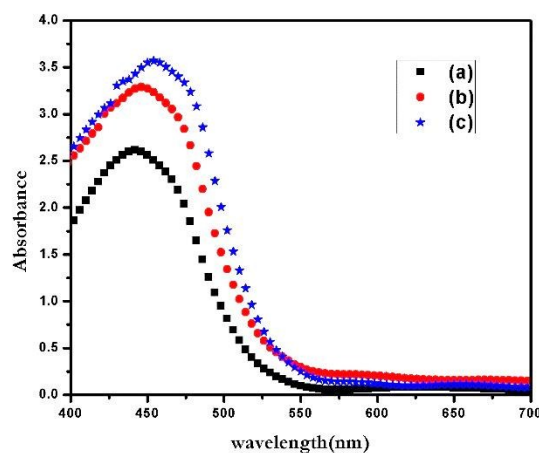


**Fig. 4.11:** Absorption spectra of (a) pristine P(EDOT-FL) film and P(EDOT-FL):PCBM blend films for a weight ratio of (a) 1:1 and (b) 1:2. all these films were prepared on ITO coated glass substrates.

### 4.5.2 Fluorescence quenching

In the PCBM blend films, there can be a possibility of simultaneous exciton generation in PCBM molecule. By comparing the absorption spectra of the polymer with that of the PCBM, the contribution of the exciton from the PCBM molecules was ruled out and it could be assumed that the entire exciton generation was substantially from the polymer molecule itself. Incorporation of PCBM molecule led to the quenching of the fluorescence intensity and the quenching increased with the concentration of PCBM (Fig. 4.12), which revealed the significant interaction of the polymer and PCBM in the excited state. In the case of films with polymer to PCBM ratio of 1:1, the fluorescence intensity was decreased by 90% and for a ratio of 1:2, fluorescent emission from the sample was almost lost. This suggested that, at higher concentration, practically all excitons got quenched at the acceptor molecules.

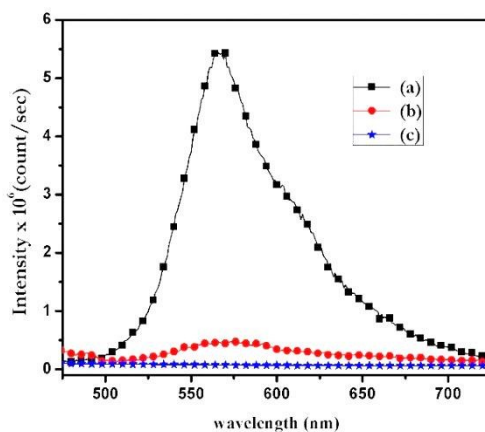


**Fig. 4.12:** Fluorescence spectra of (a) pristine P(EDOT-FL) film and P(EDOT-FL):PCBM blend films for a weight ratio of (b) 1:1 and (c) 1:2, under the excitation of photons with energy 2.80 eV

The quenching of fluorescence intensity was either due to energy transfer reaction or due to charge transfer reaction between donor and acceptor. Since P(EDOT-FL):PCBM blend films were excited with low energy photons, the photoinduced charge transfer was much faster at the P(EDOT-FL):PCBM interface [13]. This charge transfer resulted in high photogeneration efficiency for the blend films. Numerous organic composites, incorporated with PCBM exhibited faster photoinduced charge transfer at short distances [43].

Efficiency of the exciton dissociation depends on diffusion length of the exciton in the polymer, which is the distance from the exciton generation sites to the interface of the acceptor molecule. The increased quenching of fluorescence intensity with the concentration of PCBM could be treated as a measure of decrease in average distance for the exciton to travel to reach the acceptor. Also the life time of the exciton got decreased rapidly as the concentration of the PCBM increased [44]. These arguments suggest that, as the concentration of the PCBM increases, the exciton needs to take less time to find a PCBM molecule to dissociate.

### **4.5.3 Steady state photocurrent measurements in P(EDOT-FL):PCBM films**

#### **4.5.3.1 Intensity dependence of photocurrent**

To study photoconductivity of the samples, steady state photocurrent measurements were carried out in blend films for different concentrations of PCBM. Fig. 4.13 illustrates the dependence of photocurrent on the intensity of the laser beam of wavelength 488 nm by applying an electric field of  $10 \text{ V}/\mu\text{m}$ . Intensity of the light was varied by using a polarizer. The steady state photocurrent exhibited by pristine and blend films depended on the intensity

of the light in a slightly different way. The power law dependence of the photocurrent with the intensity of the incident photon flux ( $I$ ) was of the form  $J_{PH} \propto I^\beta$ , where  $\beta = 1.20$  and  $1.18$  for films with P(EDOT-FL) to PCBM ratio 1:1 and 1:2 respectively. This nearly linear dependence indicated the absence of bimolecular recombination [31,42]. The results also revealed the strong dependence of carrier generation on the concentration of PCBM.

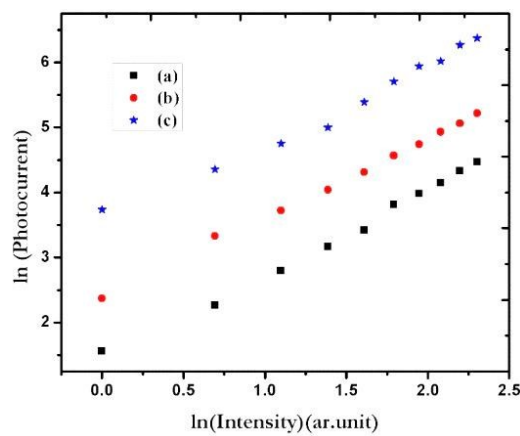


**Fig. 4.13:** The dependence of steady state photocurrent on the excitation intensity for (a) pristine P(EDOT-FL) films, and P(EDOT-FL):PCBM blend films for a weight ratio of (a) 1:1 and (b) 1:2, by applying an electric field of  $10\text{V}/\mu\text{m}$ , measured for photons of energy  $2.55\text{ eV}$ .

#### 4.5.3.2 Internal photocurrent efficiency and photoconductive sensitivity

The photocurrent measurements were carried out on PCBM blend thin films as a function of the electric field at an illumination intensity of  $125\text{ mWcm}^{-2}$ . Photoconductive sensitivity and internal photocurrent efficiency of the pristine and PCBM blend films were calculated and are plotted as a function of the electric field (Fig. 4.14 and Fig. 4.15). As the concentration of PCBM in the film was increased, internal photocurrent efficiency and thus photoconductive sensitivity increased with increase in external electric field.

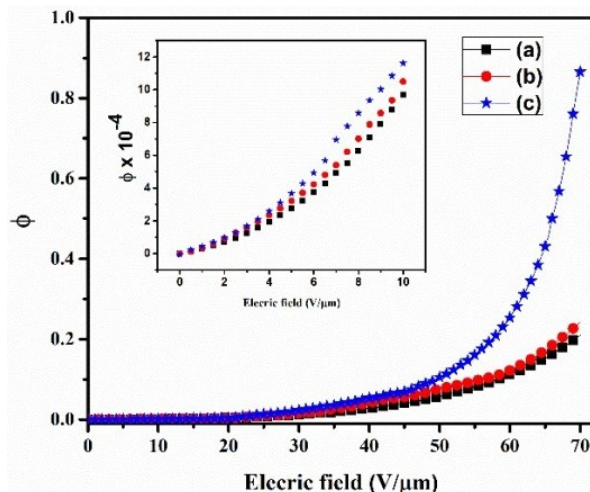


**Fig. 4.14:** The dependence of internal photocurrent efficiency on external electric field for (a) pristine P(EDOT-FL) films and P(EDOT-FL):PCBM blend films for a weight ratio of 1:1 and (b) 1:2, measured for photons of energy of 2.55 eV and an incident intensity of 125 mW/cm<sup>2</sup>.

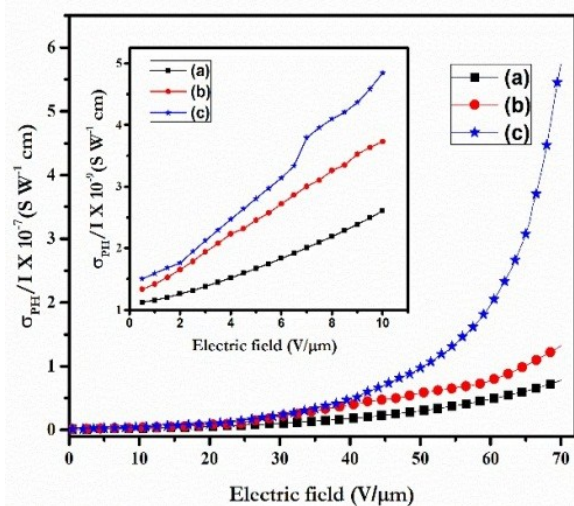


**Fig. 4.15:** The dependence of photoconductive sensitivity on external electric field for (a) pristine P(EDOT-FL) films and P(EDOT-FL):PCBM blend films for a weight ratio of 1:1 and (b) 1:2, measured for photons of energy of 2.55 eV and an incident intensity of 125 mW/cm<sup>2</sup>.

For the films with P(EDOT-FL) to PCBM ratio of 1:1, the internal photocurrent efficiency increased by 26% at an electric field of 70 V/ $\mu\text{m}$  and photoconductive sensitivity increased up to  $1.3 \times 10^{-7}$  SW<sup>-1</sup>cm. When P(EDOT-FL) to PCBM ratio was changed to 1:2, a maximum of 86% internal photocurrent efficiency and a photoconductive sensitivity of  $5.44 \times 10^{-7}$  SW<sup>-1</sup>cm were achieved. In all these samples, irrespective of PCBM concentration, the internal photocurrent efficiency was very large at higher electric fields, which suggested more efficient photogeneration at higher electric field.

It is significant that pristine P(EDOT-FL) and P(EDOT-FL):PCBM blend films exhibit good photoconductive sensitivity at low applied electric fields (<10 V/ $\mu\text{m}$ ). At 10 V/ $\mu\text{m}$ , the values of photoconductive sensitivities were 2.60, 3.73 and  $4.85 \times 10^{-9}$  SW<sup>-1</sup>cm respectively for samples with P(EDOT-FL) to PCBM ratios of 1:0, 1:1 and 1:2 respectively. Corresponding internal photocurrent efficiencies were 9.7, 10.5 and  $11.6 \times 10^{-4}$  respectively.

#### **4.6 Band diagram and photoinduced charge separation**

Photoconductivity in polymers is associated with the subsequent dissociation of the excitons formed upon irradiation and the transport of free carriers through the material via hopping. Photoinduced charge transfer can occur either between two covalently bonded donor and acceptor moieties (intramolecular charge transfer) or between moieties that are spatially very close to each other (intermolecular charge transfer) [43]. An electron transfer from donor to acceptor will be possible only if the offset between the LUMO levels of donor and acceptor is large enough to overcome the Coulombic attraction between the electron hole pairs [13].

An external electric field or excess thermal energy can lower the potential barrier due to Coulombic attraction, which leads to the increased carrier generation [45]. It has been reported that the offset between the LUMO level of the donor and the LUMO level of the acceptor should be at least 0.30 eV to drive the charge separation [46,47].

When the sensitizer PCBM is incorporated into the P(EDOT-FL), it is assumed that PCBM is uniformly distributed throughout the volume and the polymer composite is electrically neutral along with the electron accepting sensitizer. When the polymer matrix is excited, an electron is transferred from the polymer matrix to the sensitizer and the hole left is free to move through the hole transporting polymer matrix via hopping.

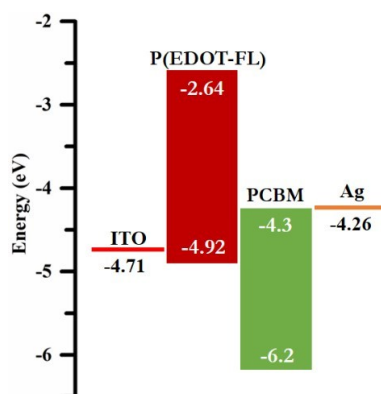


**Fig. 4.16:** Energy band diagram of P(EDOT-FL) and PCBM. Also work functions of electrodes are presented.

The LUMO level of the PCBM is at -4.3 eV [48] and the LUMO energy level of the P(EDOT-FL) calculated using CV measurements and the optical band gap was -2.19 eV [16]. Hence the energy offset between the LUMO levels of polymer and PCBM is 2.11 eV (Fig. 4.16) which is high enough to overcome the Coulombic attraction between the charges, leading

to the charge separation at the P(EDOT-FL):PCBM interface. The higher values of internal photocurrent efficiency in blend films compared to that of the pristine film is a clear indication of the effective charge separation at the P(EDOT-FL):PCBM interface.

Due to the low dielectric constant of polymers, the Coulomb interaction between electron and hole is much high, causing low photogeneration efficiency. An external electric field can increase shielding of the Coulomb field and can result in an effective exciton dissociation [49]. At steady state, photoconductivity can be related to carrier generation rate per unit volume  $G$ , which in turn is proportional to illumination intensity and the recombination rate described by the carrier life time  $\tau$  using the relation  $\sigma_{PH} = G\tau e\mu$ , where  $\mu$  is the mobility [42]. By Langevin's model for the efficiency of recombination of free carriers in amorphous solids, the carrier life time  $\tau \propto 1/\mu$ . This suggests that the increase in photoconductivity due to any increase in the mobility of the carriers as a result of the increased electric field is compensated by a decrease in carrier lifetime. Hence the increased photoconductivity at higher electric fields can be attributed to higher photogeneration efficiency of charge carrier [50].

The photocurrent and hence the photoconductivity of the pristine and blend films exhibits super linear power law dependence with the electric field, which reflects the major role of the electric field on exciton dissociation. The bimolecular recombination is inversely proportional to the external electric field [51]. So the field induced exciton dissociation dominates at higher electric field, and leads to higher photogeneration efficiency.

The photocurrent through a material is determined by the photogeneration rate and recombination rate of the free electrons and holes. Existence of strong fluorescence in the pristine film leads to higher recombination rate of excitons and free carriers, which limits the photocurrent through the film. According to the model suggested by V. I. Arkhipov *et al.* [12], the blending of conjugated polymer with electron acceptor strongly promotes the exciton dissociation. Hence the higher photogeneration efficiency at higher acceptor concentration is due to the increase in exciton dissociation rates rather than the decrease in the rate of monomolecular decay of the geminate pair of electron and hole.

## 4.7 Summary

In this chapter, a low band gap donor-acceptor conjugated copolymer, P(EDOT-FL) was studied. Studies were concentrated on pristine and PCBM blend films. The positive solvatochromism exhibited by the polymer has revealed the possibility of photoconductivity even in the pristine P(EDOT-FL) polymer film. P(EDOT-FL) thin films can withstand high electric field of  $70 \text{ V}/\mu\text{m}$  with an internal photocurrent efficiency of 20%. The performance of the P(EDOT-FL) polymer was better than the non-conjugated polymer blend, polybenzoxazine with PCBM. Hence it is suitable as a photoconducting host for photorefractive applications. Since it has good photoconducting performance in the pristine form, it can eliminate the chances of phase separation usually encountered while preparing photorefractive polymer composite can be overcome.

Incorporation of PCBM resulted in intense quenching of the fluorescence and enhanced photoconductivity. Photoconductive properties

of blend films improved with the concentration of PCBM, due to efficient exciton dissociation. The steady state photocurrent measurements on pristine P(EDOT-FL) and P(EDOT-FL):PCBM blend films also revealed that both the internal photocurrent efficiency and photoconductive sensitivity strongly depended on the concentration of PCBM and external electric field. An internal photocurrent efficiency of 86% was obtained for blend films, with P(EDOT-FL) to PCBM ratio 1:2.

The P(EDOT-FL) and P(EDOT-FL):PCBM blend films exhibited good photoresponse even at low electric fields. So the polymer material could safely operate in the low electric field region, without undergoing dielectric breakdown. The obtained values of internal photocurrent efficiency and photoconductive sensitivity at low field region were much higher compared to the values of the reported photorefractive polymer composites [52,53].

## References

- [1] B. Kippelen, K. Tamura, N. Peyghambarian, A.B. Padias, J. H. K. Hall, Photorefractivity in a functional side-chain polymer, *Phys. Rev. B.* 48 (1993) 10710–10718.
- [2] C. Zhao, C. Park, P.N. Prasad, Y. Zhang, S. Ghosal, R. Burzynski, Photorefractive polymer with side-chain second-order nonlinear optical and charge-transporting groups, *Chem. Mater.* 7 (1995) 1237–1242.
- [3] D.T. McQuade, A.E. Pullen, T.M. Swager, Conjugated polymer-based chemical sensors, *Chem. Rev.* 100 (2000) 2537–2574.
- [4] M.C. Scharber, D. Mühlbacher, M. Koppe, P. Denk, C. Waldauf, A.J. Heeger, C.J. Brabec, Design rules for donors in bulk-heterojunction solar cells- towards 10% energy-conversion efficiency, *Adv. Mater.* 18 (2006) 789–794.

- 
- [5] L. Sims, H.J. Egelhaaf, J.A. Hauch, F.R. Kogler, R. Steim, Plastic solar cells, *Adv. Funct. Mater.* 11 (2001) 15–26.
- [6] J. Thomas, C.W. Christenson, P.A. Blanche, M. Yamamoto, R.A. Norwood, N. Peyghambarian, Photoconducting polymers for photorefractive 3D display applications, *Chem. Mater.* 23 (2011) 416–429.
- [7] B. Lynn, P.A. Blanche, N. Peyghambarian, Photorefractive polymers for holography, *J. Polym. Sci. Part B Polym. Phys.* 52 (2014) 193–231.
- [8] Y. Cheng, S. Yang, C. Hsu, Synthesis of conjugated polymers for organic solar cell applications, *Chem. Rev.* 109 (2009) 5868–5923.
- [9] P. Leriche, P. Fre, A. Cravino, O. Ale, J. Roncali, Molecular engineering of the internal charge transfer in thiophene-triphenylamine hybrid  $\pi$ -conjugated systems, *J. Org. Chem.* 72 (2007) 8332–8336.
- [10] K.G. Jespersen, W.J.D. Beenken, Y. Zaushitsyn, A. Yartsev, M. Andersson, T. Pullerits, V. Sundström, The electronic states of polyfluorene copolymers with alternating donor-acceptor units, *J. Chem. Phys.* 121 (2004) 12613–12617.
- [11] S.E. Shaheen, R. Radspinner, N. Peyghambarian, G.E. Jabbour, Fabrication of bulk heterojunction plastic solar cells by screen printing, *Appl. Phys. Lett.* 79 (2001) 2996–2998.
- [12] V.I. Arkhipov, P. Heremans, H. Bässler, Why is exciton dissociation so efficient at the interface between a conjugated polymer and an electron acceptor?, *Appl. Phys. Lett.* 82 (2003) 4605–4607.
- [13] R. Koeppel, N.S. Sariciftci, Photoinduced charge and energy transfer involving fullerene derivatives, *Photochem. Photobiol. Sci.* 5 (2006) 1122–31.
- [14] E. Hendry, P.J. Hale, J. Moger, A.K. Savchenko, Coherent nonlinear optical response of graphene, *Phys. Rev. Lett.* 105 (2010) 1–4.
- [15] A. Abbas, J.J. Pillai, S. Narayanan, K. Sreekumar, R. Joseph, Study on the photoconductive properties of charge carriers in donor- acceptor copolymer P(EDOT-FL) and P(EDOT-FL): PCBM blend, *Synth. Met.* 233 (2017) 52–57.

- [16] S. Narayanan, A. Abbas, S.P. Raghunathan, K. Sreekumar, C.S. Kartha, R. Joseph, Theoretical and experimental investigations on the photoconductivity and nonlinear optical properties of donor–acceptor  $\pi$  conjugated copolymer, poly(2,5-(3,4-ethylenedioxythiophene)-alt-2,7-(9,9-dioctylfluorene)), *RSC Adv.* 5 (2015) 8657–8668.
- [17] B.L. Groenendaal, F. Jonas, D. Freitag, H. Pielartzik, J.R. Reynolds, Poly(3,4-ethylenedioxythiophene) and its derivatives: past, present, and future, *Adv. Mater.* 12 (2000) 481–494.
- [18] B.L. Groenendaal, G. Zotti, P. Aubert, S.M. Waybright, J.R. Reynolds, Electrochemistry of poly(3,4-alkylenedioxythiophene) derivatives, *Adv. Mater.* 15 (2003) 855–879.
- [19] J. Roncali, P. Blanchard, P. Fre, 3,4-Ethylenedioxythiophene (EDOT) as a versatile building block for advanced functional p-conjugated systems, *J. Mater. Chem.* 15 (2005) 1589–1610.
- [20] C.B. Nielsen, A. Angerhofer, K.A. Abboud, J.R. Reynolds, V. Gaines, Discrete photopatternable  $\pi$ -conjugated oligomers for electrochromic devices, *J. Am. Chem. Soc.* 130 (2008) 9734–9746.
- [21] B.I. Schwendeman, C.L. Gaupp, J.M. Hancock, L. Groenendaal, J.R. Reynolds, Perfluoroalkanoate-substituted PEDOT for electrochromic device applications, *Adv. Funct. Mater.* 13 (2003) 541–547.
- [22] K. Krishnamoorthy, R.S. Gokhale, A.Q. Contractor, A. Kumar, A. Asaf, A. Marg, Novel label-free DNA sensors based on poly(3,4-ethylenedioxythiophene), *Chem. Commun.* (2004) 820–821.
- [23] B. Winther-Jensen, O. Winther-Jensen, M. Forsyth, D.R. MacFarlane, High rates of oxygen reduction over a vapor phase–polymerized PEDOT electrode, *Science* 321 (2008) 671–674.
- [24] F. Wu, P. Shih, C. Shu, Highly efficient light-emitting diodes based on fluorene copolymer consisting of triarylamine units in the main chain and oxadiazole pendent groups, *Macromolecules.* 38 (2005) 9028–9036.
- [25] Y. Yang, Q. Pei, Efficient blue-green and white light-emitting electrochemical cells based on poly[9,9-bis(3,6-dioxaheptyl)-fluorene-2,7-diy], *J. Appl. Phys.* 81 (1997) 3294–3298.

- [26] F. Tran-van, C. Chevrot, O. Ste, New organic materials for light emitting devices based on dihexylfluorene-co-ethylenedioxythiophene copolymers exhibiting improved hole-injecting properties, *Synth. Met.* 131 (2002) 31–40.
- [27] W. Wu, C. Liu, W. Chen, Synthesis and characterization of new fluorene-acceptor alternating and random copolymers for light-emitting applications, *Polymer.* 47 (2006) 527–538.
- [28] E. Bundgaard, F.C. Krebs, Low band gap polymers for organic photovoltaics, *Sol. Energy Mater. Sol. Cells.* 91 (2007) 954–985.
- [29] W.A. Braunecker, S.D. Oosterhout, Z.R. Owczarczyk, N. Kopidakis, E.L. Ratcli, D.S. Ginley, D.C. Olson, Semi-random vs well-defined alternating donor-acceptor copolymers, *ACS Macro Lett.* 3 (2014) 622–627.
- [30] S.A. Jenekhe, L. Lu, M.M. Alam, New conjugated polymers with donor-acceptor architectures: synthesis and photophysics of carbazole-quinoline and phenothiazine-quinoline copolymers and oligomers exhibiting large intramolecular charge transfer, *Macromolecules.* 34 (2001) 7315–7324.
- [31] V.C. Kishore, R. Dhanya, K. Sreekumar, R. Joseph, C.S. Kartha, Spectral distribution of photocurrent in poly(6-tert-butyl-3-methyl-3,4-dihydro-2H-1,3-benzoxazine), *Synth. Met.* 158 (2008) 676–680.
- [32] V.I. Arkhipov, H. Bassler, M. Deussen, E.O. Gobel, R. Kersting, H. Kurz, U. Lemmer, R.F. Mahrt, Field-induced exciton breaking in conjugated polymers, *Phys. Rev. B.* 52 (1995) 4932–4940.
- [33] A.M. Mehranpour, S. Hashemnia, Solvatochromism in binary solvent mixtures by means of a penta-tert-butyl pyridinium N-phenolate betaine dye, *J. Chinese Chem. Soc.* 53 (2006) 759–765.
- [34] R.S. Mulliken, W.B. Person, *Molecular complexes: a lecture and reprint volume*, Wiley-Interscience, New York, London, 1969.
- [35] L. Remy, A. Clemence, B. Guillaume, F. Schmidt, C. Fiorini-Debuisscher, F. Charra, M.P. Teulade-Fichou, Synthetic strategies to derivatizable triphenylamines displaying high two-photon absorption, *J. Org. Chem.* 73 (2008) 1732–1744.

- [36] C. Reichardt, Solvatochromic dyes as solvent polarity indicators, *Chem. Rev.* 94 (1994) 2319–2358.
- [37] V.C. Kishore, R. Dhanya, K. Sreekumar, R. Joseph, C. Sudha Kartha, On the dipole moments and first-order hyperpolarizability of N,N-bis(4-bromobutyl)-4-nitrobenzenamine, *Spectrochim. Acta-Part A Mol. Biomol. Spectrosc.* 70 (2008) 1227–1230.
- [38] F.C. Grozema, L.D.A. Siebbeles, Charge mobilities in conjugated polymers measured by pulse radiolysis time-resolved microwave conductivity: from single chains to solids, *J. Phys. Chem. Lett.* 2011, 2 (2011) 2951–2958.
- [39] F. Chemie, What determines the mobility of charge carriers in conjugated polymers?, *Philos. Trans. A. Math. Phys. Eng. Sci.* 365 (2007) 1473–1487.
- [40] C. Liu, S. Chen, Charge mobility and charge traps in conjugated polymers, *Macromol. Rapid Commun.* 28 (2007) 1743–1760.
- [41] N. Tsutsumi, Molecular design of photorefractive polymers, *Polym. J.* 48 (2016) 571–588.
- [42] J.C. Scott, L.T. Pautmeier, W.E. Moerner, Photoconductivity studies of photorefractive polymers, *J. Opt. Soc. Am. B.* 9 (1992) 2059.
- [43] N. Sariciftci, L. Smilowitz, A.J. Heeger, F. Wudl, Photoinduced electron transfer from a conducting polymer to buckminsterfullerene., *Science.* 258 (1992) 1474–1476.
- [44] A. Bruno, L.X. Reynolds, J. Nelson, S.A. Haque, Determining the exciton diffusion length in a poly fluorene from ultrafast fluorescence measurements of polymer/fullerene blend films, *J. Phys. Chem. C.* 117 (2013) 19832–19838.
- [45] V. Gulbinas, Y. Zaushitsyn, H. Bässler, A. Yartsev, V. Sundström, Dynamics of charge pair generation in ladder-type poly(para-phenylene) at different excitation photon energies, *Phys. Rev. B - Condens. Matter Mater. Phys.* 70 (2004) 1–7.
- [46] M.C. Scharber, D. Mühlbacher, M. Koppe, P. Denk, C. Waldauf, A.J. Heeger, C.J. Brabec, Design rules for donors in bulk-heterojunction solar cells- towards 10 % energy-conversion efficiency, *Adv. Mater.* 18 (2006) 789–794.

- [47] B. Carsten, J.M. Szarko, Hae, J. Son, W. Wang, L. Lu, F. He, B.S. Rolczynski, S.J. Lou, L.X. Chen, L. Yu, Examining the effect of the dipole moment on charge separation in donor-acceptor polymers for organic photovoltaic applications, *J. Am. Chem. Soc.* 133 (2011) 20468–20475.
- [48] Y. Liang, Y. Wu, D. Feng, S.T. Tsai, H.-J. Son, G. Li, L. Yu, Development of new semiconducting polymers for high performance solar cells, *J. Am. Chem. Soc.* 131 (2009) 56–57.
- [49] H.S. Nalwa, S. Miyata, *Nonlinear Optics of Organic Molecules and Polymers*, CRC Press, 1996.
- [50] G. Bäuml, S. Schloter, U. Hofmann, D. Haarer, Correlation between photoconductivity and holographic response time in a photorefractive guest host polymer, *Opt. Commun.* 154 (1998) 75–78.
- [51] M. Obarowska, J. Godlewski, Electric field dependence of the bimolecular recombination rate of the charge carriers, *Synth. Met.* 109 (2000) 219–222.
- [52] T. Däubler, R. Bittner, K. Meerholz, V. Cimrová, D. Neher, Charge carrier photogeneration, trapping, and space-charge field formation in PVK-based photorefractive materials, *Phys. Rev. B.* 61 (2000) 13515–13527.
- [53] T.K. Däubler, L. Kulikovsky, D. Neher, Photoconductivity and charge-carrier photogeneration in photorefractive polymers, *Proc. SPIE.* 4462 (2002) 206–216.



## Photoconductive Aspects of Benzothiadiazole Copolymers

### Abstract

This chapter presents the photophysical and photoconductive properties of newly synthesized low band gap donor-acceptor conjugated copolymers based on 2,1,3-benzothiadiazole (BTZ), which exhibits high acceptor strength. Triphenylamine (TPA), 3-hexylthiophene (HT) and 3,4-dihexyloxythiophene (HXT) are donor moieties. The copolymers synthesized and studied are poly(benzothiadiazole-triphenylamine) labelled as P(BTZ-TPA), poly(benzothiadiazole-hexylthiophene) labelled as P(BTZ-HT) and poly(benzothiadiazole-dihexyloxythiophene) labelled as P(BTZ-HXT). Optical properties of these synthesized polymers were analyzed by recording steady state absorption and emission spectra. Band gap of the polymers was finely tuned in these polymers in accordance with the donor strength of the donor moieties. The polymers exhibited good fluorescence emission in the red region. Solvatochromic experiments were carried out using a binary mixture consisting of toluene and acetonitrile to understand the solvent dependence on the ground state and excited states P(BTZ-TPA). Carrier generation and transport of the generated carriers upon photo-excitation was studied in detail, in pristine and P(BTZ-TPA):PCBM blend films, by performing photoconductivity studies using broad spectral source and lasers of wavelengths 488 nm and 632 nm. The blend films exhibited good photoresponse over the entire visible region, with promising internal photocurrent efficiency. Quenching of fluorescence was observed in PCBM blend films. The quenching of fluorescence emission is assigned to the charge transfer reaction between copolymer and PCBM, and was confirmed by substantial increment in photoconductivity of the blend films. An internal photocurrent efficiency of 17.4% was obtained in P(BTZ-TPA):PCBM blend films for a biasing field of  $10\text{ V}/\mu\text{m}$ . The photoconductive performance of P(BTZ-HT):PCBM and P(BTZ-HXT):PCBM blend films were compared with that of P(BTZ-TPA):PCBM blend films.

## 5.1 Introduction

The concept of donor-acceptor (D-A) architecture has become an encouraging breakthrough in the design of conducting conjugated polymers. The donor-acceptor conjugated polymers are extensively used in electronic devices due to their enhanced opto-electronic properties [1]. The band gap and fluorescence emission of these polymers can be finely tuned by modifying the polymer structure through appropriate assortment of electron donating and electron accepting moieties along the polymer backbone [2]. Tuning of the band gap towards the visible regime is a necessity for enabling optoelectronic and photovoltaic applications [3,4]. In addition, the LUMO energy levels should have appropriate value for the efficient exciton dissociation at the donor-acceptor interface [5]. The conjugative coupling between donor and acceptor moieties through the  $\pi$  -bonding results in a charge transfer band, at the higher wavelength of the visible spectrum. Strength of the acceptor group and length of the  $\pi$  conjugation govern the D-A interactions. Monomer segments with high HOMO and low LUMOs are found to be effective for fabricating low band gap polymers through effective inter-chain charge transfer [6]. The D-A copolymers have versatile applications in the progressive technologies including polymer solar cell [7–11], light emitting diodes [12,13], and electrochromic devices [14–16]. The problem of inefficient charge separation in pristine conjugated polymer, upon photo-excitation, can be overcome by creating bulk heterojunction with a suitable electron acceptor. Here, the photoexcited electrons get transferred to the acceptor molecule, and the resulting positive charges (holes) in the conjugated polymer are found to be highly delocalized and mobile [9].

2,1,3-Benzothiadiazoles (BTZ) were used as electron acceptor in combination with numerous donor moieties which resulted in compounds with enhanced absorption at higher wavelength region and having lower band gap, compared with other donor-acceptor copolymers [17,18]. Hence, there is greater research interest in this moiety owing to its extensive applications in organic electronics [19]. The coplanar structure of BTZ promotes delocalization of electrons along the entire polymer chain and thus make a path way for intra/inter molecular interactions. Benzothiadiazole compounds exhibit good stability, and high values of reduction potential and electron affinity [20]. The structure of BTZ is shown in Fig. 5.1.

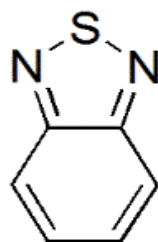


**Fig. 5.1:** Structure of 2,1,3-Benzothiadiazole

Triphenylamine (TPA), 3-hexylthiophene (HT) and 3,4-dihexyloxythiophene (HXT) are selected as donor moieties. The structure of these donor moieties are shown in Fig. 5.2. Donor strength of HT is greater than the donor strength of TPA and donor strength of HXT is greater than the donor strength of HT. The copolymers synthesized are poly(benzothiadiazole-triphenylamine), poly(benzothiadiazole-hexylthiophene) and poly(benzothiadiazole-dihexyloxythiophene). Effective donor-acceptor interaction [21] resulted in the visible absorption over a wide range and provided good charge transport [22]. By incorporating these monomers

into BTZ in a repeating polymer unit, it was expected that the band gap of the polymer could be tailored to give absorption at higher wavelength.

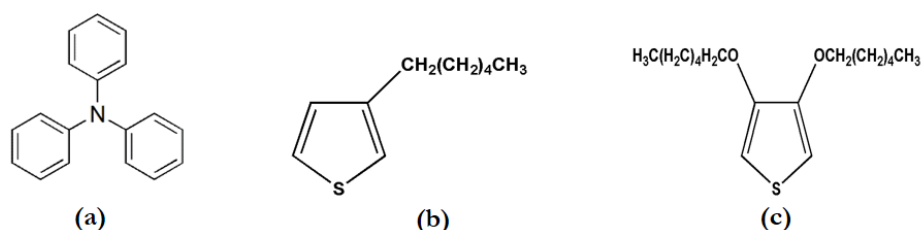


**Fig. 5.2:** Structure of (a) triphenylamine, (b) 3-hexylthiophene and (c) 3,4-dihexyloxythiophene

The goal of this work was to evaluate the optical and photoconductive properties of the newly synthesized conjugated donor-acceptor copolymers which can be used for photorefractive applications. The donor-acceptor design facilitates intrachain charge transfer through strong  $\pi$ -conjugation, up to some extent, which results in generation of free carriers upon photo-excitation with low photogeneration efficiency. However, promising results are obtained in photoconductivity experiment with the incorporation of another acceptor molecule, PCBM (phenyl-C<sub>61</sub>-butyric acid methyl ester). Photoconductivity in organic polymers depends on several factors, including photon absorption, generation of free carriers and their transport through the material. Here, detailed investigations on P(BTZ-TPA) and P(BTZ-TPA):PCBM blend were carried out in this direction by assessing absorbance and fluorescence spectra, conducting solvatochromic experiments along with steady state and transient photoconductivity studies. These results were compared with the photoconductive performance of P(BTZ-HT):PCBM and P(BTZ-HXT):PCBM blends.

## 5.2 Experimental

Optical studies were performed on spin-coated thin films, prepared on ITO coated glass substrates, having thickness of typically  $1 \mu\text{m}$ . A spin coating unit of model SPIN 150 (SPS Euorope) was used. For coating films, solutions with polymer to PCBM ratios, 1:0 (pristine) and 1:1 were initially prepared in spectroscopic grade chloroform and spin coated to get uniform films. Films were prepared by spinning the substrate at a speed of 800 rpm for 60 s. The acceleration of the spinning was fixed to 800 rpm/s. For electrical measurements, a sandwich cell structure ITO/polymer:PCBM/Ag was used. Silver electrodes of thickness  $\approx 50 \text{ nm}$  were deposited using thermal evaporation. Before the thermal evaporation of the top contact, the spin coated samples were stored for 12 h in a vacuum desiccator for the complete removal of the solvent. The active area of the device was  $3 \text{ mm}^2$ . Thickness of the films was measured using Dektak stylus profiler. The absorption spectra of the samples were taken using a Jasco V-570 UV-visible-NIR spectrophotometer. Fluorescence spectra were recorded with a Horiba Fluoromax-3 fluorescence spectrometer.

Electrical measurements were done using a Keithley 236 Source Measure unit. Steady state photocurrent measurements were done by measuring the DC current through the sample, with and without illumination on the sample. The dark current measured as a function of electric field was subtracted from the current measured after illumination to yield the photocurrent. In order to understand the spectral dependence of photocurrent, measurements were carried out by illuminating the sample with different wavelengths and measured the current for each wavelength.

A 150 W Xenon lamp was used as excitation source. The sample was illuminated for a fixed interval of time to achieve a steady state. The intensity of exciting wavelengths was measured initially using a power meter (Coherent). Normalization of the collected data was done by dividing the obtained photocurrent with the intensity of excitation wavelength. The photocurrent, as a function of intensity of illumination and applied electric fields were measured using CW lasers, He-Ne laser (632.8 nm) and optically pumped solid state diode laser (488 nm).

### 5.3 Studies on P(BTZ-TPA)

Poly(benzothiadiazole-triphenylamine) co-polymer labelled as P(BTZ-TPA) is a conjugated polymer in which 2,1,3-benzothiadiazole (BTZ) moiety acts as electron acceptor and triphenylamine (TPA) acts as donor moiety. The polymer was synthesized via Suzuki coupling method [23]. The structure of P(BTZ-TPA) is shown in Fig. 5.3. Triphenylamine (TPA) has strong electron donor nature with outstanding hole transporting properties and the derivatives of TPA have been widely investigated as active materials for solar cells [24,25]. Recently, TPA was extensively employed for constructing donor building block to develop donor-acceptor, conjugated alternating copolymer for photovoltaic applications [26].

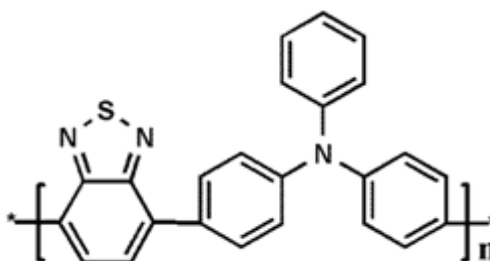


Fig. 5.3: Structure of P(BTZ-TPA)

The synthesized polymer was well dissolved in organic solvents such as chloroform, toluene, THF etc.. The number average molecular weight and weight average molecular weight were 5771 and 8674 respectively. The poly dispersity index is 1.85.

### 5.3.1 Optical properties of P(BTZ-TPA)

#### 5.3.1.1 Optical absorption

Optical absorption spectra of the samples were recorded at ambient conditions. Absorption spectra of P(BTZ-TPA) dissolved in chloroform and P(BTZ-TPA) thin films are presented in Fig. 5.4. As expected, absorption spectra revealed two distinct absorption bands. One band appeared at the higher wavelength region around 400–550 nm centered at 470 nm and other band appeared in the lower wavelength region around 300–400 nm centered at 316 nm. The band at high energy (300-400 nm) arises from the  $\pi \rightarrow \pi^*$  transitions [27] and the low energy band (400-550 nm) corresponds to the intramolecular charge transfer (ICT). During photo-excitation, the electron density around triphenylamine moiety can get transferred to the electron accepting benzothiadazole group [28]. The ICT band of P(BTZ-TPA) thin films exhibited a bathochromic shift of 10 nm and 45 nm for the peak absorption and for the onset of the absorption respectively, when compared to ICT band in solution. This red shift arises due to increased electron delocalization as well as planarization upon solid state close packing [29]. The band edge of the P(BTZ-TPA) thin film was at 603 nm and the corresponding optical band gap was 2.05 eV. This reduced band gap in the solid state form greatly enhances intramolecular charge transfer [30].

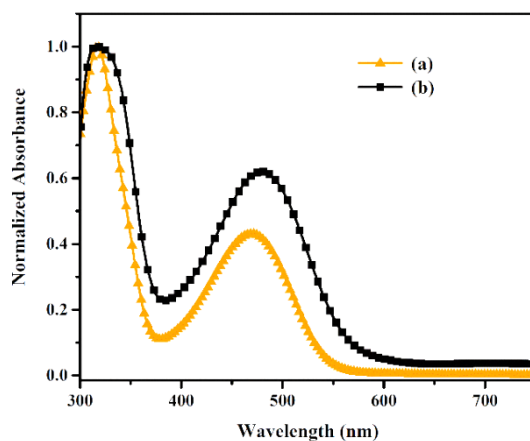


**Fig. 5.4:** Absorption spectra of (a) P(BTZ-TPA) in Chloroform (b) P(BTZ-TPA) thin film deposited over ITO coated glass substrate.

### 5.3.1.2 Fluorescence emission

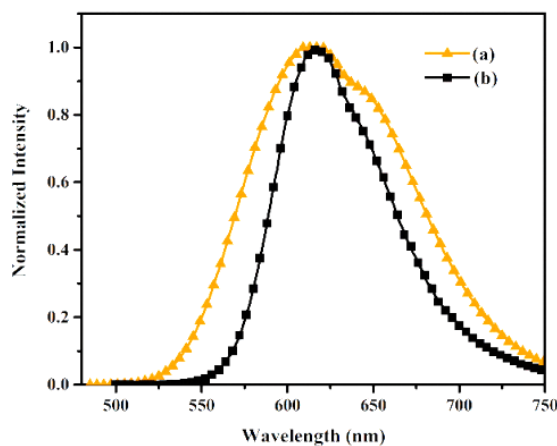


**Fig. 5.5:** Fluorescence spectra of (a) P(BTZ-TPA) solution prepared in chloroform and (b) P(BTZ-TPA) thin film prepared on ITO coated glass substrate. Both samples were excited with photons of energy 2.64 eV.

Fig. 5.5 depicts the fluorescence spectra of copolymer P(BTZ-TPA) in chloroform and spin coated films. The samples were excited with photons of energy 2.64 eV. Both in solution and in film P(BTZ-TPA) exhibited good

fluorescence emission with a peak centred at 615 nm. The emission spectra of P(BTZ-TPA) in solution was much broadened than the emission from thin films. The excitation spectrum of P(BTZ-TPA) for the emission peak at 615 nm was monitored to earn additional information on the nature of the excited state (Fig. 5.6). Excitation spectrum approximately followed the absorption spectrum and revealed that the  $\pi \rightarrow \pi^*$  transition resulted in more intense fluorescence emission.

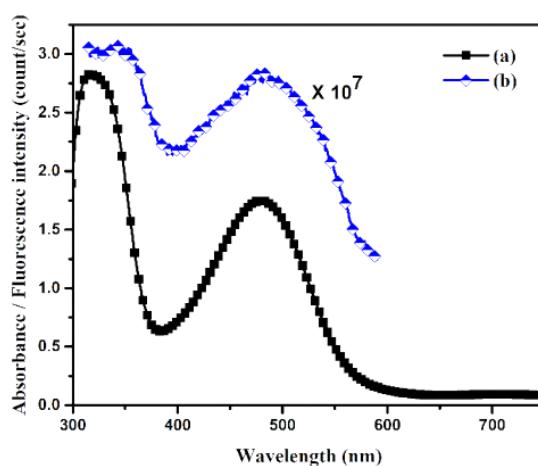


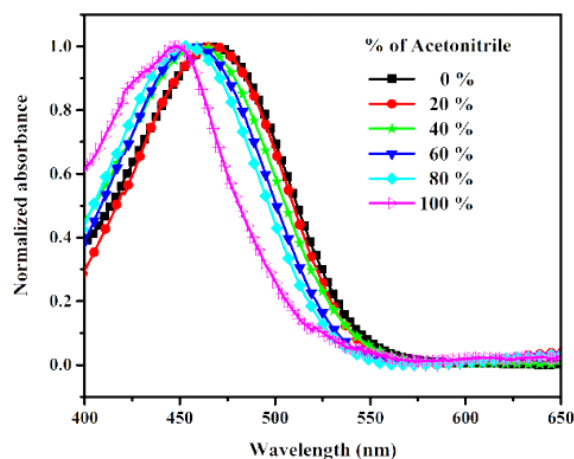
**Fig. 5.6:** (a) Absorption spectra and (b) fluorescence excitation spectra of P(BTZ-TPA) films prepared on ITO coated glass substrates.

Fluorescence quantum yield ( $\eta$ ) of P(BTZ-TPA) was calculated by comparative method, in which a dye of known absolute quantum yield was used as standard. For this, the magnitude of integrated fluorescence intensity of the polymer was plotted against absorbance of the polymer in solvent, in very dilute regime. The quantum yield was estimated by the following relation,  $\eta_{sample} = \frac{Grad_{sample}}{Grad_{standard}} \times \eta_{standard}$ , where Grad represents the gradient from the plot of integrated fluorescence intensity

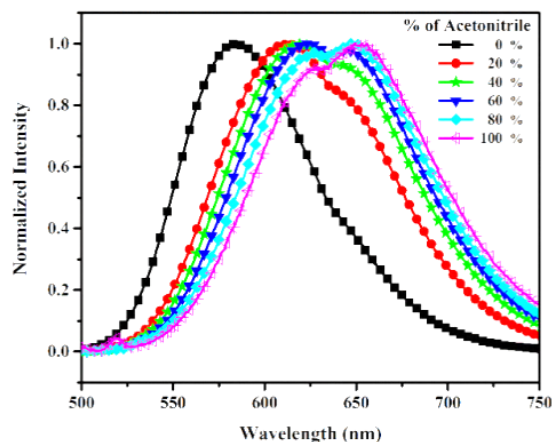
against absorbance. Here, rhodamine 6G ( $\eta_{std}=0.75$  in chloroform [31]) was used as the standard dye. The calculated value of the quantum yield of P(BTZ-TPA) was 0.23.

### 5.3.1.3 Solvatochromic analysis

Solvatochromic experiments were performed to provide insight into the details of electronic interactions up on photoexcitation. For this, absorption and emission spectra of P(BTZ-TPA) were recorded by dissolving it in a binary solvent mixture consisting of toluene and acetonitrile. The binary solvent was prepared at different proportions of individual solvents, so that the solution changed from nonpolar to polar with the increasing weight fraction of acetonitrile. In order to quantify the polarity of the binary mixtures, the solvent polarity parameter ( $E_T^N$  parameter) was calculated using standard Reichardt's dye [32].



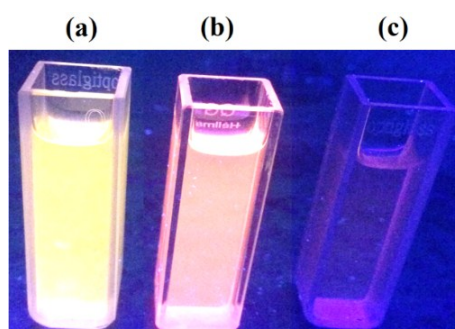
**Fig 5.7:** Normalized absorption spectra of P(BTZ-TPA) in the binary mixtures of toluene and acetonitrile, for different weight fractions of acetonitrile.



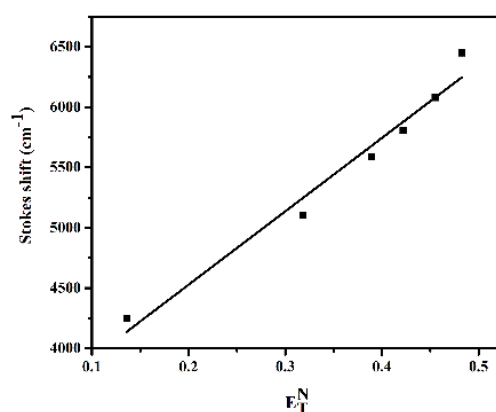
**Fig 5.8:** Normalized emission spectra of P(BTZ-TPA) in the binary mixtures of toluene and acetonitrile, for different weight fractions of acetonitrile.

Fig. 5.7 and Fig. 5.8 reveal the effects of solvent on the absorption and emission spectra of P(BTZ-TPA) in the binary solvent mixtures with varying polarities. For P(BTZ-TPA), toluene is comparatively a good solvent than acetonitrile. It was found that the intra-molecular charge transfer (ICT) band in the absorption spectra got blue shifted as the solution changed from non-polar to polar, while the emission spectra exhibited a red shift (Fig. 5.9). Also, the emission band showed spectral broadening for the same polarity variation. A comparison of the values corresponding to longest wavelength absorption maxima  $\lambda_{max}^{abs}$  and emission maxima  $\lambda_{max}^{emi}$  of P(BTZ-TPA) in these binary mixtures is shown in Table. 5.1, along with  $E_T^N$  parameters corresponding to each binary mixture. Effect of solvent on the absorption spectra was less compared to that of the emission spectra. It indicates that in comparison to excited state, the ground state energy distribution is not affected to a great extent. This is due to its less polar nature in the ground state.

A close examination on the emission spectra of P(BTZ-TPA) in toluene showed a shoulder peak at the higher wavelength region, in addition to the peak at 584 nm. But the relative intensity was much low. However, as the concentration of acetonitrile increased, relative intensity of this peak began to increase. When the fraction of the acetonitrile exceeded that of toluene, intensity of this shoulder peak began to dominate. This could be due to the aggregation induced emission from P(BTZ-TPA) due to the highly polar acetonitrile.



**Fig. 5.9:** Fluorescence emission of P(BTZ-TPA) from (a) pure toluene (b) binary mixture of toluene and acetonitrile with 60% toluene and (C) pure acetonitrile. A clear redshift is observed as the solvent polarity changes from apolar to polar.



**Fig. 5.10:** Stokes shift against the solvent polarity parameter.

Stoke's shift of the polymer in each binary solvent was calculated. Stoke's shift increased from  $4241 \text{ cm}^{-1}$  to  $6078 \text{ cm}^{-1}$  as the weight fraction of acetonitrile in the binary mixture increased. This large Stoke's shift is a signature of its charge transfer nature during photoexcitation. The large Stoke's shift observed in acetonitrile could provide information about the large transition dipole moment of the polymer [21]. Fig. 5.10 shows the variation of Stoke's shift of the polymer in each solvent with the corresponding  $E_T^N$  parameter. A linear correlation is observed. The positive solvatochromism exhibited by P(BTZ-TPA) confirms intramolecular charge transfer between donor and acceptor in the excited state [27,33,34].

**Table. 5.1:** The longest wavelength absorption maxima and emission maxima of P(BTZ-TPA) in binary mixtures of toluene and acetonitrile along with the solvent polarity parameter.

Weight fraction of acetonitrile %	$E_T^N$	$\lambda_{max}^{abs}$ (nm)	$\lambda_{max}^{emi}$ (nm)	$\nu^{abs} - \nu^{emi}$ ( $\text{cm}^{-1}$ )
0	0.136	468	584	4244
20	0.318	467	613	5100
40	0.389	460	619	5584
60	0.422	458	624	5809
80	0.455	454	627	6078
100	0.483	448	630	6448
$ \Delta\lambda_{max} $		20	46	

## 5.3.2 Steady state photocurrent measurements

### 5.3.2.1 Photocurrent action spectrum

Photoresponse of the samples were analyzed in the energy range between 1.77 eV (700 nm) and 4.14 eV (300 nm), for negatively biased ITO.

Measurements were taken for every 10 nm interval and the incident intensity was around  $1 \text{ mW/cm}^2$ . The data were normalized for constant incident flux.

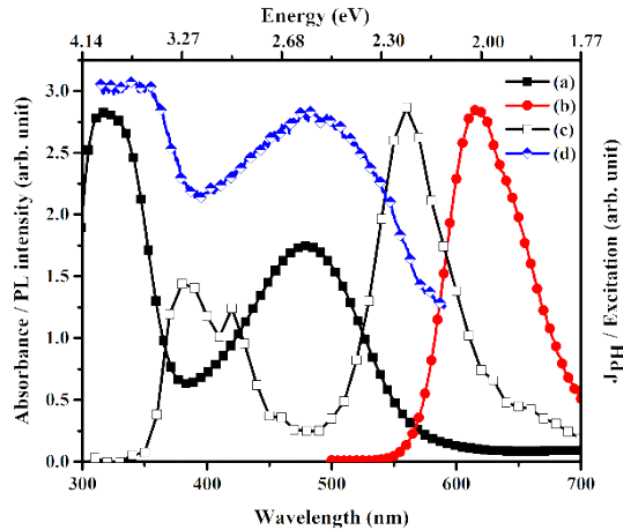


**Fig. 5.11:** (a) Absorption spectrum, (b) fluorescence spectrum, (c) photocurrent action spectrum and (d) excitation spectrum of pristine P(BTZ-TPA) thin film.

In pristine films, photocurrent measurements were taken under a biasing electric field of  $10 \text{ V}/\mu\text{m}$ . Fig. 5.11 shows the, absorption spectrum (a), fluorescence emission spectrum (b), photocurrent action spectrum (c) and fluorescence excitation spectrum (d) of pristine P(BTZ-TPA). Similar to the absorption spectrum, action spectrum exhibited dual bands, with an energy shift. It is observed that, the photocurrent increases with the energy of the incident photons, and exhibited a rapid growth after 2 eV and reached a maximum at 2.21 eV. Also, the contribution of the optical excitations near 2.21 eV to the fluorescence emission is much less. Thus most of the excitations around the band edge get dissociated and contributed to photoconductivity. Further, photocurrent decreased with

increase in energy of the incident photons above 2.21 eV. The spectral response showed a dip at 2.58 eV (480 nm), which corresponded to the absorption maxima and excitation maxima of the ICT band. Thus most of the excitons excited with this particular energy underwent recombination, resulting in a strong fluorescence emission. Further increase in energy of the incident photons led to an increased photocurrent and a maximum photocurrent was obtained at 3.26 eV (380 nm). In this energy range, the absorption and excitation spectra showed a descending nature. At the particular energy of 3.26 eV, the absorption and excitation spectra showed a dip, suggesting that most of the excitations contributed to photocurrent. Thereafter, photocurrent was decreased and below 3.65 eV (340 nm), the photocurrent was very low. Interestingly, excitations corresponding to this particular energy led predominantly to fluorescence. Hence it is concluded that, the excitations near the band edges contributed to photocurrent via exciton dissociation and the excitations at the band maxima contributed to fluorescence emission.

### 5.3.2.2 Intensity dependence of photocurrent

Intensity dependence of photocurrent was monitored by illuminating both the pristine and blend films with photons of energy 1.97 eV (632 nm) and 2.54 eV (488 nm), under a biasing electric field of  $5 \text{ V}/\mu\text{m}$  (Fig. 5.12). Intensity of the laser beams were gradually varied by using a polarizer. Photocurrent generated in the pristine films are correlated by a power law dependence of the form  $J_{PH} \propto I^\beta$ , where  $I$  is the intensity of illumination. For the pristine polymer film, values of  $\beta$  were 0.65 and 0.77 respectively when illuminated with 632 and 488 nm wavelengths. This

sub linear power law dependence is generally observed in amorphous solids [35]

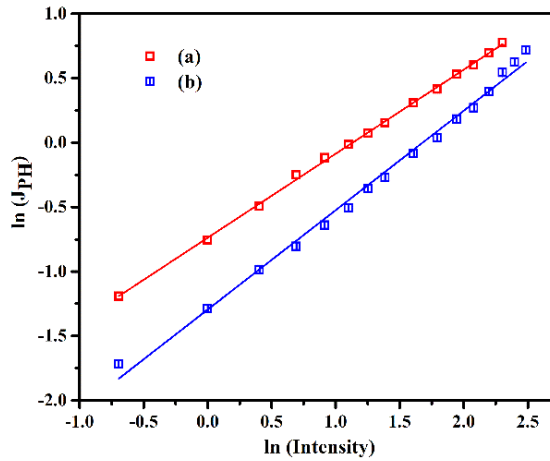


**Fig. 5.12:** Dependence of photocurrent on the intensity of illumination. (a) and (b) represent the variation in photocurrent in pristine P(BTZ-TPA) film under the irradiation of photons of energy 1.97 eV (632 nm) and 2.54 eV (488 nm) respectively.

### 5.3.2.3 Internal photocurrent efficiency and photoconductive sensitivity

Further investigations were carried out to understand the spectral response in terms of carrier generation efficiency and photoconductive sensitivity. All the photo-excited carriers under photo-excitation do not entirely contribute to the photocurrent. Some of the carriers got localized due to traps present in the films. So the experimental accuracy is limited to the calculation of the internal photocurrent efficiency ( $\phi$ ), which is defined as the number of measured free carriers per absorbed photon [36]. For this purpose, steady state photocurrent measurements were carried out on pristine polymer films using lasers of wavelength 488 nm and 632 nm, by varying the applied electric field. The intensity of incident flux was kept at  $125 \text{ mWcm}^{-2}$  throughout the

measurement. Using the measured photocurrent, internal photocurrent efficiency and photoconductive sensitivity were calculated and plotted against the applied electric field (Fig. 5.13 and Fig. 5.14).

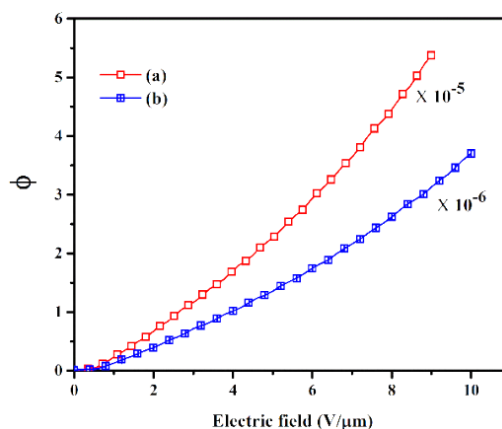


**Fig. 5.13:** Internal photocurrent efficiency as a function of electric field. (a) and (b) represent the variation of internal photocurrent in pristine P(BTZ-TPA) film under the irradiation of photons of energy 1.97 eV (632 nm) and 2.54 eV (488 nm) respectively

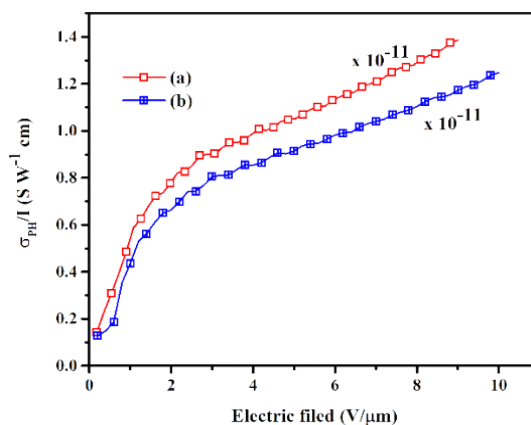


**Fig. 5.14:** Dependence of photoconductive sensitivity on applied electric field (a) and (b) represent the variation of photoconductive sensitivity in pristine P(BTZ-TPA) film under the irradiation of photons of energy 1.97 eV (632 nm) and 2.54 eV (488 nm) respectively.

The pristine samples could withstand an electric field up to  $10\text{ V}/\mu\text{m}$ . In pristine P(BTZ-TPA) polymer films, internal photocurrent efficiency of  $5.4 \times 10^{-5}$  and photoconductive sensitivity of  $1.4 \times 10^{-11}\text{ SW}^{-1}\text{cm}$  were achieved for an applied electric field of  $10\text{ V}/\mu\text{m}$ , on illuminating with 632 nm laser beam. When the illuminating source was replaced by 488 nm laser beam, internal photocurrent efficiency and photoconductive sensitivity changed to  $3.7 \times 10^{-6}$  and  $1.25 \times 10^{-11}\text{ SW}^{-1}\text{cm}$ , respectively.

## **5.4 Studies on P(BTZ-TPA):PCBM**

### **5.4.1 Optical properties of P(BTZ-TPA):PCBM**

#### **5.4.1.1 Optical absorption**

To enhance charge transfer properties, P(BTZ-TPA):PCBM blend films were prepared, in which polymer to PCBM ratio was 1:1. Optical absorption spectra of blend film as well as pristine are shown in Fig. 5.15. The absorption spectrum of PCBM thin film is shown in the inset. A  $\pi - \pi^*$  absorption peak (335 nm) is clearly observed in the absorption spectrum of PCBM thin film. The increased absorption corresponding to this characteristic peak in the blend films suggest that absorption spectrum of blend films is the superposition of absorption of copolymer and PCBM. Absence of additional features in the blend films is an indication that the ground state of the copolymer is unaffected due to the incorporation of PCBM.

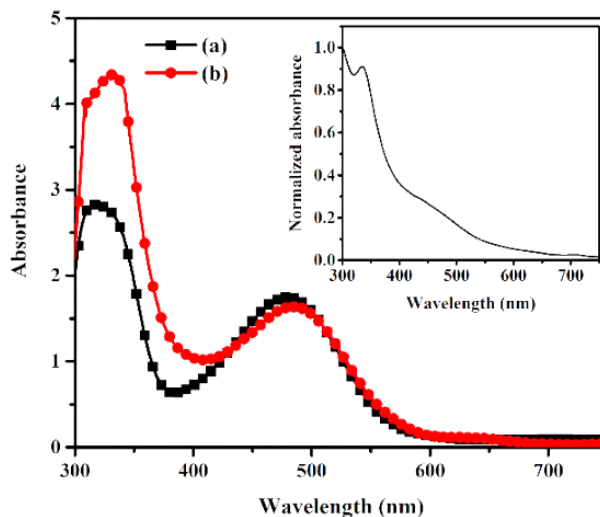


**Fig. 5.15:** Absorption spectra of (a) pristine P(BTZ-TPA) thin film and (b) P(BTZ-TPA):PCBM blend for a ratio of 1:1. Inset presents absorption spectrum of PCBM thin film. Both films were prepared on ITO coated glass substrates.

#### 5.4.1.2 Fluorescence quenching

Fig. 5.16 shows the fluorescence spectra of P(BTZ-TPA) and P(BTZ-TPA) with PCBM. P(BTZ-TPA):PCBM blend films, having polymer to PCBM ratio of 1:1 resulted in severe quenching of fluorescence emission compared to that of the pristine polymer film. The integrated fluorescence intensity (calculated as area under the curve) of the blend films is reduced to 1/84 of the pristine film. The emission spectrum of P(BTZ-TPA) has poor overlap with the absorption spectrum of PCBM. Further, emission spectrum of blend film does not exhibit any additional features. Hence energy transfer from polymer to PCBM can be ruled out and the relentless quenching of the fluorescence emission is assigned to photoinduced charge transfer and charge separation. The quenching of fluorescence in combination with the increased

photoconductivity indicates the charge transfer at the polymer:PCBM interface. In many of the conjugated polymers, this photoinduced electron transfer at the polymer-PCBM interface ensues in sub-picosecond ( $t < 100 \text{ fs}$ ) timespan to inhibit the radiative relaxation of the excitons [9,37,38].

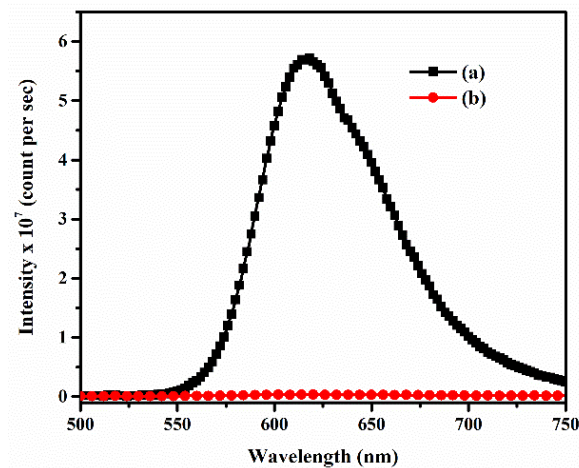


**Fig. 5.16:** Fluorescence spectra of thin films of (a) pristine P(BTZ-TPA) and (b) P(BTZ-TPA):PCBM blend for a ratio of 1:1. Films were prepared on ITO coated glass substrate, and excited with photons of energy 2.64 eV

## 5.4.2 Steady state photocurrent measurements

### 5.4.2.1 Photocurrent action spectrum

Steady state photocurrent action spectrum was recorded in the P(BTZ-TPA):PCBM blend films by measuring the photocurrent generated in the sample, while illuminating with photons having energies in the range 1.77 eV (700 nm) to 4.14 eV (300 nm). For this, sample was biased by an electric field of  $5 \text{ V}/\mu\text{m}$  and ITO was biased negatively. Measurements were taken for every 10 nm interval and the incident intensity was around  $1 \text{ mW}/\text{cm}^2$ . The obtained data were normalized to constant incident flux.

Fig. 5.17 shows the photocurrent spectrum of pristine and P(BTZ-TPA):PCBM blend films.

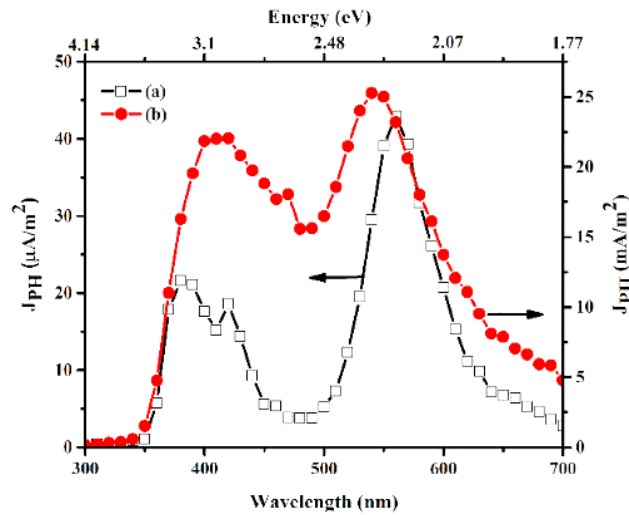


**Fig. 5.17:** Photocurrent action spectra of (a) pristine P(BTZ-TPA) thin film under a biasing electric field of  $10 V/\mu m$  and (b) P(BTZ-TPA):PCBM blend films under a biasing electric field of  $5 V/\mu m$ .

As expected, P(BTZ-TPA):PCBM blend film exhibited a substantially improved photocurrent spectral response over the entire spectral range (Fig. 5.17 b) and observed three orders of increment in photocurrent compared to that of pristine film. A good photoresponse was observed even at 1.77 eV (700 nm).

#### 5.4.2.2 Intensity dependence of photocurrent

Intensity dependence of photocurrent was monitored by illuminating the blend films and pristine films with photons of energy 1.97 eV (632 nm) and 2.54 eV (488 nm), under a biasing electric field of  $5 V/\mu m$  (Fig. 5.18). Intensity of the laser beams were gradually varied by using a polarizer.

Photocurrent generated in the blend films were correlated by a power law dependence of the form  $J_{PH} \propto I^\beta$ , where  $I$  is the intensity of illumination. For the blend film, the  $\beta$  values were 0.91 and 0.94 respectively, for the illumination of 632 nm and 488 nm wavelengths. The near linear dependence in the blend films revealed the absence of bimolecular recombination [39,40].

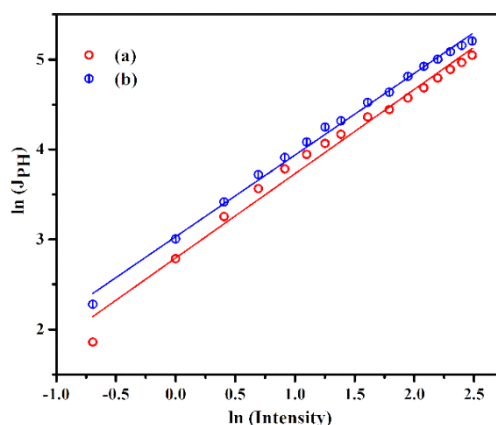


**Fig 5.18:** Dependence of photocurrent on the intensity of illumination. (a) and (b) present the variation in photocurrent in P(BTZ-TPA):PCBM blend film under the irradiation of photons of energy 1.97 eV (632 nm) and 2.54 eV (488 nm) respectively.

#### 5.4.2.3 Internal photocurrent efficiency and photoconductive sensitivity

Steady state photocurrent measurements were carried out on PCBM blend polymer films using lasers of wavelength 488 nm and 632 nm, by varying the applied electric field. The intensity of incident flux was kept at  $125 \text{ mWcm}^{-2}$  throughout the measurement. Using the measured photocurrent, internal photocurrent efficiency and photoconductive sensitivity were calculated and plotted against the applied electric field (Fig. 5.19 and Fig. 5.20).

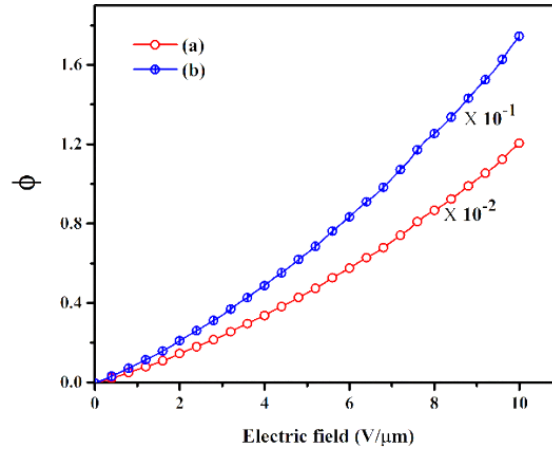


**Fig. 5.19:** Internal photocurrent efficiency as a function of electric field. (a) and (b) present the variation of internal photocurrent efficiency in P(BTZ-TPA):PCBM blend film under the irradiation of photons of energy 1.97 eV (632 nm) and 2.54 eV (488 nm) respectively.

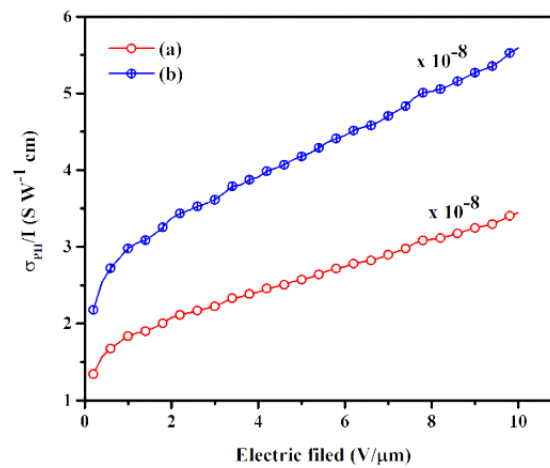


**Fig. 5.20:** Dependence of photoconductive sensitivity on applied electric field. (a) and (b) present the variation in photoconductive sensitivity in P(BTZ-TPA):PCBM blend film under the irradiation of photons of energy 1.97 eV (632 nm) and 2.54 eV (488 nm) respectively.

For P(BTZ-TPA):PCBM blend films, internal photocurrent efficiency and photoconductive sensitivity were  $1.2 \times 10^{-2}$  and  $3.47 \times 10^{-8} \text{ SW}^{-1} \text{ cm}$  respectively for 632 nm illumination and  $1.74 \times 10^{-1}$  and  $5.6 \times 10^{-8} \text{ SW}^{-1} \text{ cm}$  respectively for the illumination under 488 nm. The blend films had better photoconductive sensitivity and photocurrent efficiency than the pristine films.

## 5.5 Studies on P(BTZ-HT)

The next polymer was poly(benzothiadiazole-hexylthiophene) copolymer labelled as P(BTZ-HT). In this case, benzothiadiazole acted as the donor moiety and 3-hexylthiophene acted as acceptor moiety. The structure of the polymer is shown in Fig. 5.22. Poly(3-hexylthiophene) commonly labelled as (P3HT) is a p-type conjugated semiconducting polymer widely studied for solar cell fabrication and organic field effect transistors due to its excellent optoelectronic properties, low cost, stability and easiness of synthesis [41–44].

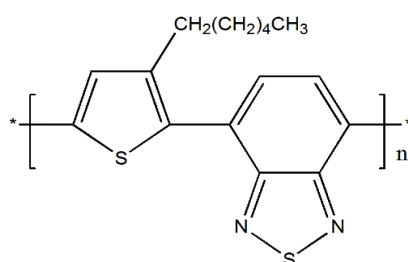


Fig. 5.21: Structure of P(BTZ-HT)

The polymer was soluble in common organic solvents such as chloroform, toluene, etc. The molecular weight of the polymer was determined using GPC. The number average molecular weight and weight

average molecular weight of the polymer were 52200 and 60500 respectively. The polydispersity index was 1.05.

## 5.5.1 Optical properties of P(BTZ-HT):PCBM

### 5.5.1.1 Optical absorption

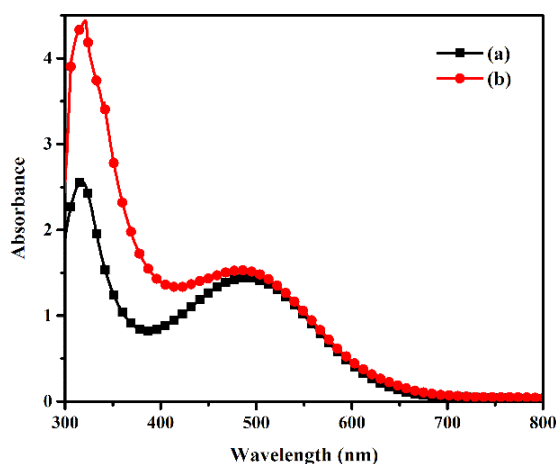


**Fig. 5.22:** Absorption spectra of (a) pristine P(BTZ-HT) thin film and (b) P(BTZ-HT):PCBM blend films for a weight ratio of 1:1.

Fig. 5.22 depicts the absorption spectra of pristine P(BTZ-HT) thin film and P(BTZ-HT):PCBM films for a polymer to PCBM weight ratio of 1:1. As in the previous case, absorption spectra of pristine film (Fig. 5.22 (a)) exhibited two distinct absorption bands. The band at higher wavelength region is centred around 490 nm which arises due to the charge transfer interaction between donor and acceptor moieties. The band in the low energy region, centred around 315 nm is due to  $\pi - \pi^*$  transition. The absorption onset of P(BTZ-HT) is at 675 nm and thus the optical band gap was calculated to be 1.84 eV.

To obtain increased carrier generation during optical excitations, P(BTZ-HT):PCBM blend films were prepared for a polymer to PCBM weight ratio of 1:1. The absorption spectrum of the blend film (Fig. 5.22 (b)) is the super position of the absorption of the polymer and absorption of the PCBM, which suggest the weak mixing of ground state wave functions.

### 5.5.1.2 Fluorescence quenching

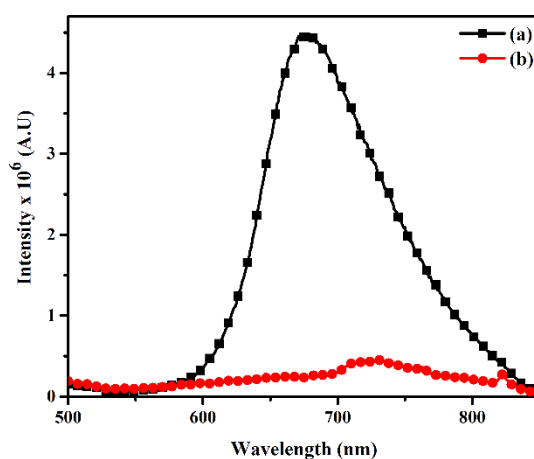


**Fig. 5.23:** Fluorescence emission from (a) pristine P(BTZ-HT) thin film and (b) P(BTZ-HT):PCBM thin film for a weight ratio of 1:1. Both the films were excited with photons of energy 2.53 eV.

Fig. 5.23 shows the fluorescence emission of the pristine P(BTZ-HT) film and P(BTZ-HT):PCBM blend films for a weight ratio of 1:1, when excited with photons of energy 2.58 eV. The pristine film exhibited good fluorescence emission with an emission maximum at 675 nm. Incorporation of PCBM reduced the fluorescence intensity. In this case, the integrated fluorescence intensity (area under the curve) was reduced only to 1/8 of the pristine film. This is a clear indication of the inefficient exciton

dissociation at the P(BTZ-HT):PCBM interface. This may reflect in the photoconductive performance of the blend films.

## 5.5.2 Steady state photocurrent measurements

### 5.5.2.1 Photocurrent action spectrum

Spectral dependence of photocurrent in the P(BTZ-HT):PCBM blend films was obtained from the photocurrent action spectrum. The sample was illuminated using the wavelengths in the entire visible region (300-700 nm). The measurements were done under a biasing electric field of  $5 \text{ V}/\mu\text{m}$ . ITO electrode was kept at negative polarity during the experiment. Similar to the previous case, the photocurrent was normalized to constant incident flux. The steady state photocurrent action spectrum is shown in Fig. 5.24. The blend films exhibited photoresponse in the entire visible region. Here also, the excitations around the band edges predominantly contributed to photocurrent.

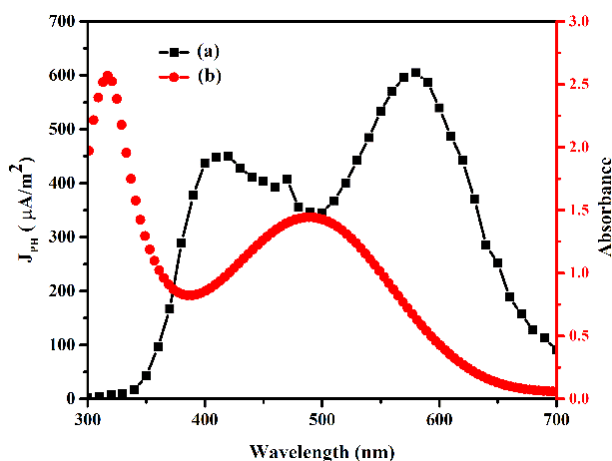


**Fig. 5.24:** (a) Steady state photocurrent action spectrum of P(BTZ-HT):PCBM blend films for a weight ratio of 1:1. (b) present the absorption spectrum of the blend films.

### 5.5.2.2 Intensity dependence of photocurrent

Dependence of photocurrent on the intensity of illumination was studied by illuminating the sample with laser beams of wavelength 632 nm and 488 nm. The ITO electrode was kept at negative polarity and an electric field of  $5 \text{ V}/\mu\text{m}$  was applied across the sample. Fig. 5.25 shows the variation of photocurrent with intensity of illumination. The intensity of illumination and photocurrent generated in the P(BTZ-HT):PCBM films are correlated by a power law dependence of the form  $J_{PH} \propto I^\beta$ , with  $\beta = 1.03$  and 1.01 respectively for the illumination of 632 and 488 nm wavelengths. This concludes the absence of bimolecular recombination in the P(BTZ-HT):PCBM blend films.

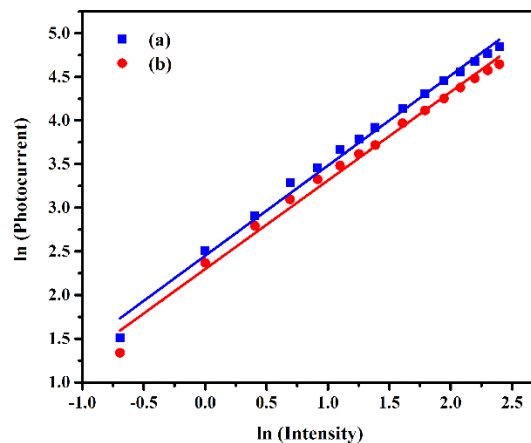


**Fig. 5.25:** Intensity dependence of photocurrent by illuminating the P(BTZ-HT):PCBM blend films with laser beams of wavelength (a) 488 nm and (b) 632 nm.

### 5.5.2.3 Internal photocurrent efficiency and photoconductive sensitivity

To estimate the internal photocurrent efficiency and photoconductive sensitivity of the P(BTZ-HT):PCBM blend films, steady state photocurrent

measurements were carried out on blend films using lasers of wavelength 488 nm and 632 nm, by varying the applied electric field. The intensity of incident flux was kept at  $125 \text{ mWcm}^{-2}$  throughout the measurement. Using the measured photocurrent, internal photocurrent efficiency and photoconductive sensitivity were calculated and plotted against the applied electric field (Fig. 5.26 and Fig. 5.27). In P(BTZ-HT):PCBM films, internal photocurrent efficiency of  $5 \times 10^{-4}$  and photoconductive sensitivity of  $1.5 \times 10^{-9} \text{ SW}^{-1}\text{cm}$  were achieved for an applied electric field of  $10 \text{ V}/\mu\text{m}$ , on illuminating with 488 nm laser beam. When the illuminating source was replaced by 632 nm laser beam, internal photocurrent efficiency and photoconductive sensitivity was changed to  $4 \times 10^{-6}$  and  $1.3 \times 10^{-9} \text{ SW}^{-1}\text{cm}$ , respectively.

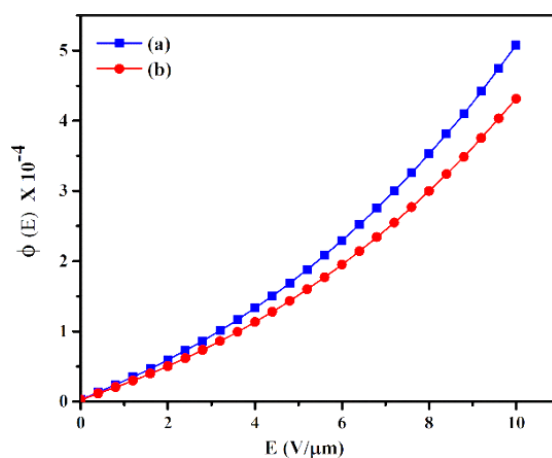


**Fig. 5.26:** Internal photocurrent efficiency as a function of electric field. (a) and (b) present the variation of internal photocurrent efficiency in P(BTZ-HT):PCBM blend film under the irradiation of photons of energy 2.54 eV (488 nm) and 1.97 eV (632 nm) respectively

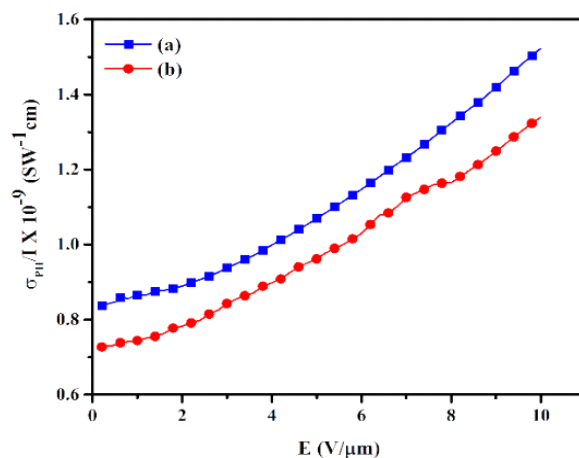


**Fig. 5.27:** Photoconductive sensitivity as a function of electric field. (a) and (b) present the variation of photoconductive sensitivity in P(BTZ-HT):PCBM blend film under the irradiation of photons of energy 2.54 eV (488 nm) and 1.97 eV (632 nm) respectively

## 5.6 Studies on P(BTZ-HXT)

A third benzothiadiazole co-polymer was synthesized by the copolymerization with dihexyloxythiophene, having comparatively greater donor strength. The structure of the polymer is shown in Fig. 5.28. The poly(benzothiadiazole-dihexyloxythiophene) copolymer is labelled as P(BTZ-HXT). 3,4-Dihexyloxythiophene is extensively used in many of the conducting polymers and electrochromic applications[45–50]

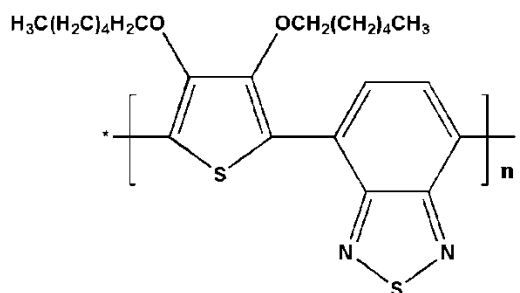


**Fig. 5.28:** Structure of P(BTZ-HXT)

This polymer also exhibited amenable solubility in common organic solvents so that the film fabrication for optical and electrical applications was feasible. On performing GPC measurement, the number average molecular weight and weight average molecular weight of the P(BTZ-HXT) were estimated as 12356 and 15445 respectively. Polydispersity index was 1.25.

## 5.6.1 Optical properties of P(BTZ-HXT):PCBM

### 5.6.1.1 Optical absorption

Fig. 5.29 shows the absorption spectrum of pristine P(BTZ-HXT) thin film and P(BTZ-HXT):PCBM films prepared for a polymer to PCBM weight ratio of 1:1. Here also, two distinct absorption bands are there in the pristine film. The charge transfer absorption band observed in the higher wavelength region was more red shifted compared to other two copolymers. In this case, the absorption onset was found to be at 752 nm and the corresponding band gap was 1.65 eV. Thus the D-A coupling significantly reduced the band gap.

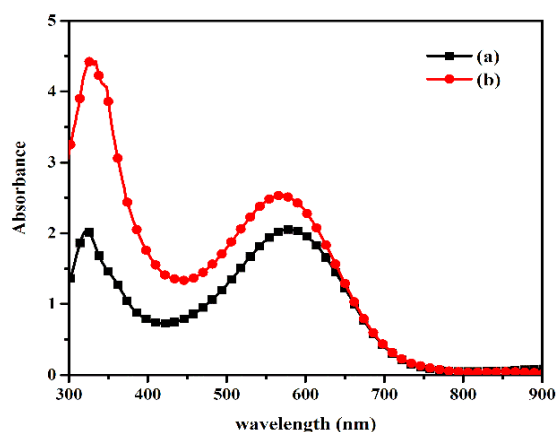


**Fig. 5.29:** Absorption spectra of (a) pristine P(BTZ-HT) thin film and (b) P(BTZ-HXT):PCBM blend films for a weight ratio of 1:1.

In order to overcome the less efficient charge transfer in the pristine polymer film, P(BTZ-HXT):PCBM blend film was prepared for a polymer to PCBM weight ratio of 1:1. Here also, no overlapping of the ground state wavefunctions was observed and the absorption of the blend films was the superposition of the absorption of the polymer and PCBM.

### 5.6.1.2 Fluorescence quenching

The fluorescence emission from the pristine P(BTZ-HXT) films and P(BTZ-HXT):PCBM films excited with photons of energy 2.16 eV is shown in Fig. 5.30. Pristine film exhibited good fluorescence emission with an emission maximum at 740 nm. Fluorescence emission from the blend films got quenched due to the presence of PCBM. The integrated fluorescence intensity of the blend film was reduced to 1/24 th of pristine film. This strongly suggest that, the exciton dissociation at the PCBM interface is not efficient as in the case of P(BTZ-TPA):PCBM blend. However, fluorescence quenching is assigned to charge transfer reaction between polymer and PCBM.

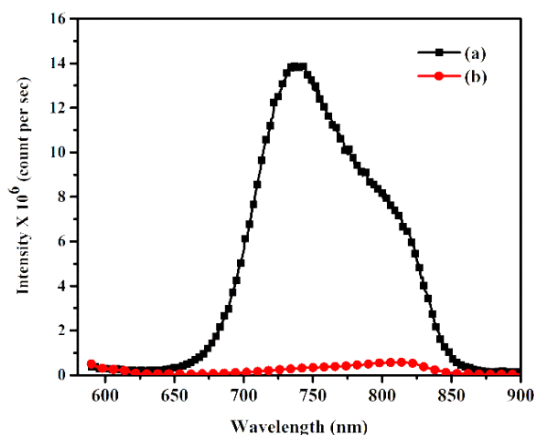
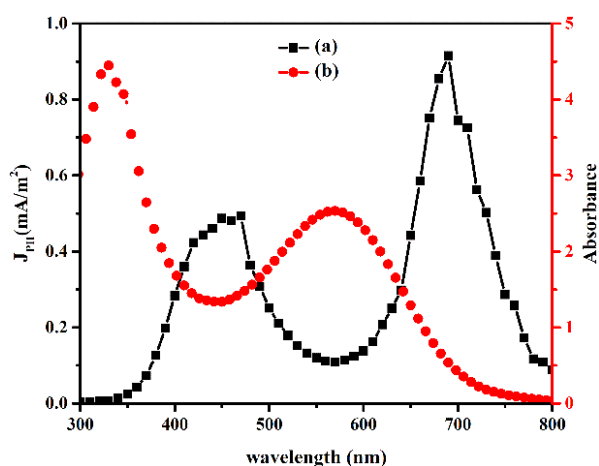


**Fig. 5.30:** Fluorescence emission from (a) pristine P(BTZ-HXT) thin film and (b) P(BTZ-HXT):PCBM thin film for a weight ratio of 1:1. Both the films were excited with photons of energy 2.16 eV.

## 5.6.2 Steady state photocurrent measurements

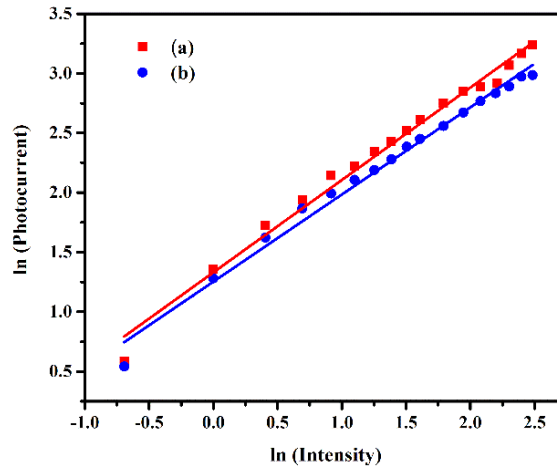
### 5.6.2.1 Photocurrent action spectrum

Steady state photocurrent action spectrum was recorded in the sandwich cell samples. Photoresponse of the samples were analyzed in the energy range between 1.55 eV (800 nm) and 4.14 eV (300 nm), for negatively biased ITO (Fig. 5.31). Measurements were taken for every 10 nm interval. The sample was biased at an electric field of  $5 \text{ V}/\mu\text{m}$ . The blend films exhibited photoresponse in the entire visible region. Here also, the excitations around the band edges predominantly contributed to photocurrent. Here, the spectral response was slightly higher compared to the spectral response of P(BTZ-HT):PCBM blend films.



**Fig. 5.31:** (a) Steady state photocurrent action spectrum of P(BTZ-HXT):PCBM blend films for a weight ratio of 1:1. (b) present the absorption spectrum of the blend films.

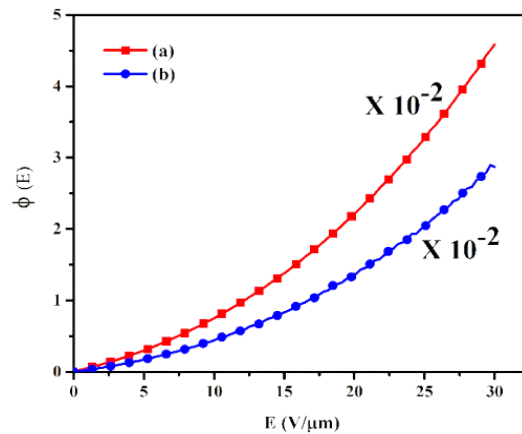
### 5.6.2.2 Intensity dependence of Photocurrent



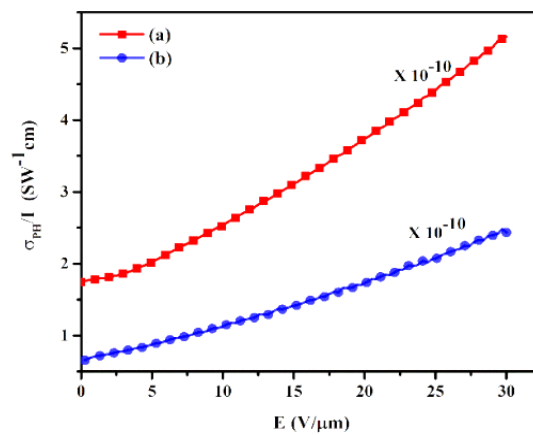
**Fig. 5.32:** Intensity dependence of photocurrent by illuminating P(BTZ-HXT):PCBM blend films with laser beams of wavelength (a) 488 nm and (b) 632 nm.

Fig. 5.32 shows the variation of photocurrent with the intensity of illumination on the P(BTZ-HXT):PCBM films. Dependence of photocurrent on the intensity of illumination was studied by illuminating the sample with laser beams of wavelength 632 nm and 488 nm. The ITO electrode was kept at negative polarity and an electric field of  $5 \text{ V}/\mu\text{m}$  was applied across the sample. The intensity of illumination and photocurrent generated in the pristine films were correlated by a power law dependence of the form  $J_{PH} \propto I^\beta$ , with  $\beta = 0.77$  and  $0.73$  respectively for the illumination of 632 and 488 nm wavelengths. This indicates the amorphous behavior of the blend films.

### 5.6.2.3 Internal photocurrent efficiency and photoconductive Sensitivity



**Fig. 5.33:** Internal photocurrent efficiency as a function of electric field. (a) and (b) present the variation of internal photocurrent efficiency in P(BTZ-HXT):PCBM blend film under the irradiation of photons of energy 1.97 eV (632 nm) and 2.54 eV (488 nm) respectively



**Fig. 5.34:** Photoconductive sensitivity as a function of electric field. (a) and (b) present the variation of photoconductive sensitivity in P(BTZ-HT):PCBM blend film under the irradiation of photons of energy 2.54 eV (488 nm) and 1.97 eV (632 nm) respectively

Internal photocurrent efficiency and photoconductive sensitivity of the P(BTZ-HXT):PCBM blend films were calculated from the measured photocurrent. For this, steady state photocurrent measurements were carried out on blend films as a function of electric field, by illuminating the sample with lasers of wavelength 488 nm and 632 nm. The intensity of incident flux was kept at  $125 \text{ mWcm}^{-2}$  throughout the measurement. The P(BTZ-HXT):PCBM blend films could withstand an electric field up to  $30 \text{ V}/\mu\text{m}$ . Fig. 5.26 and Fig. 5.27 shows the internal photocurrent efficiency and photoconductive sensitivity against the applied electric field. In P(BTZ-HXT):PCBM films, internal photocurrent efficiency of  $2.85 \times 10^{-2}$  and photoconductive sensitivity of  $5.13 \times 10^{-10} \text{ SW}^{-1}\text{cm}$  were achieved for an applied electric field of  $30 \text{ V}/\mu\text{m}$ , on illuminating with 488 nm laser beam. When the illuminating source was replaced by 632 nm laser beam, internal photocurrent efficiency and photoconductive sensitivity was changed to  $4.55 \times 10^{-2}$  and  $1.5 \times 10^{-10} \text{ SW}^{-1}\text{cm}$ , respectively.

## 5.7 The band diagram and photoconductivity

Photoconductivity in conjugated polymers is generally due to the formation of excitons, its dissociation and the transport of the generated carriers under the influence of external field. The optical absorption in conjugated polymer leads to the formation of strongly bound and highly localized Frenkel excitons. Low dielectric constant of polymers results in the formation of stable excitons by providing significantly high Coulomb binding energy between electron and hole. The exciton exhibit diffusive motion and get dissociated while reaching a donor-acceptor interface. In addition, the excitons can dissociate at impurities or on applying external

electric fields [51]. In conjugated polymers, the average diffusion length of the excitons typically lies in the range 5-14 nm [3,52]. Exciton dissociation at the interface happens only if it is energetically favorable. For effective charge separation, the LUMO energy level of the polymer donor should be higher than the LUMO energy level of the acceptor[5]. Also, the energy offset between the LUMO energy levels of donor and acceptor should be at least 0.30 eV for driving the charge separation [51,53]. Using cyclic voltammetry experiments, the HOMO and LUMO energy levels of P(BTZ-TPA), P(BTZ-HT) and P(BTZ-HXT) were identified and tabulated in Table 5.2. LUMO energy level of PCBM is at -4.3 eV [54].

**Table 5.2:** HOMO and LUMO energy levels of P(BTZ-TPA), P(BTZ-HT) and P(BTZ-HXT)

Polymer	HOMO (eV)	LUMO (eV)
P(BTZ-TPA)	-4.66	-2.59
P(BTZ-HT)	-6.03	-4.07
P(BTZ-HXT)	-5.31	-3.58

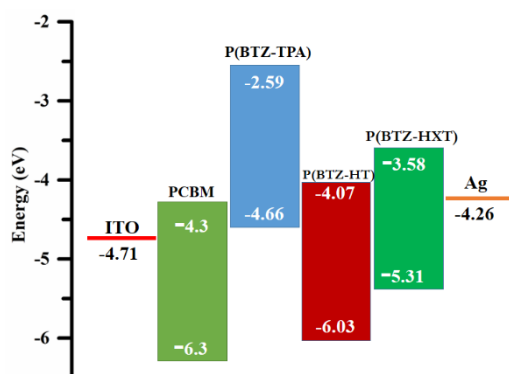


**Fig. 5.35:** Energy level diagram of P(BTZ-TPA), P(BTZ-HT), P(BTZ-HXT) and PCBM. Also the work functions of electrodes used are presented.

Photoconductivity in conjugated polymer:PCBM blend films is predominantly influenced by the exciton dissociation at the polymer:PCBM interface. Fig. 5.35 shows the energy band diagram of the copolymers and PCBM. The LUMO-LUMO offset between P(BTZ-TPA) is 1.7 eV, which highly favors exciton dissociation at the interface. For P(BTZ-HT) and PCBM, the LUMO offset is 0.27 eV, which is below the minimum requirement. So, the exciton dissociation is apparently inhibited at the P(BTZ-HT):PCBM interface. So the introduction of PCBM did not significantly contribute to photoconductivity. The LUMO-LUMO offset between P(BTZ-HXT) and PCBM is 0.72 eV, which overcomes the minimum requirement for interfacial exciton dissociation. This energy demand of the LUMO levels of polymer and PCBM is significantly reflected in the photoconductive performance.

The concept of bulk hetero-junction (interpenetrating network of polymer and PCBM) and comparatively high concentration of PCBM enhances the exciton encounter at the polymer-PCBM interface, within the limit of exciton diffusion length. The rate of dissociation of excitons at the PCBM interface is  $> 10^{12} \text{ s}^{-1}$  [55]. All these favors a high carrier generation efficiency, resulting in an enhanced photoconductivity. It is observed that internal photocurrent efficiency and photoconductive sensitivity in both pristine and blend films of all polymers exhibited super linear power law dependence with the applied electric field. The increased photoconductivity with the applied electric field can be attributed to the increased carrier generation efficiency [35].

## 5.8 Summary

Optical and photoconductive properties of three synthesized low band gap copolymers P(BTZ-TPA), P(BTZ-HT) and P(BTZ-HXT) were studied. Reduction in the band gap was observed with the increase in donor strength of the donor moieties. Thus, the band gap was finely tuned from 2.05 eV to 1.65 eV by introducing TPA, HT and HXT as donor moieties. Steady state photocurrent measurements carried out on pristine films and PCBM blended films revealed that carrier generation and photoconductivity were predominantly affected by external electric field. However, carrier generation efficiency was found to be much low, which might be due to the intense fluorescence emission. Polymer:PCBM blend films showed better performance. In P(BTZ-TPA):PCBM blend films, carrier generation efficiency of 17.4% was achieved using 488 nm laser beam illumination, at  $10 \text{ V}/\mu\text{m}$ . Significantly high values of photoconductive sensitivity and internal photocurrent efficiency obtained in the low field regime in these synthesized polymers are favorable for different optoelectronic and photorefractive applications [56].

P(BTZ-HT) and P(BTZ-HXT) polymers exhibited photon harvesting from the low energy region of the visible spectrum (due to their low band gap) compared to P(BTZ-TPA). Thus, these polymers can function as potential candidates in many of the applications, especially in photovoltaic applications. But as an acceptor, PCBM is not compatible with these polymers. By introducing suitable acceptor molecules (which should favor the energy demand), these polymers can be used for potential applications.

## References

- [1] X. Guo, M. Baumgarten, K. Müllen, Designing  $\pi$ -conjugated polymers for organic electronics, *Prog. Polym. Sci.* 38 (2013) 1832–1908.
- [2] J. Roncali, Molecular engineering of the band gap of  $\pi$ -conjugated systems: Facing technological applications, *Macromol. Rapid Commun.* 28 (2007) 1761–1775.
- [3] C.S. Cheng, Y. J. Yang, S. H. Hsu, Synthesis of conjugated polymers for organic solar cell applications, *Chem. Rev.* 109 (2009) 5868–923.
- [4] A.R. Murphy, J.M.J. Fréchet, Organic semiconducting oligomers for use in thin film transistors, *Chem. Rev.* 107 (2007) 1066–1096.
- [5] C. Soci, I.W. Hwang, D. Moses, Z. Zhu, D. Waller, R. Gaudiana, C.J. Brabec, A.J. Heeger, Photoconductivity of a low-bandgap conjugated polymer, *Adv. Funct. Mater.* 17 (2007) 632–636.
- [6] H.A.M. van Mullekom, J. Vekemans, E.W. Meijer, Band-gap engineering of donor-acceptor-substituted pi-conjugated polymers, *Chem. Eur. J.* 4 (1998) 1235–1243.
- [7] P. Dutta, H. Park, W.H. Lee, I.N. Kang, S.H. Lee, Synthesis, characterization and bulk-heterojunction photovoltaic applications of new naphtho[1,2-b:5,6-b']dithiophene–quinoxaline containing narrow band gap D–A conjugated polymers, *Polym. Chem.* 5 (2014) 132–143.
- [8] T. Jia, Q. Hou, K. Xiong, Q. Li, L. Hou, Synthesis and photovoltaic properties of benzo[1,2-b:3,4-b]thiophene-based conjugated copolymers with a pendent acceptor, *J. Mater. Sci. Mater. Electron.* 25 (2014) 1639–1646.
- [9] L. Sims, H.J. Egelhaaf, J.A. Hauch, F.R. Kogler, R. Steim, Plastic solar cells, *Adv. Funct. Mater.* 11 (2001) 15–26.
- [10] X. Guo, H. Xin, F.S. Kim, A.D.T. Liyanage, S.A. Jenekhe, M.D. Watson, Thieno[3,4-c]pyrrole-4,6-dione-based donor-acceptor conjugated polymers for solar cells, *Macromolecules.* 44 (2011) 269–277.
- [11] A. Facchetti, Polymer donor-polymer acceptor (all-polymer) solar cells, *Mater. Today.* 16 (2013) 123–132.

- [12] Q. Huang, G.A. Evmenenko, P. Dutta, P. Lee, N.R. Armstrong, T.J. Marks, Covalently bound hole-injecting nanostructures. Systematics of molecular architecture, thickness, saturation, and electron-blocking characteristics on organic light-emitting diode luminance, turn-on voltage, and quantum efficiency, *J. Am. Chem. Soc.* 127 (2005) 10227–10242.
- [13] N.R. Evans, L.S. Devi, C.S.K. Mak, S.E. Watkins, S.I. Pascu, A. Köhler, R.H. Friend, C.K. Williams, A.B. Holmes, Triplet energy back transfer in conjugated polymers with pendant phosphorescent iridium complexes, *J. Am. Chem. Soc.* 128 (2006) 6647–6656.
- [14] P. Shi, C.M. Amb, A.L. Dyer, J.R. Reynolds, Fast switching water processable electrochromic polymers, *ACS Appl. Mater. Interfaces.* 4 (2012) 6512–6521.
- [15] P.M. Beaujuge, J.R. Reynolds, Color control in pi-conjugated organic polymers for use in electrochromic devices., *Chem. Rev.* 110 (2010) 268–320.
- [16] E. Kaya, A. Balan, D. Baran, A. Cirpan, L. Toppare, Electrochromic and optical studies of solution processable benzotriazole and fluorene containing copolymers, *Org. Electron. Physics, Mater. Appl.* 12 (2011) 202–209.
- [17] S. Narayanan, A. Abbas, S.P. Raghunathan, K. Sreekumar, C.S. Kartha, R. Joseph, Theoretical and experimental investigations on the photoconductivity and nonlinear optical properties of donor–acceptor  $\pi$  conjugated copolymer, poly(2,5-(3,4-ethylenedioxythiophene)-alt-2,7-(9,9-dioctylfluorene)), *RSC Adv.* 5 (2015) 8657–8668.
- [18] S.W. Chang, T. Muto, T. Kondo, M. Liao, M. Horie, Double acceptor donor–acceptor alternating conjugated polymers containing cyclopentadithiophene, benzothiadiazole and thienopyrroledione: toward subtractive color organic photovoltaics, *Polym. J.* 49 (2016) 113–122.
- [19] S. Ellinger, K.R. Graham, P. Shi, R.T. Farley, T.T. Steckler, R.N. Brookins, P. Taraneekar, J. Mei, L.A. Padilha, T.R. Ensley, H. Hu, S. Webster, D.J. Hagan, E.W. Van Stryland, K.S. Schanze, J.R. Reynolds, Donor-acceptor-donor-based  $\pi$ -conjugated oligomers for nonlinear optics and near-IR emission, *Chem. Mater.* 23 (2011) 3805–3817.

- [20] K.H. Ong, S.L. Lim, J. Li, H.K. Wong, H.S. Tan, T.T. Lin, L.C.H. Moh, J.C. de Mello, Z.K. Chen, Design and synthesis of benzothiadiazole-oligothiophene polymers for organic solar cell applications, *Polym. Chem.* 4 (2013) 1863–1873.
- [21] T. Michinobu, K. Okoshi, H. Osako, H. Kumazawa, K. Shigehara, Band-gap tuning of carbazole-containing donor-acceptor type conjugated polymers by acceptor moieties and  $\pi$ -spacer groups, *Polymer.* 49 (2008) 192–199.
- [22] P.M. Beaujuge, W. Pisula, H.N. Tsao, S. Ellinger, J.R. Reynolds, Tailoring structure-property relationships in dithienosilole- benzothiadiazole donor-acceptor copolymers, *J. Am. Chem. Soc.* 131 (2009) 7514–7515.
- [23] Unpublished work.
- [24] X. Wang, L. Lv, W. Gu, X. Wang, T. Dong, Z. Yang, H. Cao, H. Huang, Novel triphenylamine-based copolymers for all-polymer solar cells, *Dye. Pigment.* 140 (2017) 141–149.
- [25] Y. Shang, Y. Wen, S. Li, S. Du, X. He, L. Cai, Y. Li, L. Yang, H. Gao, Y. Song, A triphenylamine-containing donor-acceptor molecule for stable, reversible, ultrahigh density data storage, *J. Am. Chem. Soc.* 129 (2007) 11674–11675.
- [26] C. Duan, W. Cai, F. Huang, J. Zhang, M. Wang, T. Yang, C. Zhong, X. Gong, Y. Cao, Novel silafluorene-based conjugated polymers with pendant acceptor groups for high performance solar cells, *Macromolecules.* 43 (2010) 5262–5268.
- [27] G. Paramaguru, R. Vijay Solomon, S. Jagadeeswari, P. Venuvalingam, R. Renganathan, Tuning the photophysical properties of 2-quinolinone-based donor-acceptor molecules through N-versus O-alkylation: insights from experimental and theoretical investigations, *European J. Org. Chem.* (2014) 753–766.
- [28] P.M. Beaujuge, C.M. Amb, J.R. Reynolds, Spectral engineering in  $\pi$ -conjugated polymers with intramolecular donor-acceptor interactions, *Acc. Chem. Res.* 43 (2010) 1396–1407.

- [29] W.A. Braunecker, S.D. Oosterhout, Z.R. Owczarczyk, N. Kopidakis, E.L. Ratcli, D.S. Ginley, D.C. Olson, Semi-random vs well-defined alternating donor-acceptor copolymers, *ACS Macro Lett.* 3 (2014) 622–627.
- [30] C. Winder, N.S. Sariciftci, Low bandgap polymers for photon harvesting in bulk heterojunction solar cells, *J. Mater. Chem.* 14 (2004) 1077.
- [31] R. Reisfeld, R. Zusman, Y. Cohen, M. Eyal, The spectroscopic behaviour of rhodamine 6G in polar and non-polar solvents and in thin glass and PMMA films, *Chem. Phys. Lett.* 147 (1988) 142–147.
- [32] V.C. Kishore, R. Dhanya, K. Sreekumar, R. Joseph, C. Sudha Kartha, On the dipole moments and first-order hyperpolarizability of N,N-bis(4-bromobutyl)-4-nitrobenzenamine, *Spectrochim. Acta - Part A Mol. Biomol. Spectrosc.* 70 (2008) 1227–1230.
- [33] N. Banerji, E. Gagnon, P. Morgantini, S. Valouch, A.R. Mohebbi, J. Seo, M. Leclerc, A.J. Heeger, Breaking down the problem: optical transitions, electronic structure, and photoconductivity in conjugated polymer PCDTBT and in its separate building blocks, *Am. Chem. Soc.* 116 (2012) 11456–11469.
- [34] S.A. Jenekhe, L. Lu, M.M. Alam, New conjugated polymers with donor-acceptor architectures: synthesis and photophysics of carbazole-quinoline and phenothiazine-quinoline copolymers and oligomers exhibiting large intramolecular charge transfer, *Macromolecules.* 34 (2001) 7315–7324.
- [35] G. Bäuml, S. Schloter, U. Hofmann, D. Haarer, Correlation between photoconductivity and holographic response time in a photorefractive guest host polymer, *Opt. Commun.* 154 (1998) 75–78.
- [36] B. Lynn, P.A. Blanche, N. Peyghambarian, Photorefractive polymers for holography, *J. Polym. Sci. Part B Polym. Phys.* 52 (2014) 193–231.
- [37] L.G. Kaake, J.J. Jasieniak, R.C. Bakus, G.C. Welch, D. Moses, G.C. Bazan, A.J. Heeger, Photoinduced charge generation in a molecular bulk heterojunction material, *J. Am. Chem. Soc.* 134 (2012) 19828–19838.
- [38] S.M. Falke, C.A. Rozzi, D. Brida, M. Maiuri, M. Amato, E. Sommer, A. De Sio, A. Rubio, G. Cerullo, E. Molinari, C. Lienau, Coherent ultrafast charge transfer in an organic photovoltaic blend, *Science.* 344 (2014) 1001–1005.

- [39] J.C. Scott, L.T. Pautmeier, W.E. Moerner, Photoconductivity studies of photorefractive polymers, *J. Opt. Soc. Am. B.* 9 (1992) 2059.
- [40] T.K. Däubler, L. Kulikovskiy, D. Neher, Photoconductivity and charge-carrier photogeneration in photorefractive polymers, *Proc. SPIE.* 4462 (2002) 206–216.
- [41] J. Skindhøj, J.W. Perry, S.R. Marder, Development of electrooptic polymers for high voltage instrument transformers, *Nanoscale.* 2285 (2018) 10395–10402.
- [42] K. Mahesh, S. Karpagam, F. Goubard, Conductive and photoactive nature of conjugated polymer based on thiophene functionalized thiazole or benzothiadiazole, *Express Polym. Lett.* 12 (2018) 238–255.
- [43] P.R. Berger, M. Kim, Polymer solar cells: P3HT : PCBM and beyond, *J. Renew. Sustain. Energy.* 10 (2018) 13508.
- [44] B. Xu, G. Sai-anand, Improving photovoltaic properties of P3HT:IC60 BA through the incorporation of small molecules, *Polymers.* 10 (2018) 1–10.
- [45] B.L. Groenendaal, F. Jonas, D. Freitag, H. Pielartzik, J.R. Reynolds, Poly(3,4-ethylenedioxythiophene) and its derivatives: past, present, and future, *Adv. Mater.* 12 (2000) 481–494.
- [46] M.P. De Jong, L.J. Van Ijzendoorn, M.J.A. De Voigt, Stability of the interface between indium-tin-oxide and poly(3,4- ethylenedioxythiophene)/ poly(styrenesulfonate) in polymer light-emitting diodes, *Appl. Phys. Lett.* 77 (2000) 2255.
- [47] O. Bubnova, Z.U. Khan, A. Malti, S. Braun, M. Fahlman, M. Berggren, X. Crispin, Optimization of the thermoelectric figure of merit in the conducting polymer poly(3, 4-ethylenedioxythiophene ), *Nat. Mater.* 10 (2011) 429–433.
- [48] B.J. Ouyang, C. Chu, F. Chen, Q. Xu, Y. Yang, High-conductivity poly(3,4-ethylenedioxythiophene):poly(styrenesulfonate) film and its application in polymer optoelectronic devices, *Adv. Energy Mater.* 15 (2005) 203–208.
- [49] S. Kirchmeyer, K. Reuter, Scientific importance, properties and growing applications of poly(3,4-ethylenedioxythiophene), *J. Mater. Chem.* 15 (2005) 2077–2088.

- [50] B.H.W. Heuer, R. Wehrmann, S. Kirchmeyer, Electrochromic window based on conducting poly(3,4-ethylenedioxythiophene)-poly(styrene sulfonate), *Adv. Funct. Mater.* 12 (2002) 89–94.
- [51] M.C. Scharber, D. Mühlbacher, M. Koppe, P. Denk, C. Waldauf, A.J. Heeger, C.J. Brabec, Design rules for donors in bulk-heterojunction solar cells- towards 10% energy-conversion efficiency, *Adv. Mater.* 18 (2006) 789–794.
- [52] A. Kohler, D.A. dos Santos, D. Beljonne, Z. Shuai, J.L. Brédas, A.B. Holmes, A. Kraus, K. Müllen, R.H. Friend, Charge separation in localized and delocalized electronic states in polymeric semiconductors, *Nature.* 392 (1998) 903–906.
- [53] B. Carsten, J.M. Szarko, Hae, J. Son, W. Wang, L. Lu, F. He, B.S. Rolczynski, S.J. Lou, L.X. Chen, L. Yu, Examining the effect of the dipole moment on charge separation in donor-acceptor polymers for organic photovoltaic applications, *J. Am. Chem. Soc.* 133 (2011) 20468–20475.
- [54] Y. Liang, Y. Wu, D. Feng, S.T. Tsai, H.-J. Son, G. Li, L. Yu, Development of new semiconducting polymers for high performance solar cells, *J. Am. Chem. Soc.* 131 (2009) 56–57.
- [55] R. Koeppe, N.S. Sariciftci, Photoinduced charge and energy transfer involving fullerene derivatives., *Photochem. Photobiol. Sci.* 5 (2006) 1122–31.
- [56] G. Ramos, T. Belenguer, D. Levy, A highly photoconductive poly(vinylcarbazole)/2,4,7-trinitro-9-fluorenone sol-gel material that follows a classical charge-generation model, *J. Phys. Chem. B.* 110 (2006) 24780–24785.



### 6.1 Summary of the present work

The goal of the present work was to develop photorefractive polymer systems based on photoconducting polymers. Photorefractive materials are now being studied for erasable holographic recording. Photorefractive effect is the inhomogeneous variation in the refractive index of a material when exposed to non-uniform illumination. Photoconductivity and electro-optic effects are the two essential properties to exhibit photorefractive effect. The present thesis reports the studies made on synthesized polymers (both non-conjugated and conjugated polymers) which could be used as photorefractive materials for holographic recording.

Photoconducting properties of three non-conjugated polymers based on polybenzoxazine were studied. The polymers studied were poly(6-tert-butyl-3-phenyl-3,4-dihydro-2H-1,3-benzoxazine) labelled as PBZ, poly([4-(6-tert-butyl-4H-benzo[e][1,3]oxazin-3-yl)phenyl]phenyldiazene) labelled as AZO-PBZ and poly(4-tert-butyl-2-{{ethyl(4-nitrophenyl)amino}methyl}6{{methyl(4-phenylazophenyl)-amino}methyl}phenol) labelled as AZO-PNA. Cyclic voltammetry experiments were performed to determine the HOMO and LUMO energy levels of the polymers. From the onset of the absorption of the polymer thin film, the optical band gap ( $E_g$ ) was calculated. Steady state photoconductivity experiments were performed on the spin-coated films of the polymers. None of the polymers exhibited

photoconductivity in the pristine form. When the polymers were blended with PCBM, the polymers exhibited photoconductivity. The benzoxazine polymer: PCBM blend films were prepared for polymer to PCBM ratios of 1:0.5 and 1:1. Further increase in concentration of PCBM produced films with less optical clarity. The steady state photoconductivity experiments were carried out in the blend films and the internal photocurrent efficiency ( $\phi$ ) and photoconductive sensitivity ( $\frac{\sigma_{ph}}{I}$ ) of the benzoxazine polymer: PCBM blend films were calculated as a function of electric field. The main results are tabulated in Table 6.1.

**Table 6.1:** Photoconducting performance of benzoxazine polymer: PCBM blend films.

Sample		$E_g$ (eV)	$E_{max}$ (V/ $\mu m$ )	$\phi_{max}$ for 488 nm	$\left(\frac{\sigma_{ph}}{I}\right)_{max}$ $SW^{-1}cm$
PBZ:PCBM	1:0	2.90	40		
	1:0.5		40	$1.40 \times 10^{-5}$	$6.15 \times 10^{-12}$
	1:1		40	$1.74 \times 10^{-5}$	$8.14 \times 10^{-12}$
AZO-PBZ:PCBM	1:0	2.45	30		
	1:0.5		30	$4.15 \times 10^{-5}$	$3.13 \times 10^{-11}$
	1:1		30	$6.2 \times 10^{-5}$	$5.57 \times 10^{-11}$
AZO-PNA:PCBM	1:0	2.80	55		
	1:0.5		55	$7.9 \times 10^{-4}$	$1.31 \times 10^{-10}$
	1:1		55	$9.52 \times 10^{-4}$	$1.59 \times 10^{-10}$

From Table 6.1, it is obvious that band gap of the polymers occurs in the higher frequency region of the visible spectrum. The values corresponding to the internal photocurrent efficiency and photoconductive sensitivities are comparable with the typical photorefractive polymer systems. So, trials were carried out to check the validity of these polymers

to exhibit photorefractivity. Photorefractive devices were successfully prepared using PBZ and showed asymmetric energy transfer in two beam coupling experiment. A photorefractive gain of  $87.45 \text{ cm}^{-1}$  was obtained at an electric field of  $35 \text{ V}/\mu\text{m}$ . Photorefractive device preparation with other two polymers viz. AZO-PBZ and AZO-PNA was not successful. But the photoconductive performance of these two polymers are much better than PBZ. Hence, once the sample preparation is successful, better photorefractive performance can be expected from these polymers.

**Table 6.2** Photorefractive composites available from the literature and corresponding diffraction efficiency

Year	Photorefractive composite	Diffraction efficiency (%)
1991	bisA-NPDA+DEH	$2 \times 10^{-3}$
1992	PVK+C <sub>60</sub> +DEANST	$2 \times 10^{-3}$
1994	PVK+TNF+DMNPAA+ECZ	95
1999	PVK+CdS+TCP+NPP	8
1999	PVK+ECZ+TNFDM+FTCN	24
2003	PPT-CZ+C <sub>60</sub> +DDCST	93
2008	PATPD-CANN+FDCT+ECZ	90
2012	PVK+TNF+7-DCST+CzEPA	68
2013	P-IP-DC+PCBM	67
2013	PTAA+7-DCST+ECZ+PCBM	4.64

For a comparative study, the maximum diffraction efficiencies exhibited by different polymer composites is tabulated in Table 6.2 [1–8]. The data described in the table are reported as obtained by conducting the four wave mixing experiment and hence could not compare with our results.

The photoconductive properties of donor acceptor conjugated copolymers were also studied. The donor-acceptor segments in the repeat units reduced the band gap and provided absorption towards the higher

wavelength region of the visible spectrum. Initially, studies were concentrated on poly(2,5-(3,4-ethylenedioxythiophene)-alt-2,7-(9,9-dioctylfluorene)) labelled as P(EDOT-FL). The HOMO and LUMO energy levels of the polymer was calculated from CV experiment. Unlike the benzoxazine polymers, pristine P(EDOT-FL) films exhibited photoconductivity. However, the photogeneration efficiency was much less. To enhance the charge transfer properties, P(EDOT-FL):PCBM blend films were prepared for a polymer to PCBM weight ratios of 1:1 and 1:2. The polymer could withstand electric field up to  $70 \text{ V}/\mu\text{m}$ . An internal photocurrent efficiency of 86% was obtained for the blend films with polymer to PCBM ratio of 1:2, at an electric field of  $70 \text{ V}/\mu\text{m}$ . Also, the P(EDOT-FL) film and P(EDOT-FL):PCBM blend films exhibited good photoresponse even at low electric fields. So the polymer material could safely operate in the low electric field region, without undergoing dielectric breakdown. Here also, the photorefractive device fabrication was not successful. Due to the enhanced photoconductive performance of this polymer, one can expect better photorefractive performance in P(EDOT-FL) polymer system.

Further, the photoconductivity studies of three donor-acceptor conjugated polymers consisting of 2,1,3-benzothiadiazole (BTZ) acceptor moiety were carried out. Triphenylamine (TPA), 3-hexylthiophene (HT) and 3,4-dihexyloxythiophene (HXT) were used as donor moieties. The copolymers were labelled as P(BTZ-TPA), P(BTZ-HT) and P(BTZ-HXT). Band gap of the polymers were finely tuned in accordance with the donor strength of the donor moieties. Donor strength of donor moieties were in the order  $\text{HXT} > \text{HT} > \text{TPA}$  and consequently the lowest band gap was obtained for P(BTZ-HXT). Polymer:PCBM blend films (with ratio 1:1)

were prepared to overcome the low carrier generation efficiency of the pristine polymers. P(BTZ-TPA):PCBM blend exhibited higher internal photocurrent efficiency due to higher LUMO-LUMO offset of polymer and PCBM. Other two polymers showed low band gap compared to P(BTZ-TPA), but the photogeneration efficiency was much less compared to P(BTZ-TPA):PCBM blend films. This is due to the insufficient LUMO-LUMO offset between polymer and PCBM which was confirmed by CV measurements. Hence it was concluded that for P(BTZ-HT) and P(BTZ-HXT) polymers, PCBM was not a suitable acceptor for the photogeneration process. Because of the low synthesis yield of these polymers, studies towards the photorefractive effect could not be done. A comparison of the photoconductive performance of the above donor-acceptor conjugated polymers is given in Table 6.3.

**Table 6.3:** Photoconducting performance of P(EDOT-FL):PCBM, P(BTZ-TPA):PCBM, P(BTZ-HT):PCBM and P(BTZ-HXT):PCBM films.

Sample		$E_g$ (eV)	$\phi$ at $10\text{ V}/\mu\text{m}$ (for 488 nm)	$\left(\frac{\sigma_{ph}}{I}\right)$ at $10\text{ V}/\mu\text{m}$ (for 488 nm) $SW^{-1}cm$	$E_{max}$ ( $V/\mu m$ )	$\phi_{max}$ For 488 nm	$\left(\frac{\sigma_{ph}}{I}\right)_{max}$ $SW^{-1}cm$
P(EDOT-FL):PCBM	1:0	2.40	$9.70 \times 10^{-4}$	$2.60 \times 10^{-9}$	70	0.2	$7.0 \times 10^{-8}$
	1:1		$1.05 \times 10^{-3}$	$3.73 \times 10^{-9}$	70	0.26	$1.3 \times 10^{-7}$
	1:2		$1.16 \times 10^{-3}$	$4.85 \times 10^{-9}$	70	0.86	$5.4 \times 10^{-7}$
P(BTZ-TPA):PCBM	1:0	2.02	$3.70 \times 10^{-6}$	$1.25 \times 10^{-11}$	10	$3.70 \times 10^{-6}$	$1.25 \times 10^{-11}$
	1:1		$1.74 \times 10^{-1}$	$5.60 \times 10^{-8}$	10	$1.74 \times 10^{-1}$	$5.60 \times 10^{-8}$
P(BTZ-HT):PCBM	1:0	1.84			10		
	1:1		$5.00 \times 10^{-4}$	$1.50 \times 10^{-9}$	10	$5.00 \times 10^{-4}$	$1.50 \times 10^{-9}$
P(BTZ-HXT):PCBM	1:0	1.65			30		
	1:1		$7.50 \times 10^{-3}$	$1.10 \times 10^{-10}$	30	0.028	$5.1 \times 10^{-10}$

From Table 6.3, it may be noted that only P(EDOT-FL) and its blend with PCBM can withstand higher electric field up to  $70 \text{ V}/\mu\text{m}$ . Now, comparing the internal photocurrent efficiencies of the pristine polymer and blend films measured at an electric field of  $10 \text{ V}/\mu\text{m}$ , it could be seen that highest photocurrent efficiency of 17.4% was achieved for the P(BTZ-TPA):PCBM blend films for a weight ratio of 1:1, which was two orders higher than that of other polymers or blend films. Another point worth mentioning here is that an internal photocurrent efficiency greater than or comparable to this value (17.4%) could only be achieved in pristine P(EDOT-FL) and P(EDOT-FL):PCBM films at a higher electric field of  $70 \text{ V}/\mu\text{m}$ . Hence, considering that a low field regime is more desirable for photorefractive and photoconducting applications, P(BTZ-TPA):PCBM composite is more suitable compared to other polymers studied.

Many of the reported photorefractive polymer systems face problems such as phase separation of the components in the guest-host systems and dielectric breakdown in the presence of high external electric field. The studied donor-acceptor conjugated copolymers exhibited photoconductivity in pristine form with enough photogeneration efficiency in the low field regime. Hence it is expected that the breakdown at higher field can be avoided by using these polymers. These polymers are not guest host systems and hence the problem of phase separation can also be avoided. But we could not observe any erasing effect in the prepared photorefractive device. Usually either by applying high DC field or by uniform illumination one can erase the recorded grating [8–11]. This has to be further studied and optimised to erase and rerecord gratings in the present system.

## 6.2 Future scope

The present thesis was focused on the development of photorefractive polymers. Out of the seven polymers studied, photorefractive effect could be studied in poly(6-tert-butyl-3-phenyl-3,4-dihydro-2H-1,3-benzoxazine) alone. For other polymers, the experiment could not be conducted due to the inadequacies regarding the device fabrication. The ground state dipole moment of PBZ, AZO-PBZ, AZO-PNA and P(EDOT-FL) molecules were determined experimentally by Guggenheim and Smith method (G-S method). The respective permanent dipole moment values of PBZ, AZO-PBZ, AZO-PNA and P(EDOT-FL) were obtained as 2.65, 4.89, 5.65 and 6.11 D. This suggested the existence of charge asymmetry in the polymers, which could generate second order nonlinear effect. Relative second harmonic efficiency of PBZ, AZO-PBZ, P(EDOT-FL) and P(BTZ-TPA) were estimated by Kurtz-Perry powder technique and the obtained relative efficiencies (with respect to KDP) were 0.17, 0.3, 0.075 and 2.75 respectively. The observation of second harmonic emission from polymer systems is an indication of presence of  $\chi^{(2)}$  and hence the Pockel's effect. Hence, these polymers might be suitable for electro-optic applications and could be used as photorefractive polymers for holographic recording. Further studies are needed for fully exploiting these materials.

The conjugated polymers studied showed higher photogeneration of charge carriers in the presence of acceptor PCBM. So these polymers could be successfully used for photovoltaic and other optoelectronic applications also. Among the polymers studied, P(BTZ-HXI) exhibited the lowest band gap of 1.65 eV which is quite suitable for photovoltaic application.

However, for P(BTZ-HXT) an acceptor other than PCBM may be better for efficient photocarrier generation.

## References

- [1] J.A. Herlocker, K.B. Ferrio, E. Hendrickx, B.D. Guenther, S. Mery, B. Kippelen, N. Peyghambarian, J.A. Herlocker, K.B. Ferrio, E. Hendrickx, B.D. Guenther, S. Mery, B. Kippelen, Direct observation of orientation limit in a fast photorefractive polymer composite Direct observation of orientation limit in a fast photorefractive polymer composite, 2253 (2007) 18–21.
- [2] K. Kinashi, H. Shinkai, W. Sakai, N. Tsutsumi, Photorefractive device using self-assembled monolayer coated indium-tin-oxide electrodes, *Org. Electron.* 14 (2013) 2987–2993.
- [3] I.K. Moon, J. Choi, N. Kim, High-Performance Photorefractive Composite Based on Non-conjugated Main-Chain , Hole-Transporting Polymer, *Macromol. Chem. Phys.* 214 (2013) 478–485.
- [4] K. Meerholz, B.L. Volodin, Sandalphon, & Kippelen, B., N. Peyghambarian, A photorefractive polymer with high optical gain and diffraction efficiency near 100 %, *Nature.* 371 (1994) 497–500.
- [5] O. Kwon, S. Lee, G. Montemezzani, P. Gu, Highly efficient photorefractive composites based on layered photoconductive polymers, *J. Opt. Soc. Am. B.* 20 (2003) 2307–2312.
- [6] N. Tsutsumi, K. Kinashi, A. Nonomura, W. Sakai, Quickly Updatable Hologram Images Using Poly(N-vinyl Carbazole) (PVCz) Photorefractive Polymer Composite, (2012) 1477–1486.
- [7] J. Thomas, C.W. Christenson, P.A. Blanche, M. Yamamoto, R.A. Norwood, N. Peyghambarian, Photoconducting polymers for

- photorefractive 3D display applications, *Chem. Mater.* 23 (2011) 416–429.
- [8] J. Thomas, R.A. Norwood, N. Peyghambarian, Nonlinear optical polymers for photorefractive applications, *J. Mater. Chem.* 19 (2009) 7476–7489.
- [9] S. Köber, M. Salvador, K. Meerholz, Organic photorefractive materials and applications, *Adv. Mater.* 23 (2011) 4725–4763.
- [10] W. Lin, S. Rokutanda, T. Gu, D. Flores, P. Wang, G. Li, P.S. Hilaire, J. Thomas, R.A. Norwood, M. Yamamoto, N. Peyghambarian, An updatable holographic three-dimensional display, *Nature*. 451 (2008) 694–698.
- [11] P. Blanche, S. Tay, R. Voorakaranam, P. Saint-hilaire, C. Christenson, T. Gu, W. Lin, D. Flores, P. Wang, M. Yamamoto, J. Thomas, R.A. Norwood, N. Peyghambarian, An Updatable Holographic Display for 3D Visualization, *J. Display Techn.* 4 (2008) 424–430.

